

Hyperspectral imaging for the characterization of Athabasca oil sands core

by

Michelle Alexandra Speta

A thesis submitted in partial fulfillment of the requirements for the degree of

Doctor of Philosophy

Department of Earth and Atmospheric Sciences
University of Alberta

© Michelle Alexandra Speta, 2016

Abstract

The Athabasca oil sands of northeastern Alberta, Canada, are one of the largest accumulations of crude bitumen in the world. Drill core sampling is the principal method for investigating subsurface geology in the oil sands industry. Cores are logged to record sedimentological characteristics and sub-sampled for total bitumen content (TBC) determination. However, these processes are time- and labour-intensive, and in the case of TBC analysis, destructive to the core. Hyperspectral imaging is a remote sensing technique that combines reflectance spectroscopy with digital imaging. This study investigates the application of hyperspectral imaging for the characterization of Athabasca oil sands drill core with three specific objectives: 1) spectral determination of TBC in core samples, 2) visual enhancement of sedimentological features in oil-saturated sediments, and 3) automated classification of lithological units in core imagery.

Two spectral models for the determination of TBC were tested on four suites of fresh core and one suite of dry core from different locations and depths in the Athabasca deposit. The models produce greyscale images that show the spatial distribution of oil saturation at a per-pixel scale (~1 mm). For all cores and both models, spectral TBC results were highly correlated with Dean-Stark data ($R^2 = 0.94-0.99$). The margin of error in the spectral predictions for three of the fresh cores was comparable to that of Dean-Stark analysis (± 1.5 wt %). A fourth fresh core and the dry core had higher margins of error ($\pm 2.5-3.3$ wt %) due to some instances of overestimation in high grade samples (>10 wt %). Surface roughness was identified as a possible source of error in the spectral TBC estimates.

Logging oil sands core can be challenging because sedimentary and biogenic features are often difficult to see in the bitumen-saturated sediment. Shortwave infrared (SWIR; 1.0-2.5 μm) hyperspectral imagery, using the three-band combination of 2.16 μm , 2.20 μm and 2.35 μm , was found to greatly enhance the visibility of sedimentological features in massive-appearing oil

sand. This combination of wavelength bands produced near-natural colour images that in many cases revealed features completely invisible to the unaided eye. A spatial resolution of at least 0.25 mm/pixel is required for accurate trace fossil identification, but most sedimentary structures can be accurately identified even at lower resolutions (1.2-1.5 mm/pixel). Enhanced visibility of features is due to variable reflectance that for large-scale sedimentary structures (>1 cm) is attributed primarily to changes in grain size and bitumen content. Variable reflectance across smaller-scale (<1 cm) sedimentary structures or trace fossils is mainly attributed to differences in clay content.

Finally, SWIR and longwave infrared (LWIR; 8-12 μm) imagery of oil sand core was investigated for the automated mapping of five common rock types (oil sand, barren sand, siltstone, mudstone, and siderite) using the spectral angle mapper (SAM) classification technique. Detailed maps that are consistent with visual inspection of the core were successfully produced with both datasets. In cases of disagreement, the SWIR imagery was more accurate for mapping the spatial distribution of oil sand and the LWIR imagery was more accurate for the discrimination of barren sand, siltstone and mudstone. Improvements in the mapping methodology, such as using a spectral TBC model to map oil sands at different bitumen saturation thresholds, or using spectral subsets of the image data for SAM input, enhanced the mapping results. The combined results of this thesis demonstrate the immense potential of hyperspectral imaging for facilitating the processes of routine oil sands core logging and bitumen content analysis.

Preface

Chapter 1, 2, 5 and 6 of this thesis are my original work. Chapter 3 of this thesis has been published as: Speta, M., Rivard, B., Feng, J., Lipsett, M., Gingras, M., 2015, Hyperspectral imaging for the determination of bitumen content in Athabasca oil sands core samples, *AAPG Bulletin*, 99(7), 1245-1259. The spectral models for bitumen content estimation were developed by J. Feng and B. Rivard. I was responsible for data collection, data analysis and interpretation, and manuscript composition. J. Feng assisted with data collection and interpretation. B. Rivard was the supervisory author and was involved with manuscript composition and data interpretation. M. Gingras was involved in the sedimentological aspects of this work and M. Lipsett was involved in statistical analysis of the results.

Chapter 4 of this thesis has been accepted for publication as: Speta, M., Gingras, M., Rivard, B., Shortwave infrared hyperspectral imaging: A novel method for the enhancement of sedimentary and biogenic features in oil-saturated core, *Journal of Sedimentary Research*. I was responsible for data collection and manuscript composition. J. Feng and P. Lypaczewski assisted with data collection. M. Gingras assisted with the sedimentological aspects of this research. B. Rivard was the supervisory author and assisted with manuscript composition.

Acknowledgements

There are many people that I am extremely grateful to for their involvement and support in both my research and my life over the past 4.5 years. Thank you to my supervisor, Dr. Benoit Rivard, who took me on as a student even though I had absolutely zero knowledge of remote sensing. Thank you for allowing me to take on this project and for supporting me as I chased down opportunities to grow both my research and my professional network, even though that meant I sometimes pushed you out of your comfort zone. Thank you also for giving me the opportunity to gain mentorship experience through working with Paulina Hauf (and thank you to Paulina for being a great mentee!).

Thank you to Dr. Jilu Feng, who not only helped with all the core scanning for this thesis, but was always willing to answer my questions, no matter how big or small. Thank you for always having an open door, you are an amazing teacher! Thank you also to Dr. Murray Gingras. Your enthusiasm is contagious and I always left our meetings feeling inspired.

The first year of my thesis was funded by an NSERC CGS-M scholarship. In subsequent years, I am grateful for funding I received from industry partners (Devon Canada, Cenovus Energy), as well as various scholarships from both the province and the university. Devon Canada provided core samples that were integral to the third chapter of this thesis. The core that I used for all three research papers was donated to the Department of Earth & Atmospheric Sciences' teaching and research collection by Imperial Oil.

Lisa Budney, Igor Jakab, Mark Labbe and Andrew Locock were extremely helpful during various stages of my degree, assisting with everything from getting access to core, collecting ancillary data, sample photography, and printing. Thank you to Iman Entezari, Dominica Harrison, David Turner and Alina Shchepetkina for being great colleagues and collaborators. I am also immensely grateful to Erica Dunn. Thank you for being such a constant, steady source of support. I will carry your wise words with me for many years to come!

Finally, I thank my friends and family. Big thank you to my parents for their unwavering, unconditional support and love, and to friends within the department and all around the world for cheering me on and keeping me sane. And last, but certainly not least, thank you to David Dockman, my true partner in everything.

Table of Contents

Chapter 1

Introduction..... 1

 1.1 Background & Research Objectives..... 1

 1.2 Hyperspectral Imaging..... 4

 1.3 Thesis Layout..... 7

References..... 9

Chapter 2

The Athabasca Oil Sands..... 11

 2.1 The McMurray Formation..... 11

 2.2 Origin of the Resource..... 13

 2.3 Depositional History & Facies Classification..... 15

 2.4 Extraction of the Resource..... 18

References..... 20

Chapter 3

Hyperspectral imaging for the determination of bitumen content in Athabasca oil sands core samples..... 24

 3.1 Introduction..... 24

 3.2 Study Area & Samples..... 27

 3.2.1 *Geological Context*..... 27

 3.2.2 *Samples*..... 29

 3.3 Methods..... 31

 3.3.1 *Collection of Spectral Imagery*..... 31

 3.3.2 *Spectral Models for TBC Prediction*..... 31

 3.3.3 *Viewing Spectral TBC Results*..... 34

 3.3.4 *Evaluating Spectral TBC Results*..... 34

 3.4 Results..... 37

3.5 Discussion.....	40
3.5.1 <i>Fresh Core</i>	40
3.5.2 <i>Dry Core</i>	43
3.6 Conclusions.....	45
References.....	47

Chapter 4

Shortwave infrared hyperspectral imaging: A novel method for enhancing the visibility of sedimentary and biogenic features in oil-saturated core..... 50

4.1 Introduction.....	50
4.2 Samples.....	54
4.3 Methods.....	55
4.4 Results.....	57
4.4.1 <i>Band Selection</i>	57
4.4.2 <i>Sedimentary Structures</i>	60
4.4.3 <i>Trace Fossils</i>	60
4.5 Discussion.....	65
4.6 Advantages of Hyperspectral Imaging.....	69
4.7 Limitations of the Technique.....	69
4.8 Conclusions.....	70
References.....	72

Chapter 5

Automated lithological mapping of McMurray Formation oil sands core with shortwave (1.0-2.5 μm) and longwave infrared (8-12 μm) hyperspectral imaging.....75

5.1 Introduction.....	75
5.2 Oil Sands Reflectance Spectroscopy	77
5.3 Study Area & Samples.....	80
5.3.1 <i>Geological Context</i>	80
5.3.2 <i>Samples</i>	80

5.4 Methods.....	83
5.4.1 Data Collection.....	83
5.4.2 Data Analysis.....	85
5.5 Results.....	88
5.5.1 FTIR & LWIR Rock Type Spectra.....	88
5.5.2 Rietveld Analysis	90
5.5.3 SWIR Rock Type Spectra.....	91
5.5.4 Lithological Core Maps.....	93
5.6 Discussion.....	98
5.7 Conclusions.....	102
References.....	103
Chapter 6	
Conclusions.....	107
6.1 Summary & Contributions.....	107
6.2 Future Work.....	111
6.2.1 Clay Characterization.....	111
6.2.2 Beyond the McMurray Formation.....	113
References.....	114
Appendix A	
Detailed Rietveld analysis results.....	116

List of Tables

Table 3.1 Core samples used in this study.....	30
Table 3.2 Technical specifications of the SisuROCK SWIR sensor and associated data.....	30
Table 3.3 Results of linear regression analysis for individual fresh cores for both spectral models. RMS error is given in units of \pm wt % TBC.....	38
Table 4.1 Technical specifications of the SisuROCK shortwave infrared camera and associated hyperspectral imagery.....	56
Table 5.1 SWIR and LWIR absorption features typical of the McMurray Formation rocks investigated in this study.....	79
Table 5.2 Number of spot measurements averaged for each representative spectrum.....	85
Table 5.3 Quartz and clay mineral content (in wt %) of barren sand, siltstone and mudstone as determined by Rietveld analysis.	91

List of Figures

- Figure 1.1** Terminology commonly used to describe the different wavelength regions of the electromagnetic spectrum that are pertinent to mineral spectroscopy and remote sensing. All wavelengths are in units of μm . VIS = visible, NIR = near infrared, TIR = thermal infrared, SWIR = shortwave infrared, MWIR = mid-wave infrared, LWIR = longwave infrared. The wavelength regions that are investigated in this study are shown in bold. The causes of absorption features in the different parts of the spectrum are also indicated.5
- Figure 2.1** The oil sands of northeastern Alberta, Canada. All samples used in this study are from the Athabasca deposit. Modified from Ranger and Gingras (2003).12
- Figure 2.2** Basic stratigraphy of the Athabasca oil sands deposit. The McMurray Formation is primary reservoir unit and the focus of this study. Oil saturation extends into the Wabiskaw Member and the Grand Rapids Formation in the south and west ends of the deposit. Modified from Mossop and Flach (1983).12
- Figure 3.1** The oil sands deposits of northeastern Alberta, Canada, and the basic stratigraphy of the Athabasca deposit. All samples used in this study are from the Athabasca deposit, where the primary reservoir is the McMurray Formation. Modified from Ranger and Gingras (2003).27
- Figure 3.2** Ore grade distribution for the samples used for this study ($n = 430$). Total bitumen content (wt %) values are based on Dean-Stark analysis data for core A-D and bitumen mass fraction calculations for core E. Frequency is absolute (i.e. number of Dean-Stark samples).30
- Figure 3.3** Representative reflectance spectra of oil sand and shale. Arrows indicate bitumen absorption features in the oil sand spectrum and clay mineral absorption features in the shale spectrum.32
- Figure 3.4** Photo of a box from core E (left), its greyscale TBC image (middle) and a vertical TBC profile (right). The greyscale represents the range of pixel values in the image where black means void of bitumen and white means highest grade. The yellow rectangle and line show examples of rectangular and linear region of interests that can be used to calculate mean spectral TBCs for comparison to Dean-Stark values. The vertical TBC profile represents variation in TBC as a function of depth at the mm scale, and is derived from pixel values along the red line shown on the greyscale TBC image. Core diameter = 6 cm.35
- Figure 3.5** Correlation plot showing the relationship between the mean spectral TBC obtained from rectangular regions of interest vs. linear regions of interest for Dean-Stark samples in core A ($n = 61$). Results are shown for both spectral models. The equation of the regression line (dashed) and the coefficient of determination (R^2) is provided on each plot.37
- Figure 3.6** Correlation plots showing the linear regression results for all 5 suites of core. Broadband model results are in the left column and wavelet model results are given in the right column. Fresh cores are shown in the top row of plots and the dry core is shown in the bottom row. Regressions were forced through the origin. The equation of the dashed regression line, R^2 ,

and the RMS error are provided on each plot. The number of Dean-Stark samples is given by n .
 39

Figure 3.7 Photos of boxes from fresh core B showing rough surface textures that may be a source of error in the spectral results. The left image is an example of a Type 2 problematic sample: coarse grained and loosely consolidated. The right image is a Type 3 problematic sample: fractured surface and cross-bedding with uneven bitumen distribution..... 44

Figure 3.8 Photos showing examples of two boxes from dry core E where one was overestimated and the other performed well. As shown in the inset photos, the overestimated sample shows cross-bedding defined by variable grain size and bitumen distribution. The beds impart a micro-topography to the sample surface where finer grained, oil-rich beds are higher and coarser grained, oil-poor beds are lower. A sample with similar cross-bedding but uniform oil distribution is shown for comparison. In this case, the bedding is clearly visible because of grain size variation, however the bitumen content does not appear to vary between the stripes. This sample has a smoother surface texture as all beds have similar prominence. 44

Figure 4.1 The oil sands deposits of northeastern Alberta, Canada, and the stratigraphy of the Athabasca deposit. Star indicates approximate location of drill core used in this study. Map modified from Ranger and Gingras (2003), stratigraphic column modified from Mossop and Flach (1983)..... 51

Figure 4.2 Schematic diagram of a hyperspectral data cube for a box of oil sands core. x and y represent the spatial coordinates of the pixels in the digital image and λ represents wavelength. Reflectance measurements are recorded at wavelength intervals known as bands, which are illustrated as layers in the data cube. The red box represents a pixel with its corresponding spectrum shown. Portions of the spectrum are shaded according to the legend to indicate bitumen (1700 nm and 2300 nm; dark gray), clay mineral (1400 nm and 2300 nm; light gray) and water (1900 nm; blue) absorption features. 53

Figure 4.3 A schematic diagram of the hyperspectral imaging system used in this study. The inset shows the interior of the camera housing with the following labelled components: A) SWIR camera, B) quartz lamps, C) Spectralon™ panel, and D) box of core. The spectral camera is fixed and the platform carrying the core sample moves below it at rate set by the user..... 56

Figure 4.4 Conventional litholog of the core sample used in this study. Core was logged at a scale of 1:150 by C. Ciszkowski. Locations of boxes shown in Figure 4.6 are indicated in red.... 58

Figure 4.5 Examples of spectral imagery of the same section of core, with a photo (A) for reference. B is a single band grayscale image and C is a three-band color composite image. The reflectance spectra shown (D) are average spectra from the mudstone (dashed line, indicated by “m” on the images) and oil sand (solid line, indicated by “os” on the images) sections of this core. The light gray shaded region of the spectrum represents the range of wavelength bands in which sedimentary features were enhanced in single band imagery. The dark gray band represents the wavelength shown in the single band image. The red, green and blue bands show the three-band combination that was used to make the color composite images presented in this study. While both single-band and three-band images enhance the contrast of sedimentary

features, color composites images allow for the discrimination of lithology. In image C, the green tone of the oil sand makes it easy to distinguish from the pale blue-toned mudstone, while in image B, bright sections of oil sand could easily be confused with equally bright mudstone.59

Figure 4.6 Examples of spectral imagery where the visibility of sedimentary structures and trace fossils is enhanced relative to the corresponding photographs, which are shown at the same scale. Low resolution images show the full core box and high resolution images are shown as sections of the sample as indicated with red and blue rectangles. Colored arrows indicate ichnofossils as per the legend. A1) The oil sand looks entirely structureless, but spectral imagery reveals a contact between low angle planar-tabular cross-bedded sand and massive sand. A2) Spectral imagery reveals cross-bedded sand abruptly overlaying massive sand. This contact is clear at both high and low resolution. A vertical burrow is also revealed in the high resolution spectral image. B1) Large-scale cross-stratification can be inferred in the photo due to grain size variability across the beds, but the spectral image clearly differentiates finer grained (125-500 μm) dark stripes from coarser grained (500-1000 μm) bright stripes at both low and high resolution. B2) Without grain size variability, the oil sands appear structureless. However, high resolution spectral imagery reveals current ripples. C1) Current ripples are cryptic in the photo but clearly defined in the high resolution spectral image, which also reveals the climbing nature of the ripples and intercalated sigmoidal bedding. C2) Current ripples can be discerned in the photo when there is erosion along bedding surfaces and parting planes are visible, but the high resolution spectral image reveals details such as individual foreset laminae and mm-scale escape traces. D1) Low degree of bioturbation. No primary sedimentary fabric or ichnofabric is visible in the photos. Spectral imagery reveals current ripples with abundant escape traces. D2) Moderate to high degree of bioturbation. Biogenic disturbance of primary sedimentary fabric can be inferred from the photo but discrete trace fossils are not visible if not mud-filled. Spectral image reveals escape traces as well as *Cylindrichnus* in the oil-saturated sand. E1) Moderate degree of bioturbation. Disturbance of primary sedimentary fabric is clear in mudstone bed, but ambiguous in the oil sand. Spectral image improves visual contrast of trace fossils in both the mudstone and the oil sand sections. *Planolites*, *Thalassinoides* and *Cylindrichnus* can be identified as well as numerous undiagnosed burrows. E2) Moderate degree of bioturbation. Little indication of biogenic disturbance of the sediment can be deduced from the photo. Spectral image reveals *Planolites*, *Cylindrichnus*, and undiagnosed burrows. F1) High degree of bioturbation. The magnitude of biogenic disturbance is evident from the mottled texture of the interbedded mud and sand in the photo. Spectral images reveal the full extent of the bioturbation and facilitate the identification of trace fossils, including *Planolites* and *Teichichnus*. A 17 cm long sand-filled diastasis crack (Cowan and James, 1992) can also be identified. F2) High degree of bioturbation. Abundant *Planolites*, *Teichichnus*, and *Skolithos*, as well as numerous undiagnosed burrows, are clear in the spectral image.....63

Figure 4.7 An example of low resolution spectral imagery that demonstrates why a higher resolution is required for accurate identification of trace fossils. At low resolution (left), the features enclosed in the red rectangle may appear like vertical burrows. At high resolution (right), it becomes clear that these features are merely surficial fractures.64

Figure 4.8 From left to right: Photo, color composite spectral image and grayscale bitumen content image of oil sands sections that showed Type 1 (A) and Type 2 (B) spectral response. In the bitumen content images, black represents 0 wt % and white represents 18 wt % oil, as shown

in the color bar legend. b = bright domain, d = dark domain, m = mudstone. Bitumen content images were produced using a spectral model described in Speta et al. (2015). 67

Figure 4.9 Average spectra for bright (solid lines) and dark (dashed lines) domains for Type 1 (red) and Type 2 (blue) samples. Spectra are the average of 4000-6000 pixels collected from multiple sections of core showing each type of spectral response. Plot A shows whole spectra, with gray boxes showing the wavelength ranges to which continuum-removal was applied. Plot B is the continuum-removed view of the 1700 nm bitumen absorption feature and plot C shows the continuum-removed view of the 2200 clay absorption feature. 68

Figure 5.1 The oil sands deposits of northeastern Alberta, Canada, and the stratigraphy of the Athabasca deposit. Map modified from Ranger and Gingras (2003), stratigraphic column modified from Mossop and Flach (1983). 81

Figure 5.2 A litholog of the core used in this study. Sand/sandstone, siltstone and mudstone are colour-coded as per the legend and other phases are indicated by symbols. Bitumen saturation is not indicated. Core was logged by C. Cizkowski at a scale of 1:150. Core boxes that are shown as lithological maps in Figure 5.6 are indicated by the red boxes. 82

Figure 5.3 An example of SWIR (middle) and LWIR (right) imagery of a box of oil sands core with a photo for reference (left). Arrows indicate type sections and squares indicate spot measurements for oil sands (red) and siderite (cyan). The spectral images are colour composites consisting of wavelength bands at 2.16, 2.20 and 2.35 μm for SWIR and bands at 8.13, 9.98 and 11.81 μm for LWIR. In this schematic, the LWIR image has been re-sized to same dimensions as the SWIR image. 86

Figure 5.4 LWIR spectra of the five rock types investigated in this study, colour-coded as per the legend. A) Full resolution FTIR point spectra (294 bands). Spectra shown are the average of all point spectra collected for each rock type. A pure quartz sand spectrum is also shown for comparison. B) Resampled, mean normalized FTIR point spectra (35 bands). Full resolution FTIR results were resampled to the same spectral resolution as the LWIR spectral imagery to allow direct comparison of the two data sets. C) Mean normalized LWIR image spectra (35 bands). Spectra shown are the average of all spot spectra collected for each rock type from the LWIR imagery. 89

Figure 5.5 A) SWIR spectra (256 bands) of the different rock types investigated in this study, colour-coded as per the legend. B), C), and D) show the continuum-removed views of the 1.4, 1.9 and 2.2 μm features, respectively, for barren sand, siltstone and mudstone. 92

Figure 5.6 Examples of SWIR and LWIR mapping results. SWIR maps have an additional colour-coded unit (grey) representing cardboard. These pixels are unclassified in the LWIR maps because cardboard is not spectrally active in this wavelength range. A) Intraclast breccia with a matrix of high-grade oil sand. A bitumen-stained clast is classified as part of the oil sand matrix in the SWIR, but correctly mapped as barren sand in the LWIR (white box). B) Interbedded sandstone and siltstone with varying degrees of bitumen saturation in the sands. SWIR and LWIR results are comparable with the exception of two barren sand sections that incorrectly classified as oil sand in the LWIR map (white boxes). Spectral mapping results are consistent

with visual inspection of the core, both of which disagree with the classification of this core on the conventional litholog (Figure 5.2). C) Oil sand with grain striping. The whole core is correctly classified as oil sand for both datasets. Unclassified beds in the SWIR map (white arrows) correspond to fine grained stripes. D) Oil sand with siderite clasts. Siderite is correctly classified in both maps, as is the oil sand. The grainy appearance of the LWIR map is likely due to lower signal to noise ratio in the LWIR data relative to the SWIR data. E) An example of a mudstone-rich core where the SWIR and LWIR results are comparable. A contact between mudstone and barren sand that is difficult to discern visually is clearly defined in both maps (white arrow). F) An example of a mudstone-rich core where mudstone is misclassified as barren sand in the SWIR results (white box). A coal seam (white arrow) is misclassified as mudstone in the SWIR. Since a coal end-member was not included in the SAM classification, coal would be expected to remain unclassified as in the LWIR map.95

Figure 5.7 Mean spectrum of the problematic section in the LWIR map of core B. This section of barren sand is misclassified as oil sand. Comparison to the end-member spectra of oil sand and barren sand clearly show the spectral similarity of the misclassified section to the oil sand end-member.97

Figure 5.8 Mean spectra of coarse (red) and fine (black) grain stripes from a high resolution (0.25 mm/pixel) SWIR image of core C (not shown). Each spectrum is the mean of ~10,500 pixels. Fine-grained stripes have much lower spectral contrast than coarse-grained stripes, which may explain why they are not matched to the oil sand end-member by the SAM tool.97

Figure 5.9 Core A mapped in the SWIR using a spectral subset of 2.099 μm to 2.286 μm . The original SWIR map, where the entire spectral range of 1.0-2.5 μm was used, is shown for comparison. Breccia clasts, mapped incorrectly as barren sand when using the whole spectral range, are correctly classified as siltstone using the spectral subset.101

Figure 5.10 Core A as mapped in the SWIR, LWIR and using both datasets together. A spectral model for total bitumen content (TBC) was applied to the SWIR imagery to map oil sand with threshold values of 3 wt %, 6 wt % and 10 wt % TBC. Pixels mapped as oil sands were transferred to LWIR imagery and SAM was used to map the remaining rock types.101

List of Abbreviations

CSS	<i>Cyclic steam stimulation</i>
Fm.	<i>Formation</i>
FTIR	<i>Fourier Transform infrared</i>
IHS	<i>Inclined heterolithic stratification</i>
LWIR	<i>Longwave infrared</i>
MBI	<i>Methylene blue index</i>
Mbr.	<i>Member</i>
µm	<i>micrometer</i>
nm	<i>nanometer</i>
RGB	<i>Red, green, blue</i>
RMS	<i>Root mean square</i>
ROI	<i>Region of interest</i>
SAGD	<i>Steam assisted gravity drainage</i>
SAGP	<i>Steam and gas push</i>
SAM	<i>Spectral angle mapper</i>
SWIR	<i>Shortwave infrared</i>
TBC	<i>Total bitumen content</i>
VIS	<i>Visible</i>
VNIR	<i>Visible to near infrared</i>
wt %	<i>Weight percent</i>
XRD	<i>X-ray diffraction</i>

Chapter 1

Introduction

1.1 Background & Research Objectives

The Athabasca oil sands deposit in northeastern Alberta, Canada, is host to one of the world's largest petroleum reservoirs. Oil sands are a naturally occurring mixture of uncemented quartz sand, clay minerals, water, and an extra-heavy oil known as bitumen. Drill core sampling is the principal method for investigating the subsurface in oil sands industry operations. Cores are logged to collect sedimentological data, and to calibrate petrophysical well log data, and they are sub-sampled for the determination of key reservoir properties (e.g. porosity, permeability). Drill core sampling is especially crucial in deposits like the Athabasca, which is highly heterogeneous, geologically complex and characterized by a lack of vertical and lateral continuity. In the oil sands, whole cores are split longitudinally: one half (also known as the A-half or "2/3 core") is stored in a freezer for laboratory analyses and the other half (the B-half or "1/3 core") is stored at room temperature for viewing. A-half cores must be frozen to prevent the loss of volatiles, which is critical for accurate ore grade determination. Ore grade, or total bitumen content (TBC), is one of the primary variables controlling the economic recovery of bitumen from oil sands. The industry standard method for TBC determination is a process known as Dean-Stark analysis (Bulmer and Starr, 1979). Dean-Stark analysis involves using a Soxhlet extraction apparatus to distill water and bitumen from crushed ore that has been sub-sampled from the core. The bitumen content is determined either by weight difference or direct measurement of the extracted oil.

Viewing half (B-side) cores are logged manually by trained geologists. The objective of core logging is to record the sedimentological characteristics of the rock as a function of depth for the purposes of facies analysis and, ultimately, geological modeling. Geologists' observations are recorded as a strip log with colour-coded lithological units shown as a vertical grain-size profile. Symbols are used to denote sedimentary structures, trace fossils, and accessory phases. Logging

oil sands core is a time- and labour-intensive task. Oil-saturated sections are in particular challenging to log because sedimentary and biogenic structures are difficult to see in oil-saturated strata. Traditionally done by paper and pencil, core logging in the oil sands industry today is done digitally. High-resolution photographs of core are used along with borehole imagery and petrophysical data to create digital core logs. However, even when done digitally, core logging is still time-consuming and a considerable amount of expert knowledge is required. The accuracy of the results inevitably depends on the experience and skill of the logger.

The purpose of this research is to investigate the application of hyperspectral imaging for the characterization of Athabasca oil sands drill core samples. Hyperspectral imaging, also known as imaging spectroscopy, can be defined as the combination of reflectance spectroscopy and digital imaging. Reflectance spectroscopy is the measurement of the reflectance of light from a target material as a function of wavelength (Clark, 1999). The nature of the target material, such a rock or mineral, can be determined based on its reflectance spectrum because the absorption of light is controlled primarily by chemical composition. A digital image is a two-dimensional array of picture elements, or pixels, that are arranged in rows and columns. In hyperspectral imaging, a high resolution digital image of a target is produced and a reflectance measurement, or spectrum, is collected in every pixel of the digital image. In the context of drill core imaging, pixels are sub-millimeter in scale. The term “hyperspectral” refers to the fact that reflectance is measured in hundreds of narrow, contiguous intervals, known as bands, resulting in a highly detailed and smooth reflectance spectrum. During the course of this study, three specific research objectives were explored:

1. Bitumen content determination

Shaw and Kratochvil (1990) and Donkor et al. (1995) first demonstrated that reflectance spectroscopy can be used for bitumen content estimation in oil sands. These early studies were done using relatively low spectral resolution spectrometers. More recently, Lyder et al. (2010)

investigated hyperspectral data, using wavelet analysis to identify the absorption features that are most strongly correlated to bitumen abundance. Based on their results, Rivard et al. (2010) developed a number of spectral models for the estimation of bitumen content from point measurements of crushed ore. This research resulted in improvements in the accuracy of bitumen content estimates and allowed for the transition from point spectroscopy to imaging spectroscopy, which is tested in this study. The first research objective of this thesis is to investigate whether these existing spectral models can be applied for the determination of bitumen content from hyperspectral imagery of oil sands drill core samples in various states of preservation (i.e. fresh vs. dry) and from different locations and depths in the Athabasca deposit.

2. Visual enhancement of sedimentological features

Logging oil sands core can be challenging because sedimentary structures and trace fossils are difficult to see in fine-grained, well-sorted, oil-saturated sediments. A wide variety of methods for facilitating the qualitative analysis of sedimentary drill cores are becoming increasingly popular, such as x-ray radiography, x-ray computed tomography (CT scanning), magnetic resonance imaging (MRI) and confocal macro/microscopy (Rothwell, 2006). However, the application of these methods has been almost exclusively to deep marine sediments. Published work on imaging of oil sands core is limited to ultraviolet and infrared photography, but these studies have focused on using the imagery for integrating core and well log data (Phillips et al., 1991) or quantifying mud beds (Georgi et al., 1992). The second objective of this study is to investigate shortwave infrared (1.0-2.5 μm) hyperspectral imagery as a means of enhancing the visibility of important sedimentological features in oil-saturated sections of Athabasca deposit core. Hyperspectral imagery can be viewed one wavelength band at a time, or as three-band colour combinations. Knowing the spectral characteristics of oils sands minerals and bitumen, the contrast of the different constituents can be emphasized or suppressed in spectral imagery by viewing different combinations of wavelength bands.

3. Automated lithological mapping

Kruse (1996) first demonstrated that hyperspectral imaging could be used to identify and map the spatial distribution of minerals in split core samples. Since then, hyperspectral imaging has been used for the classification of minerals and rocks in a wide variety of cores, including sulfide-bearing igneous and metamorphic rocks (Feng et al., 2011; Kruse et al., 2012), iron oxide-copper-gold deposits (Huntington et al., 2006; Tappert et al., 2011), rare earth element deposits (Turner et al., 2014), and kimberlites (Tappert et al., 2015). However, all of these studies have focused on igneous and metamorphic rocks and their associated minerals. Published spectral studies of sedimentary drill core samples have been limited to point measurements for the investigation of the reflectance properties of sedimentary rocks and minerals (e.g. Lang et al., 1990). The third research objective of this thesis is to investigate whether the spatial distribution of various sedimentary rock types can be mapped in shortwave (1.0-2.5 μm) and longwave infrared (8-12 μm) hyperspectral imagery of oil sands drill core using an automated classification technique.

1.2 Hyperspectral Imaging

Hyperspectral imaging as an earth observation remote sensing technique has been a rapidly growing field of research since the early 1980s. The geological application of hyperspectral imaging is based on the fact that many minerals can be identified by the wavelengths at which absorption features appear in their reflectance spectra. The high spectral resolution provided by hyperspectral imaging is well suited for geological studies because the absorption features of minerals are typically narrow (on the order of 10s of nm) and can have subtle variations in their shape based on the mineral's chemical composition and crystal structure (Clark et al., 1990; Clark, 1999). Since the pioneering work of G. R. Hunt and J. W. Salisbury in the 1970s, reflectance spectroscopy has become an established technique for the determination of mineralogy and rock type in geological remote sensing investigations. Such studies typically conduct measurements in the ultraviolet through infrared regions of the electromagnetic

spectrum. This study focuses on two parts of the infrared wavelength range: the shortwave infrared (SWIR, 1.0-2.5 μm) and the longwave infrared (LWIR, 8-12 μm). The terminology used to describe the different wavelength regions of the electromagnetic spectrum pertinent to mineral spectroscopy vary between fields of study (e.g. spectroscopy, chemistry, astronomy, remote sensing). The terminology used in this study is defined in Figure 1.1.

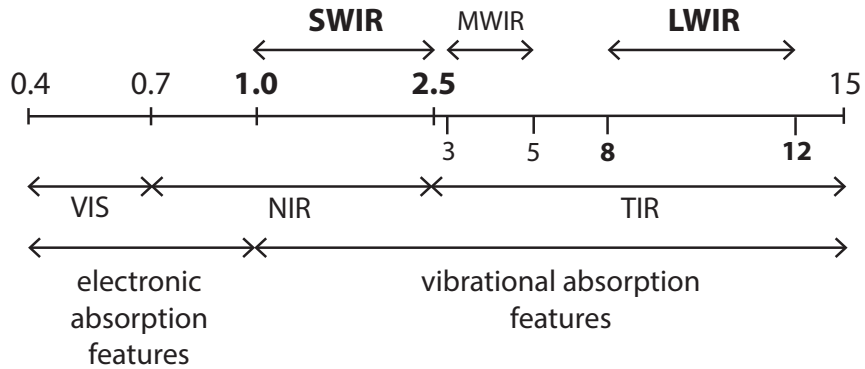


Figure 1.1 Terminology commonly used to describe the different wavelength regions of the electromagnetic spectrum that are pertinent to mineral spectroscopy and remote sensing. All wavelengths are in units of μm . VIS = visible, NIR = near infrared, TIR = thermal infrared, SWIR = shortwave infrared, MWIR = mid-wave infrared, LWIR = longwave infrared. The wavelength regions that are investigated in this study are shown in bold. The causes of absorption features in the different parts of the spectrum are also indicated.

The reflectance spectrum of a rock is the sum of the reflectance spectra of its constituent minerals. The causes of absorptions in mineral spectra can be divided into two categories: electronic and vibrational. Electronic absorption features are caused by the migration of electrons in response to the incident light energy, which occurs in the ultraviolet (UV) to the near infrared (NIR) part of the electromagnetic spectrum (Hunt and Salisbury, 1970; Hunt, 1977). Electronic absorption features are most common in transition metal-bearing minerals. Electrons in atoms are stored in discrete, quantized energy states known as orbitals. Transition metal cations have unfilled outer electron shells (d-orbitals). As a result, the energy level of the d-orbitals is split when the cation becomes part of a coordination complex, or crystal field. At a specific wavelength, the incident energy will match the energy gap between the high and low orbitals, promoting an electron to the higher level orbital and absorbing the light energy.

This phenomenon is known as crystal field splitting and is commonly caused by ferrous iron (Fe^{2+}), ferric iron (Fe^{3+}), nickel (Ni^{2+}), copper (Cu^{2+}), manganese (Mn^{2+}) and chromium (Cr^{3+}) (Hunt, 1977). Electronic absorption features can also be caused by conduction band transitions (where electrons migrate between broad energy bands, rather than discrete energy levels), charge transfers (where electrons migrate directly between neighbouring ions) or colour centers (where defects in crystal lattices create a new discrete energy level). These absorption features typically appear as broad, smooth troughs in reflectance spectra.

Vibrational absorption features are caused by molecular bond vibrations that cause a change in the molecule's dipole moment (Clark, 1999). They tend to be sharp and narrow and appear at longer wavelengths, starting in the SWIR (Hunt and Salisbury, 1970; Hunt, 1977). Vibrational absorption features are typically caused by water, hydroxide, silica and carbonate molecules. A molecule with N number of atoms has $3N-6$ fundamental modes of vibration, each denoted by the Greek letter ν (e.g. ν_1, ν_2). Vibrations that are multiples of fundamentals are known as overtones (e.g. $2\nu_1$) and additive vibrations are known as combinations (e.g. $2\nu_1 + \nu_2$). Overtones and combinations can be observed in the SWIR, while fundamentals begin to appear in the LWIR (Salisbury et al., 1991). At wavelengths shorter than $8 \mu\text{m}$, vibrational absorption features manifest as troughs in reflectance spectra. At wavelengths longer than $8 \mu\text{m}$, vibrational features in minerals primarily appear as peaks in reflectance.

The counterintuitive phenomenon of reflectance peaks as absorption features can be explained by the relationship between three mathematical variables that describe the response of a particulate material to incident radiant energy: the complex index of refraction, the absorption coefficient, and the Fresnel reflection coefficient. The complex index of refraction (n) has a real and an imaginary component. The real part (n_r) describes the velocity of the light with respect to velocity in a vacuum, and the imaginary part (n_i) describes the attenuation of the light by absorption. The absorption coefficient (k_p) is a measure of the absorptivity of a material. It is

directly proportional to the imaginary component of the complex index of refraction, as shown by Equation 1, where λ = wavelength. The Fresnel reflection coefficient (R) is a measure of the reflectivity of a material. It is related to the complex index of refraction as shown by Equation 2.

$$\text{Eq. 1: } k\rho = \frac{4\pi n_i}{\lambda} \qquad \text{Eq. 2: } R = \frac{(n_r - 1)^2 + n_i^2}{(n_r + 1)^2 + n_i^2}$$

In the SWIR, n_i tends to be smaller than n_r and thus increases in the absorption coefficient correspond to decreases in the Fresnel reflection coefficient. SWIR absorption features are thus represented by troughs in reflectance spectra. However, in the LWIR, the magnitude of n_i can become much greater than n_r , in which case high absorption coefficients will correspond to high Fresnel reflection coefficients. Consequently, in the LWIR, strong absorption features correspond to reflectance peaks known as Reststrahlen bands. Weaker absorption features (i.e. lower $k\rho$) correspond to reflectance troughs.

1.3 Thesis Layout

An overview of the geology of the Athabasca oil sands is provided in Chapter 2. The body of this thesis, Chapters 3, 4 and 5, is formed by three stand-alone manuscripts published (or to be published) in peer-reviewed journals. A summary of the contributions of this thesis and a discussion of avenues for future research is provided in Chapter 6.

Chapter 3: This chapter details the first research objective – the estimation of total bitumen content of fresh and dry drill core samples from different locations across the Athabasca deposit. This work was presented at GeoConvention 2014: Focus (May 12-16, 2014) and has been published as:

Speta, M., Rivard, B., Feng, J., Lipsett, M., Gingras, M. 2015. Hyperspectral imaging for the determination of bitumen content in Athabasca oil sands core samples. *AAPG Bulletin*, 99(7), 1245-1259.

Chapter 4: This chapter details the second research objective – enhancing the visibility of sedimentary and biogenic features in oil-saturated sections of Athabasca oil sands core. This work was presented at GeoConvention 2015: Geoscience New Horizons (May 4-8, 2015). This chapter was accepted for publication as a Research Methods paper on Dec. 13, 2015:

Speta, M., Gingras, M., Rivard, B. Shortwave infrared hyperspectral imaging: A novel method for the enhancement of sedimentary and biogenic features in oil-saturated core. *Journal of Sedimentary Research*.

Chapter 5: This chapter details the third research objective – lithological mapping of Athabasca oil sands core using an automated spectral classification technique. This research will be presented at the 2016 AAPG Annual Convention and Exhibition (June 19-22, 2016). A modified version of this chapter will be submitted for publication as:

Speta, M., Rivard, B., Feng, J. Automated mapping of lithological units in McMurray Formation oil sands core with shortwave (1.0-2.5 μm) and longwave infrared (8-12 μm) hyperspectral imaging.

References

- Bulmer, J.T., and Starr, J., 1979, *Syn crude Analytical Methods for Oil Sand and Bitumen Processing*, Alberta Oil Sands Technology and Research Authority (AOSTRA), Edmonton, AB, 173 p.
- Clark, R.N., 1999, Spectroscopy of rocks and minerals, and principles of spectroscopy, in: A.N. Rencz (Ed.), *Remote Sensing for the Earth Sciences: Manual of Remote Sensing*, John Wiley & Sons, Inc., p. 3–58.
- Clark, R.N., King, T.V.V., Klejwa, M., and Swayze, G.A., 1990, High spectral resolution reflectance spectroscopy of minerals, *Journal of Geophysical Research*, v. 95, no. B8, p. 12653–12680.
- Donkor, K.K., Kratochvil, B., and Thompson, G.R., 1995, Analysis of Athabasca oil sand by near-infrared-diffuse reflectance spectroscopy, *Analyst*, v. 120, p. 2713–2717.
- Feng, J., Rivard, B., Gallie, A., and Sanchez-Azofeifa, A., 2011, Rock type classification of drill core using continuous wavelet analysis applied to thermal infrared reflectance spectra, *International Journal of Remote Sensing*, v. 32, no. 16, p. 4489–4510.
- Georgi, D.T., Phillips, C., and Hardman, R., 1992, Applications of digital core image analysis to thin-bed evaluation, SCA Conference Paper #9206, Society of Core Analysts 6th Technical Conference, p. 1–12.
- Hunt, G.R., 1977, Spectral signatures of particulate minerals in the visible and near infrared, *Geophysics*, v. 42, no. 3, p. 501–513.
- Hunt, G.R., and Salisbury, J.W., 1970, Visible and near-infrared spectra of minerals and rocks: I. Silicate Minerals, *Modern Geology*, v. 1, p. 283–300.
- Huntington, J.F., Mauger, A.J., Skirrow, R.G., Bastrakov, E.N., Connor, P., Mason, P., Keeling, J.L., Coward, D.A., Berman, M., Phillips, R., Whitbourn, L.B., and Heithersay, P.S., 2006, Automated mineralogical core logging at the Emmie Bluff iron oxide-copper-gold prospect, *MESA Journal*, v. 41, p. 38–44.
- Kruse, F.A., 1996, Identification and mapping of minerals in drill core using hyperspectral image analysis of infrared reflectance spectra, *International Journal of Remote Sensing*, v. 17, no. 9, p. 1623–1632.
- Kruse, F.A., Bedell, R.L., Taranik, J.V., Peppin, W.A., Weatherbee, O., and Calvin, W.M., 2012, Mapping alteration minerals at prospect, outcrop and drill core scales using imaging spectroscopy, *International Journal of Remote Sensing*, v. 33, no. 6, p. 1780–1798.
- Lang, H.R., Bartholomew, M.J., Grove, C.I., and Paylor, E.D., 1990, Spectral reflectance characterization (0.4 to 2.5 and 8.0 to 12.0 μm) of Phanerozoic strata, Wind River Basin and Southern Bighorn Basin Areas, Wyoming, *Journal of Sedimentary Petrology*, v. 60, no. 4, p. 504–524.
- Lyder, D., Feng, J., Rivard, B., Gallie, A., and Cloutis, E., 2010, Remote bitumen content estimation of Athabasca oil sand from hyperspectral infrared reflectance spectra using Gaussian singlets and derivative of Gaussian wavelets, *Fuel*, v. 89, no. 3, p. 760–767.

- Phillips, C., DiFoggio, R., and Burleigh, K., 1991, Extracting information from digital images of core, SCA Conference Paper #9125, Society of Core Analysts 5th Technical Conference, p. 1–20.
- Rivard, B., Lyder, D., Feng, J., Gallie, A., Cloutis, E., Dougan, P., Gonzalez, S., Cox, D., and Lipsett, M.G., 2010, Bitumen content estimation of Athabasca oil sand from broad band infrared reflectance spectra, *The Canadian Journal of Chemical Engineering*, v. 88, p. 830–838.
- Rothwell, R.G., 2006, *New Techniques in Sediment Core Analysis*, Geological Society Special Publication No. 267, London, 266 p.
- Salisbury, J.W., Walter, L.S., Vergo, N., and D’Aria, D.M., 1991, *Infrared (2.1-25 μm) Spectra of Minerals*, The Johns Hopkins University Press, Baltimore, MD, 267 p.
- Shaw, R.C., and Kratochvil, B., 1990, Near-infrared diffuse reflectance analysis of Athabasca oil sand, *Analytical Chemistry*, v. 62, no. 2, p. 167–174.
- Tappert, M., Rivard, B., Giles, D., Tappert, R., and Mauger, A., 2011, Automated drill core logging using visible and near-infrared reflectance spectroscopy: A case study from the Olympic Dam IOCG deposit, South Australia, *Economic Geology*, v. 106, p. 289–296.
- Tappert, M.C., Rivard, B., Fulop, A., Rogge, D., Feng, J., Tappert, R., and Stalder, R., 2015, Characterizing kimberlite dilution by crustal rocks at the Snap Lake diamond mine using SWIR (1.90-2.36 μm) and LWIR (8.1-11.1 μm) hyperspectral imagery collected from drill core, *Economic Geology*, v. 110, no. 6, p. 1375–1387.
- Turner, D.J., Rivard, B., and Groat, L.A., 2014, Visible and short-wave infrared reflectance spectroscopy of REE fluorocarbonates, *American Mineralogist*, v. 99, no. 7, p. 1335–1346.

Chapter 2

The Athabasca Oil Sands

2.1 The McMurray Formation

Oil sands are found in three different deposits in northeastern Alberta, Canada: Athabasca, Cold Lake and Peace River (Figure 2.1). The Athabasca is by far the largest of the three and the most intensely studied. The main reservoir unit in the Athabasca deposit is the Lower Cretaceous McMurray Formation. The McMurray Formation makes up the lower subdivision of the Mannville Group (Figure 2.2). It unconformably overlies Devonian carbonates and is conformably overlain by marine shales of the Clearwater Formation. The upper boundary of the McMurray Formation is defined by the appearance of glauconite in the Wabiskaw Member, which is the sandy basal unit of the Clearwater Formation (Carrigy, 1959; Carrigy, 1963). The thickness of the McMurray Formation ranges from <10 m to >100 m (Hein et al., 2000), with an average of 40-60 m (Ranger, 1994). In the southern and western end of the Athabasca deposit, bitumen saturation extends into the Wabiskaw Member. In some studies, the western end of the Athabasca is treated as a separate deposit known as the Wabasca, or the Athabasca West (e.g. Hein et al., 2000). In this area, the Grand Rapids Formation, which overlies the Clearwater Formation, is also oil-saturated. The Grand Rapids Formation is the uppermost formation of the Mannville Group.

This study focuses on the McMurray Formation, which is predominantly sandstone with lesser siltstone and shale (Carrigy, 1963). The sands are mineralogically mature, predominantly composed of quartz sand (>80%) with minor amounts of clay minerals (<10%) and trace amounts of feldspars and carbonates (Bayliss and Levinson, 1976). Pyrite and siderite are the most common accessory phases, and coal seams and paleosol horizons can be observed throughout the formation. The quartz sands are very fine to fine sand sized (62.5-250 μm) and moderately well to well sorted (Mossop, 1980). The McMurray underwent very little post-

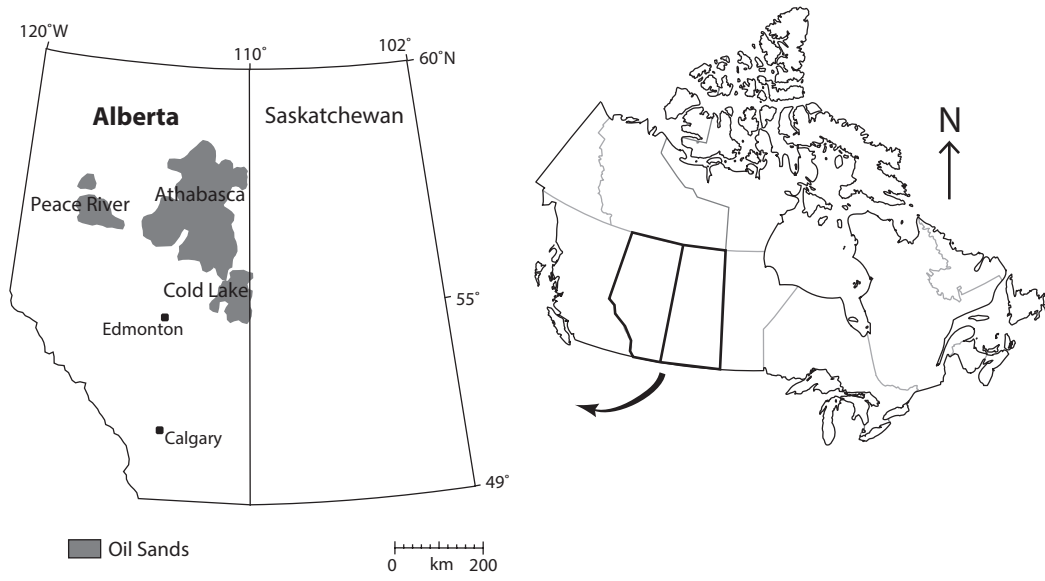


Figure 2.1 The oil sands of northeastern Alberta, Canada. All samples used in this study are from the Athabasca deposit. Modified from Ranger and Gingras (2003).

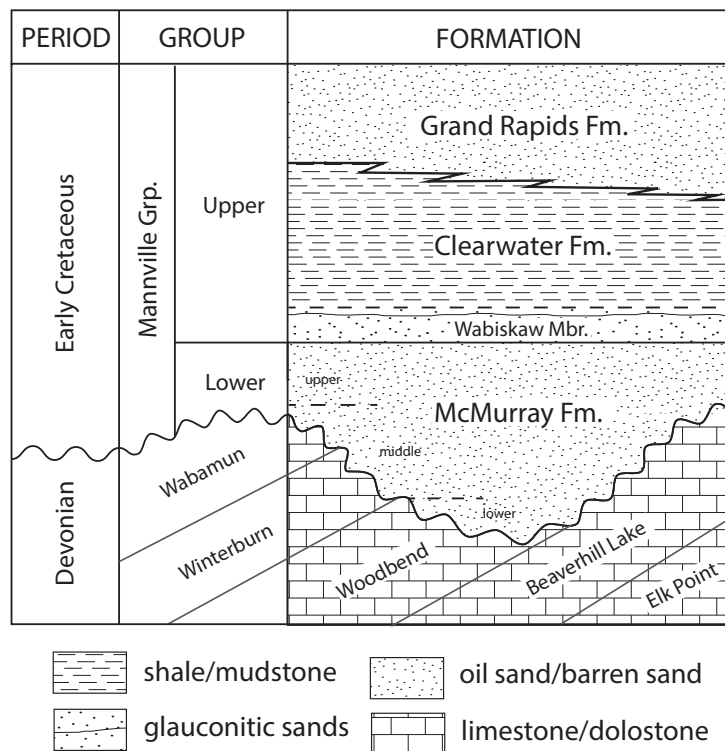


Figure 2.2 Basic stratigraphy of the Athabasca oil sands deposit. The McMurray Formation is primary reservoir unit and the focus of this study. Oil saturation extends into the Wabiskaw Member and the Grand Rapids Formation in the south and west ends of the deposit. Modified from Moss and Flach (1983).

depositional diagenesis, resulting in a lack of mineral cement (hence the use of the term “sands” rather than “sandstones”). Accordingly, the formation has very high porosity (25-35%) and all permeable zones are either oil or water saturated. Bitumen saturation can be as high as 18% by weight (wt %) (Mossop, 1980).

2.2 Origin of the Resource

The McMurray sands were deposited in Early Cretaceous time, when present-day northeastern Alberta was a broad, north-trending basin with three major river valley systems that drained into the Boreal Sea (Mossop, 1980). Little was known about the source of the sediment until a recent U-Pb detrital zircon provenance study by Benyon et al. (2014). Their findings revealed that the McMurray sediments were primarily derived from the Appalachians of eastern North America. Input from the Cordilleran region of western North America and the Canadian Shield was also identified in the upper and lower members, respectively.

The origin of the oil is an ongoing area of study. Despite decades of intensive research, both the source beds and the timing of the oil emplacement continue to be points of debate in the literature. Bitumen is an extra-heavy oil (8-10° API) that does not flow freely due to its high density and viscosity. In the early 1990s, researchers came to the consensus that the Athabasca bitumen did not form in place. The idea of long-distance migration of a precursor light oil came to be accepted through several lines of evidence, including: 1) the pervasive distribution of the oil throughout the permeable zones of the McMurray Formation, 2) the fact that host and surrounding rocks in the Athabasca have not been subjected to high enough pressure and temperatures for oil to form, and 3) the presence of a mappable, discrete bitumen-water contact where the conventional density relationship of oil overlying water is observed, despite the fact that the present day bitumen is denser than water (Mossop, 1980; Ranger, 1994).

It is widely agreed that the source beds for the Athabasca bitumen are in the foreland basin

of the Canadian Rocky Mountains, where the required pressure-temperature conditions for oil generation were met during Cordilleran mountain building. Early work by Creaney and Allan (1990) established that the Athabasca bitumen came from a combination of four source beds: Lower Jurassic Fernie Formation (Gordondale Member), Lower Mississippian Exshaw Formation, Triassic Doig Formation (Phosphate Zone) and Upper Devonian Duvernay Formation. Since then, the degree of input from the different units has been intensely debated. Riediger (1994) and Riediger et al. (2000) have argued that the Exshaw Formation is the main source bed based on biomarker and basin modelling studies, while other geochemical investigations and basin models have found that the Gordondale Member is the primary source bed (Higley et al., 2009; Berbesi et al., 2012; Finlay et al., 2012). The most recent results from a geochemical study of biodegradation-resistant biomarkers suggest that the Gordondale Member is the main source bed for the Peace River oil sands, while the Exshaw Formation is the main source for the Athabasca deposit (Adams et al., 2013). Regardless of the exact source, the precursor light oil migrated northeast several hundreds of kilometers up-dip to its present day location, where it was broken down to heavy oil by biodegradation (Head et al., 2003; Larter et al., 2006; Zhou et al., 2008).

The mechanism behind the up-dip migration of the oil is thought to be driven by the Laramide Orogeny (80-55 Ma). The two theories are: 1) topographically-driven hydrodynamic flow; uplift during the Laramide would have caused a hydraulic gradient from high head in the southwest to low head in the northeast (Garven, 1989), and 2) compaction and buoyancy flow; also known as “the squeegee model”, compaction from the Laramide Orogeny would have pushed both oil and water northeast, with the up-dip movement being facilitated by the oil’s buoyancy (Ranger, 1994). The latter theory is supported by field observations of the southwest-dipping bitumen-water contact (Ranger, 1994), and by the results of a basin modeling study by Adams et al. (2004).

Trapping of the light oil in its present-day location was both stratigraphic and structural. Ranger (1994) first demonstrated evidence for a partial anticline trap by restoring the bitumen-water contact horizon to horizontal. This work was recently expanded by Tozer et al. (2014), who conducted a basin-scale structural reconstruction of the Athabasca deposit. Based on their results, the Athabasca can be divided into six trap domains: a giant four-way anticlinal trap in the central part of the deposit, a stratigraphic trap formed by the on-lapping of Clearwater Formation shales onto Precambrian basement rocks in the northeast, and bitumen traps in the north, south, southwest and western ends of the Athabasca deposit. Bitumen traps refer to the self-sealing of the light precursor oil by oil that has already been biodegraded and thus immobilized.

Timing of oil emplacement is also controversial. Ranger's (1994) reconstruction of the bitumen-water contact indicated that oil must have been emplaced and biodegraded by 75-65 Ma. Tozer et al. (2014) found that the majority of oil charge occurred 84-78 Ma. Meanwhile, direct Re-Os dating of the Athabasca bitumen by Selby and Creaser (2005) revealed a much earlier age of emplacement – 112 Ma. However, the reliability of Re-Os dating of petroleum has recently been brought to question as it has been experimentally demonstrated that the isotopic geochronometer may be reset if oil comes in contact with formation water during migration (Mahdaoui et al., 2015). Most studies agree that the peak oil generation occurred in the Late Cretaceous (<100 Ma). The process of biodegradation is believed to have lasted 20-35 million years, and charge and biodegradation are believed to have been coeval (Adams et al., 2013).

2.3 Depositional History & Facies Classification

There is also a considerable amount of debate in the literature about the depositional history of the McMurray Formation. The McMurray Formation is commonly divided into three informal stratigraphic members - lower, middle and upper (Figure 2.2). This three-fold stratigraphic division is commonly correlated with a three-fold facies model of a lower fluvial member, middle estuarine member and an upper marine member (Stewart and MacCallum, 1978; Flach and

Mossop, 1985). Despite evidence that fully marine conditions were never reached in McMurray time (e.g. Ranger and Pemberton, 1997), this model remains in widespread use, especially in the industry. Known as the incised-valley fill model, it interprets the McMurray Formation as the amalgamation of incised valley fill complexes. The vertical stacking of narrow estuarine channel sands segregated by impermeable shales results in the observed lack of lateral continuity. This model is largely based on small-scale studies and drill core samples. More recently, in-depth regional scale studies have resulted in the development of two alternative models. While the incised-valley fill model suggests that the McMurray was deposited during fluctuating periods of maximal regression (to incise the valleys) and maximal transgression (to fill the valleys), Ranger and Gingras (2003; 2008a; 2008b) propose that the McMurray was deposited in a series of progradational (regressive) pulses during a period of overall transgression. They also use a three-fold stratigraphic sub-division for the formation, but their model proposes an overall tide-dominated estuarine sequence with greater fluvial influence at the bottom and greater marine influence at the top. Around the same time, Flach and Hein (2001) and Hein and Cotterill (2006) proposed a sequence stratigraphic model where the McMurray sediments represent a continuous transgressive sequence. They argue for a two-fold stratigraphic sub-division of the formation; a fluvial lower member that represents deposition during the initial lowstands systems tract, and an estuarine-marine upper member that represents the transgressive and highstands systems tracts. The estuarine and marine portions are grouped because they are interpreted as being in gradational contact, while Ranger and Gingras (2003; 2008a; 2008b) interpret this contact as erosional. Coarsening-upward units in the upper member, interpreted as progradational in Ranger and Gingras' work, are interpreted as aggradational by Flach and Hein (2001) and Hein and Cotterill (2006).

The debate on the depositional history of the McMurray Formation has resulted in a multitude of facies classification schemes for the Athabasca deposit. A facies is a body of rock characterized by a particular combination of lithological, sedimentological and biological features that

distinguish it from the bodies of rock surrounding it (Dalrymple, 2010). Facies analysis is the interpretation of facies in the context of the depositional processes that formed them. Facies analysis in the McMurray Formation is challenging because of its geological complexity; facies are laterally discontinuous and have a high degree of internal heterogeneity in terms of sedimentary structures, degree of bioturbation and trace fossil assemblages. Five facies that appear in most McMurray Formation facies schemes are clean sands, inclined heterolithic stratification (IHS), interbedded sandstones and mudstones, intraclast breccia and unbioturbated mudstone/shale. The clean sands represent the main reservoir units of the McMurray Formation and occur throughout the whole formation. These sands can be planar or cross-bedded, and sedimentary structures that are indicative of both fluvial influence (e.g. current ripple cross-bedding) and a tidal influence (e.g. herringbone cross-stratification, rhythmic bedding) can be observed (Harris, 2003; Ranger and Gingras, 2003; Hein and Cotterill, 2006; Crerar and Arnott, 2007). However, the clean sands often appear structureless because sedimentary structures can be difficult to see due to oil saturation.

Inclined heterolithic stratification (IHS) refers to interbedded sands and muds that are originally deposited at an angle, typically by the lateral accretion of point bars in a channelized environment (Thomas et al., 1987). IHS is the most common facies in the McMurray and makes up the bulk of the middle part of the formation. Like the clean sand facies, sand-dominated IHS (<10% mud) is an economic target. McMurray IHS is typically interpreted as having been deposited in tide-dominated estuarine distributary channels, with sand-dominated successions being from either the head or mouth of the estuary and mud-dominated successions from the central zone (Lettley et al., 2007). Ichnological evidence for the estuarine nature of the McMurray IHS was first presented in 1982 by Pemberton et al., who documented brackish trace fossil assemblages in IHS outcrops. Trace fossils that are commonly found in the upper and middle McMurray Formation include *Planolites*, *Teichichinus*, *Cylindrinchnus*, *Skolithos*, *Palaeophycus*, *Astersoma*, *Chondrites*, *Bergaueria*, *Thalassinoides*, and *Gyrolithes* (Pemberton

et al., 1982; Ranger and Pemberton, 1992; Bechtel et al., 1994; Hein et al., 2000; Lettley et al., 2007). Terrestrial trace fossils have been documented in the lower McMurray (Ranger and Gingras, 2003) and rooted horizons appear throughout the formation (Hein and Cotterill, 2006).

The interbedded sandstone and mudstone facies consists of planar to gently dipping interbedded very fine to fine sands and muds. This facies occurs throughout the whole formation, but is predominantly found in the upper McMurray, which is characterized by horizontal strata. Tidal and wave sedimentary structures (e.g. oscillation ripples, synaeresis cracks) are associated with this facies (Ranger and Gingras, 2003), which has been interpreted as being deposited in a tidal flat environment (Harris, 2003; Crerar and Arnott, 2007).

Intraclast breccia consists of mudstone or siltstone clasts (ranging from 0.5 mm to 1 m in size) in a matrix of massive or cross-stratified sand. This facies appears throughout the McMurray Formation. Brackish trace fossils have been identified in the mudstone clasts leading to the interpretation of the breccia forming either as a result of overbank collapse in the estuarine channel (Ranger and Gingras, 2003; Crerar and Arnott, 2007), or as channel margin rip-up clasts (Harris, 2003). Intraclast breccia units are thin in terms of their vertical extent (<1 m) and are typically found in close association with clean sand or IHS reservoir units.

Finally, thick intervals (2-30 m) of unbioturbated mudstone/shale have been documented throughout the middle McMurray. Despite their immense thickness, these facies units have little lateral extent, which distinguishes these mudstones/shales as a unique facies. Sometimes referred to as “mud plugs”, the unbioturbated muds are interpreted as abandoned channel fills caused by overbank flooding (Ranger and Gingras, 2003; Hein and Cotterill, 2006).

2.4 Extraction of the Resource

Because of its high density and viscosity, bitumen cannot be extracted by conventional means.

The oil is recovered either by open-pit mining or by in-situ recovery. Open-pit mining is economically viable in reservoirs that have less than 75 m of overburden (Masliyah et al., 2011). The Athabasca is the only deposit with surface-mineable ore and commercial mining operations have been running in the area since 1967. Oil sand is mined using trucks and shovels. The mined ore is processed by hot water extraction, a method for separating bitumen from sand that was first developed by Dr. Karl Clark in the 1920s. Hot water extraction involves aerating a slurry of crushed oil sand and caustic solvents to create a bitumen froth that is skimmed away in gravity separation vessels (Masliyah et al., 2004). The residual solids are then pumped into tailings ponds for settling and drying. Bitumen recovery in mining operations is typically 88-95% (Masliyah et al., 2004).

More than 95% of Alberta's bitumen is too deep to be extracted by open-pit mining (Alberta Energy Regulator, 2015). In-situ recovery refers to a variety of sub-surface methods that extract bitumen by decreasing its viscosity such that it can flow and be pumped to the surface. In-situ recovery is safe and economically viable in reservoirs that are 200-1000 m deep (Butler, 1997). Steam assisted gravity drainage (SAGD), first developed by Dr. Roger Butler in the late 1970s, is the most common in-situ extraction method in the Alberta oil sands. It involves drilling a pair of horizontal wells where the top well is used to inject steam into the formation, and the bottom well pumps the heated oil to the surface. Bitumen recovery is typically up to 55% (Butler, 1998). Another in-situ method used in the industry is cyclic steam stimulation (CSS), where a single well is used for repeated cycles of steam injection and pumping oil (Butler, 1994). Methods that are under development include Vapex, where a mixture of non-condensable gas and a volatile liquid solvent are injected into the formation to reduce the viscosity of the oil, and SAGP, or steam and gas push, where non-condensable gas is added to the injected steam (Butler, 1998).

References

- Adams, J., Larter, S., Bennett, B., Huang, H., Westrich, J., Larter, S., Bennett, B., Huang, H., Westrich, J., and van Kruisdijk, C., 2013, The dynamic interplay of oil mixing, charge timing, and biodegradation in forming the Alberta oil sands: Insights from geologic modeling and biogeochemistry, in: Hein, F.J., Leckie, D., Larter, S., and Suter, J.R. (Eds.), *Heavy-oil and Oil-sand Petroleum Systems in Alberta and Beyond*, AAPG Studies in Geology 64, American Association of Petroleum Geologists, p. 23–102.
- Adams, J.J., Rostron, B.J., and Mendoza, C.A., 2004, Coupled fluid flow, heat and mass transport, and erosion in the Alberta basin: Implications for the origin of the Athabasca oil sands, *Canadian Journal of Earth Sciences*, v. 41, no. 9, p. 1077–1095.
- Alberta Energy Regulator, 2015, Alberta's Energy Reserves 2014 and Supply/Demand Outlook 2015-2024, Report #ST98-2015, Calgary, AB, 299 p.
- Bayliss, P., and Levinson, A.A., 1976, Mineralogical review of the Alberta oil sand deposits (Lower Cretaceous, Mannville Group), *Bulletin of Canadian Petroleum Geology*, v. 24, no. 2, p. 211–224.
- Bechtel, D.J., Yuill, C.N., Ranger, M.J., and Pemberton, S.G., 1994, Ichnology of inclined heterolithic stratification in the McMurray Formation, northeastern Alberta (abs.), Exploration Update '94 - Western Canadian and International Expertise Program Book, Canadian Society of Petroleum Geologists, Calgary, AB, p. 362.
- Benyon, C., Leier, A., Leckie, D.A., Webb, A., Hubbard, S.M., and Gehrels, G., 2014, Provenance of the Cretaceous Athabasca oil sands, Canada: Implications for continental-scale sediment transport, *Journal of Sedimentary Research*, v. 84, no. 2, p. 136–143.
- Berbesi, L.A., di Primio, R., Anka, Z., Horsfield, B., and Higley, D.K., 2012, Source rock contributions to the Lower Cretaceous heavy oil accumulations in Alberta: A basin modeling study, *AAPG Bulletin*, v. 96, no. 7, p. 1211–1234.
- Butler, R., 1994, Steam-assisted gravity drainage: Concept, development, performance and future, *Journal of Canadian Petroleum Technology*, v. 33, no. 2, p. 44–50.
- Butler, R.M., 1997, *Thermal Recovery of Oil and Bitumen*, 3rd Edition, GravDrain Inc., Calgary, AB, 528 p.
- Butler, R., 1998, SAGD comes of age!, *Journal of Canadian Petroleum Technology*, v. 37, no. 7, p. 9–12.
- Carrigy, M.A., 1959, Geology of the McMurray Formation, Pt. III: General geology of the McMurray area, Research Council of Alberta, Geological Division – Memoir 1, 130 p.
- Carrigy, M.A., 1963, Criteria for differentiating the McMurray and Clearwater Formations in the Athabasca oil sands, Research Council of Alberta, Geological Division - Bulletin 14, 32 p.
- Creaney, S., and Allan, J., 1990, Hydrocarbon generation and migration in the Western Canada Sedimentary Basin, in: Brooks, J. (Ed.), *Classic Petroleum Provinces*, Geological Society Special Publication No. 50, London, p. 189–203.
- Crerar, E., and Arnott, R., 2007, Facies distribution and stratigraphic architecture of the Lower

- Cretaceous McMurray Formation, Lewis Property, northeastern Alberta, *Bulletin of Canadian Petroleum Geology*, v. 55, no. 2, p. 99–124.
- Dalrymple, R.W., 2010, Interpreting sedimentary successions: Facies, facies analysis and facies models, in: James, N.P. and Dalrymple, R.W. (Eds.), *Facies Models 4*, Geological Association of Canada, St. John's, NL, p. 3–18.
- Finlay, A.J., Selby, D., and Osborne, M.J., 2012, Petroleum source rock identification of United Kingdom Atlantic Margin oil fields and the western Canadian oil sands using platinum, palladium, osmium and rhenium: Implications for global petroleum systems, *Earth and Planetary Science Letters*, v. 313-314, p. 95–104.
- Flach, P.D., and Hein, F.J., 2001, Outcrop-core correlation of channel and non-channel facies, McMurray Formation, Fort MacKay area, NE Alberta (abs.), CSPG Rock the Foundation Convention Extended Abstracts, June 18-22, 2001, Calgary, AB, p. 132–133.
- Flach, P.D., and Mossop, G.D. 1985, Depositional environment of Lower Cretaceous McMurray Formation, Athabasca oil sands, Alberta, *AAPG Bulletin*, v. 69, no. 8, p. 1195–1207.
- Garven, G., 1989, A hydrogeologic model for the formation of the giant oil sands deposits of the Western Canada sedimentary basin, *American Journal of Science*, v. 289, no. 2, p. 105–166.
- Harris, C., 2003, Aspects of the sedimentology, ichnology, stratigraphy, and reservoir character of the McMurray Formation, northeast Alberta, MSc thesis, University of Alberta, Edmonton, AB, 209 p.
- Head, I.M., Jones, D.M., and Larter, S.R., 2003, Biological activity in the deep subsurface and the origin of heavy oil, *Nature*, v. 426, no. 6964, p. 344–352.
- Hein, F.J., and Cotterill, D.K., 2006, The Athabasca oil sands — A regional geological perspective, Fort McMurray area, Alberta, Canada, *Natural Resources Research*, v. 15, no. 2, p. 85–102.
- Hein, F.J., Cotterill, D.K., and Berhane, H., 2000, An atlas of lithofacies of the McMurray Formation Athabasca oil sands deposit, northeastern Alberta: Surface and subsurface, Earth Sciences Report 2000-07, Alberta Geological Survey, Edmonton, AB, 217 p.
- Higley, D.K., Lewan, M.D., Roberts, L.N.R., and Henry, M., 2009, Timing and petroleum sources for the Lower Cretaceous Mannville Group oil sands of northern Alberta based on 4-D modeling, *AAPG Bulletin*, v. 93, no. 2, p. 203–230.
- Larter, S., Huang, H., Adams, J., Bennett, B., Jokanola, O., Oldenburg, T., Jones, M., Head, I., Riediger, C., and Fowler, M., 2006, The controls on the composition of biodegraded oils in the deep subsurface - Part II: Geological controls on subsurface biodegradation fluxes and constraints on reservoir-fluid property prediction, *AAPG Bulletin*, v. 90, no. 6, p. 921–938.
- Lettley, C.D., Pemberton, S.G., Gingras, M.K., Ranger, M., and Blakney, B.J., 2007, Integrating sedimentology and ichnology to shed light on the system dynamics and paleogeography of an ancient riverine estuary, in: MacEachern, J.A., Bann, K.L., Gingras, M.K., and Pemberton, S.G. (Eds.), *Applied Ichnology*, SEPM (Society for Sedimentary Geology) Short Course Notes Vol. 52, p. 147–165.
- Mahdaoui, F., Michels, R., Reisberg, L., Pujol, M., and Poirier, Y., 2015, Behavior of Re and Os during contact between an aqueous solution and oil: Consequences for the application of the

- Re–Os geochronometer to petroleum, *Geochimica et Cosmochimica Acta*, v. 158, p. 1–21.
- Masliyah, J., Czarnecki, J., and Xu, Z., 2011, *Handbook on Theory and Practice of Bitumen Recovery from Athabasca Oil Sands*, Kingsley Knowledge Publishing, 468 p.
- Masliyah, J., Zhou, Z.J., Xu, Z., Czarnecki, J., and Hamza, H., 2004, Understanding water-based bitumen extraction from Athabasca oil sands, *The Canadian Journal of Chemical Engineering*, v. 82, p. 628–654.
- Mossop, G., 1980, Geology of the Athabasca Oil Sands, *Science*, v. 207, no. 4427, p. 145–152.
- Mossop, G.D., and Flach, P.D., 1983, Deep channel sedimentation in the Lower Cretaceous McMurray Formation, Athabasca Oil Sands, Alberta, *Sedimentology*, v. 30, p. 493–509.
- Pemberton, S.G., Flach, P.D., and Mossop, G.D., 1982, Trace fossils from the Athabasca oil sands, Alberta, Canada, *Science*, v. 217, no. 4562, p. 825–827.
- Ranger, M., 1994, A basin study of the southern Athabasca oil sands deposit, PhD thesis, University of Alberta, Edmonton, AB, 289 p.
- Ranger, M.J., and Gingras, M.K., 2003, *Geology of the Athabasca Oil Sands: Field Guide & Overview*, I.C.E. 2004: CSPG CHOA CWLS Joint Conference Field Trips & Short Courses, Calgary, AB, Canadian Society of Petroleum Geologists, 123 p.
- Ranger, M., and Gingras, M., 2008a, Depositional history of the McMurray Formation: A model driven by outcrop observation, *Reservoir*, v. 35, no. 3, p. 17–18.
- Ranger, M.J., and Gingras, M.K., 2008b, Stratigraphy and sequence stratigraphic surfaces of the McMurray Formation (abs.), AAPG Hedberg Research Conference - Heavy Oil and Bitumen in Foreland Basins: From Processes to Products, Banff, AB, AAPG Search and Discovery Article #90075, 6 p.
- Ranger, M.J., and Pemberton, S.G., 1997, Elements of a stratigraphic framework for the McMurray Formation in south Athabasca area, Alberta, in: Pemberton, S.G. and James, D.P. (Eds.), *Petroleum Geology of the Cretaceous Mannville Group, Western Canada*, CSPG Memoir 18, Canadian Society of Petroleum Geologists, p. 263–291.
- Ranger, M.J., and Pemberton, S.G., 1992, The sedimentology and ichnology of estuarine point bars in the McMurray Formation of the Athabasca oil sands deposit, northeastern Alberta, Canada, in: Pemberton, S.G. (Ed.), *Applications of Ichnology to Petroleum Exploration: A Core Workshop*, SEPM (Society for Sedimentary Geology), p. 401–421.
- Riediger, C.L., 1994, Migration of “Nordegg” oil in the Western Canada Basin. How much and how far?, *Bulletin of Canadian Petroleum Geology*, v. 42, no. 1, p. 63–73.
- Riediger, C., Ness, S., Fowler, M., and Akpulat, T., 2000, Timing of oil migration, Paleozoic and Cretaceous bitumen and heavy oil deposits, eastern Alberta (abs.), GeoCanada 2000 - The Millenium Geoscience Summit, Calgary, AB, p. 4.
- Selby, D., and Creaser, R.A., 2005, Direct radiometric dating of hydrocarbon deposits using rhenium-osmium isotopes, *Science*, v. 308, no. 5726, p. 1293–1295.
- Stewart, G.A., and MacCallum, G.T., 1978, *Athabasca Oil Sands Guidebook*, Canadian Society of Petroleum Geologists, Calgary, AB, 33 p.

Thomas, R.G., Smith, D.G., Wood, J.M., Visser, J., Calverley-Range, E.A., and Koster, E.H., 1987, Inclined heterolithic stratification-terminology, description, interpretation and significance, *Sedimentary Geology*, v. 53, p. 123–179.

Tozer, R.S.J., Choi, A.P., Pietras, J.T., and Tanasichuk, D.J., 2014, Athabasca oil sands: Megatrap restoration and charge timing, *AAPG Bulletin*, v. 98, no. 3, p. 429–447.

Zhou, S., Huang, H., and Liu, Y., 2008, Biodegradation and origin of oil sands in the Western Canada Sedimentary Basin, *Petroleum Science*, v. 5, no. 2, p. 87–94.

Chapter 3

Hyperspectral imaging for the determination of bitumen content in Athabasca oil sands core samples

A version of this chapter has been published as: Speta M., Rivard, B., Feng, J., Lipsett, M., Gingras, M.K., 2015, Hyperspectral imaging for the determination of bitumen content in Athabasca oil sands core samples, *AAPG Bulletin*, v. 99, n. 7, pp. 1245-1259.

3.1 Introduction

The oil sands of northeastern Alberta, Canada, represent some of the world's largest proven unconventional oil reserves. Oil sands are primarily composed of quartz sand, clay, water and bitumen. Bitumen is an extra-heavy oil ($API = 8-10^\circ$) that is essentially solid at standard ambient conditions and thus cannot be extracted by conventional methods. The oil is recovered either by surface mining of shallow reservoirs (<75 m) or through a variety of in-situ methods that heat the solid bitumen or add solvents to facilitate flow through deep reservoirs (>200 m). The bitumen content, or ore grade, of oil sands is often reported by weight. Bitumen saturation in the Athabasca deposit ranges from low grade (<6 wt %), to mid-grade (6-10 wt %), to high grade (>10 wt %), up to 18 weight percent (wt %) (Mossop, 1980). The economical cut-off is typically ~ 7 wt % (Masliyah et al., 2011). Detailed knowledge about the total bitumen content (TBC) of an oil sands reservoir is critical for all stages of industry operations from reserve estimation, production planning, and geological modeling through to efficient processing.

Drill core sampling is the principal method of investigating subsurface geology in oil sands industry operations and data from drill core analyses are often the basis of reservoir models. Experienced geologists visually estimate the ore grade of core samples based on their colour. Sub-samples are then collected from the core and sent to a laboratory for exact oil content determination by a process known as Dean-Stark analysis (Bulmer and Starr, 1979). This procedure utilizes a soxhlet extraction apparatus to distill the water and oil from the solids. TBC

is determined either by weight difference or direct measurement and reported as a bulk mass fraction. Complete evaporation of the solvent used for oil extraction, which is required for the direct measurement method, may take up to several days (Bulmer and Starr, 1979). The more popular weight difference method does not require this final step, making it both less expensive and faster, but it is also considered less accurate. Dean-Stark analysis is only effective for oil sands core that has not undergone any oxidation or volatile loss, and for this purpose core samples are typically kept frozen after drilling. Freezing core is expensive and complicates transport and storage.

Hyperspectral imaging is a remote sensing technique that may provide a means to expedite the estimation of TBC. Also known as imaging spectroscopy, hyperspectral imaging combines reflectance spectroscopy with high resolution digital imaging. A digital image of the target is acquired with ~ 1 mm per pixel detail and a reflectance measurement for a specified wavelength interval is collected in each pixel of the image. Reflectance is measured in hundreds of contiguous intervals, known as bands, providing a smooth, continuous spectrum. Because the absorption of light is controlled by chemical composition, geological materials such as minerals or bitumen can be identified based on the wavelengths at which absorption features appear in reflectance spectra. Quantitative information can be obtained as the intensity of absorption is controlled by the relative abundance of the target material.

The use of reflectance spectroscopy for bitumen content estimation is not a new concept. The Wright & Wright Oil Sands Monitor (Thompson, 1983) is an example of a simple broadband system that estimates bitumen content in crushed ore based on the ratio of light reflectance at $2.22 \mu\text{m}$ to that at $2.33 \mu\text{m}$. This system has been used to determine the amount of caustic additives required for hot water processing of mined ore, however very little has been published on it besides a test of the method by Lyder et al. (2010), where a precision of ± 3 wt % TBC was reported. With the advent of hyperspectral sensors, higher resolution can be obtained. Lyder et

al. (2010) used Gaussian fitting and wavelet analysis to identify the absorption features most strongly correlated to bitumen content in reflectance spectra of homogenized ore collected with a hyperspectral point spectrometer. Based on their results, Rivard et al. (2010) designed a number of spectral models for the online monitoring of TBC in crushed ore destined for processing. Their most accurate and robust model produced TBC estimates within ± 1.1 - 1.5 wt % of Dean-Stark values without the need for site-specific calibration.

Working with drill core samples, as opposed to crushed ore, requires a number of additional considerations. The age of the core sample and the extended range of minerals (e.g. clays, carbonates) will affect the reflectance response. Calibration is required for bitumen-free zones such as shale, fractures and man-made materials (e.g. the core box). Proof of concept for using reflectance spectroscopy for TBC estimation in core samples was demonstrated by Shaw and Kratochvil (1990). They used a point spectrometer to measure reflectance in 1 cm^2 windows along the length of a 4 m section of core that had been dehydrated by exposure to ambient conditions for more than 5 years. TBC estimates were obtained by applying a regression model developed from samples of crushed ore collected from the same core. Follow up studies investigated optimization of the regression model (Donkor et al., 1995) and the relationship between the spacing of the reflectance measurements and the accuracy of the results (Gao and Kratochvil, 2002).

This study presents the first application, to the authors' knowledge, of hyperspectral imaging to oil sands core samples for the purposes of TBC estimation. Using imaging spectroscopy means TBC can be estimated for the entire sample surface, rather than just in spot measurements, and the high resolution imagery provides the opportunity to examine the spatial distribution of the oil in the core. The objective of this study is to evaluate whether hyperspectral imaging has the potential to be an alternative method for ore grade determination in both fresh and dry oil sands core samples. We proceed from the adaptation of one of Rivard et al.'s (2010) models for

use on drill core, which resulted in the development of two models referred to in this study as “broadband” and “wavelet”. Through this analysis, we explore the effects of moisture content and surface texture on the TBC estimate. Ideally, a predictive model for TBC would be robust in that it could be applied to core samples in any state of preservation from any location, depth or industry operator in the Athabasca deposit.

3.2 Study Area & Samples

3.2.1 Geological Context

The oil sands of northeastern Alberta, Canada, are hosted in three major deposits: Athabasca, Cold Lake and Peace River (Figure 3.1). The Athabasca deposit is the largest and is the only reservoir with bitumen that is shallow enough to be extracted by surface mining. The main oil-saturated unit of interest in the Athabasca deposit is the Lower Cretaceous McMurray Formation. As shown in Figure 3.1, the McMurray Formation unconformably overlies Devonian carbonates. Its upper boundary is defined by the appearance of glauconite in the marine sandstones and shales of the Wabiskaw Member of the Clearwater Formation (Carrigy, 1959). The thickness of the McMurray Formation ranges from <10 m to >100 m (Hein et al., 2000), but averages 40-60 m (Ranger, 1994).

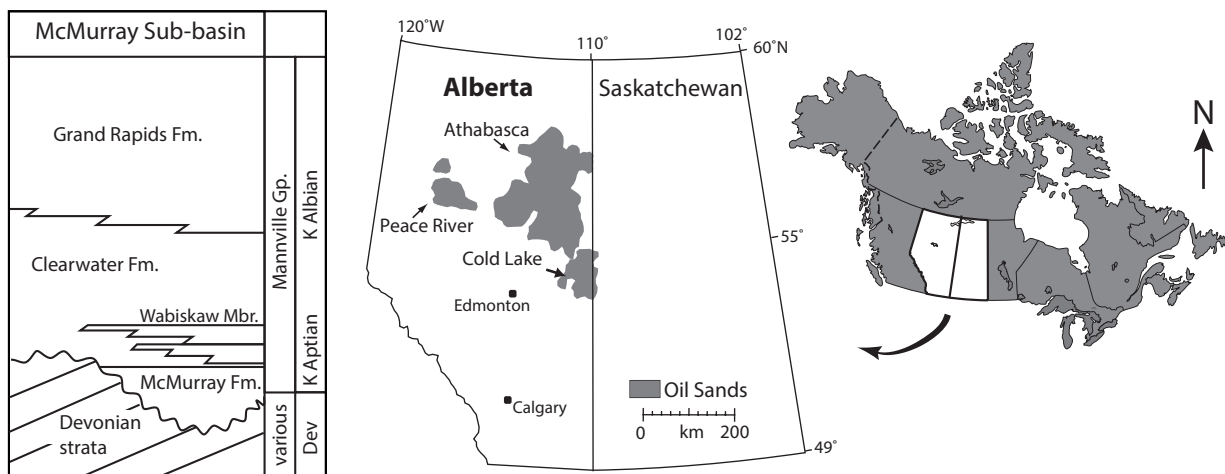


Figure 3.1 The oil sands deposits of northeastern Alberta, Canada, and the basic stratigraphy of the Athabasca deposit. All samples used in this study are from the Athabasca deposit, where the primary reservoir is the McMurray Formation. Modified from Ranger and Gingras (2003).

The McMurray Formation is commonly divided into three informal units that correlate to a three-fold facies model of a lower fluvial member, a middle estuarine member and an upper marine member (Stewart and MacCallum, 1978; Flach and Mossop, 1985). The most common interpretation of the formation's depositional history is that it was created by the amalgamation of incised valley fill complexes. Other interpretations include a estuarine-deltaic model where the McMurray Formation represents progradational pulses during a period of overall transgression (Ranger and Gingras, 2003; 2008), and a sequence stratigraphic model where the McMurray Formation represents continuous deposition over the course of a transgressive systems tract (Flach and Hein, 2001; Hein and Cotterill, 2006).

The McMurray sands are predominantly quartzose (>80%) with minor lithic components (Bayliss and Levinson, 1976). Little was known about the provenance of the sediment until a recent detrital zircon study by Benyon et al. (2014) identified the Appalachians of eastern North America as the primary source region, and the Cordilleran region of western North America and the Canadian Shield of north and east-central Canada as secondary sources. The origin of the Athabasca bitumen is an ongoing area of research. A light precursor oil is believed to have formed in source beds southwest of the deposit in the foreland basin of the Rocky Mountains. The degree of input from various source units has been intensely debated, with some geochemical and basin modeling studies reporting that the Gordondale Member of the Lower Jurassic Fernie Formation is the primary source bed (Higley et al., 2009; Berbesi et al., 2012; Finlay et al., 2012), and others the Mississippian Exshaw Formation (Adams et al., 2013). In either case, the precursor oil migrated hundreds of kilometers northeast to its present day location, where it was broken down to heavy oil by biodegradation (Head et al., 2003; Larter et al., 2006; Zhou et al., 2008). The timing of oil migration and biodegradation has also been the subject of debate. Structural reconstructions of bitumen-water contacts observed in the Athabasca deposit by Ranger (1994) suggested oil emplacement must have been completed by Late Cretaceous time (75-65 Ma). More recent geochemical studies suggest the oil could have been

emplaced as early as 112 Ma (Selby and Creaser, 2005).

3.2.2 Samples

Five suites of core from the Athabasca deposit were investigated in this study (Table 3.1). Core samples were selected from different locations within the deposit (location proprietary) and from both shallow and deep reservoirs. Freshly drilled oil sands cores, enclosed in an aluminum or plastic casing, are slabbed longitudinally. One half is stored in a freezer for laboratory analyses (also known as the A-side or “2/3 core”) and the other half is kept out for viewing (B-side or “1/3 core”). The core samples used in this study are the viewing (B) halves and the age of the sample provided in Table 3.1 refers to the length of time it has been exposed to ambient conditions. Each suite of core is classified as either “fresh” or “dry”, where oil sand sections of the fresh core are moist and pliable, while dry core sections are completely hardened and visibly dehydrated. The dry core also lacks the characteristic bituminous smell of oil sand. The five suites encompass a broad distribution of low to high ore grades (Figure 3.2), which makes this sample set well suited for evaluating the performance of the predictive spectral models.

The core samples used in this study are from three different operators, where A and B are from the first, C and D are from the second and E is from a third. Dean-Stark analysis was conducted at commercial laboratories and the industry operator that provided each suite of core also provided the Dean-Stark data. The weight difference method was used to determine bitumen content for fresh cores A and B. No information on the method used was available for cores C, D or E. In the Dean-Stark process, sections of core ranging from 10-30 cm in length are collected and homogenized prior to oil extraction. The lengths of core sub-sampled from the frozen A-side cores for Dean-Stark analysis are also marked on the boxes of the viewing B-side cores used in this study, allowing the Dean-Stark intervals to be easily identified in spectral imagery.

Table 3.1 Core samples used in this study.

	Core Suite	Age (years)	Number of Dean-Stark Samples	Ore Grade Range (wt %)	Depth Interval (m)
Fresh	A	~1	61	0.0-16.1	425-490
	B	~1	96	0.0-16.5	400-480
	C	<2	42	0.0-17.8	10-90
	D	<2	54	0.0-17.9	5-90
Dry	E	>15	177	0.1-17.6	7-125

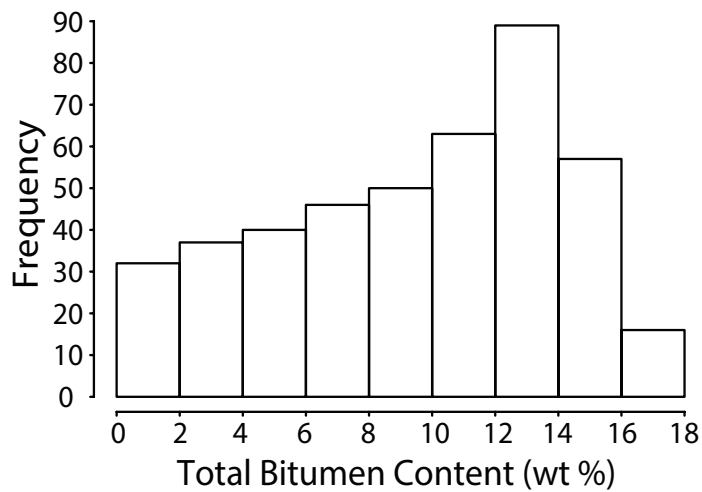


Figure 3.2 Ore grade distribution for the samples used for this study ($n = 430$). Total bitumen content (wt %) values are based on Dean-Stark analysis data for core A-D and bitumen mass fraction calculations for core E. Frequency is absolute (i.e. number of Dean-Stark samples).

Table 3.2 Technical specifications of the SisuROCK SWIR sensor and associated data.

Spectral Range	Number of Spectral Bands	Spectral Resolution	Bandwidth	Pixel Size
970-2500 nm	256	10 nm	6.3 nm	0.2-2.0 mm

3.3 Methods

3.3.1 Collection of Spectral Imagery

Spectral imagery of the five sets of core was collected with a SisuROCK core imaging system, developed and manufactured by Spectral Imaging (Specim) Ltd., Finland. The SisuROCK system is specifically designed for scanning drill core samples and no special sample preparation is required. Cores are loaded on to a platform that is capable of holding samples up to 1.5 m in length, 0.65 m in width and 50 kg in weight. The main body of the unit used for this study contains two high resolution spectral cameras and a set of quartz halogen lamps that illuminate the sample. The spectral sensors measure reflectance in the visible-near infrared (VNIR; 0.4-1.0 μm) and shortwave infrared (SWIR; 1.0-2.5 μm). In this study, data was collected in the SWIR because the materials of interest (bitumen, clays, water) are spectrally active in this wavelength region. Table 3.2 summarizes the technical specifications of the SWIR sensor and associated hyperspectral data. The SWIR sensor measures radiance in 256 spectral bands. The reflectance in each spectral band is obtained by normalization of the radiance measured in each pixel against that of a Spectralon™ panel at the head of the scanning platform. The platform moves past the sensors at a rate set by the user. In this study, imagery was collected at a spatial resolution of 1.2 mm/pixel. Up to four boxes of core were scanned at a time and it took less than 2 minutes to complete a scan (including calibration measurements). The depth of sensitivity of the reflectance measurements is on the order of tens of microns, thus these measurements are surficial in nature.

3.3.2 Spectral Models for TBC Prediction

Converting a reflectance measurement to an ore grade estimate requires a mathematical model based on absorption features that are correlated to bitumen abundance. A reflectance spectrum (Figure 3.3) is made up of a background continuum and absorption features (Rivard et al., 2008). The background continuum, or overall shape of the spectrum, is influenced by the physical properties of the surface (e.g. roughness, particle size) and by some compositional characteristics (e.g. moisture content, opaque minerals). These factors are referred to as non-wavelength specific

because they affect the spectrum as a whole. Absorption features, on the other hand, are caused by electronic and vibrational processes at the molecular level, which cause them to appear at specific wavelengths in the spectrum (Hunt, 1977).

With the exception of quartz, the constituents of oil sands (bitumen, clays and water) are spectrally active in the SWIR. A typical SWIR spectrum of oil-saturated sand (Figure 3.3) is dominated by bitumen absorption features around 1.7 μm and 2.3 μm , caused by C-H bond vibrations in the oil (Cloutis, 1989). Shale/mudstone spectra are dominated by clay mineral absorption features around 1.4 and 2.2 μm due to O-H and OH-cation bond vibrations (Hunt and Salisbury, 1970). A strong infrared absorber, water affects the overall reflectance of the spectrum, and O-H and H-O-H bond vibrations in water also produce absorption features around 1.4 μm and 1.9 μm (Clark, 1999).

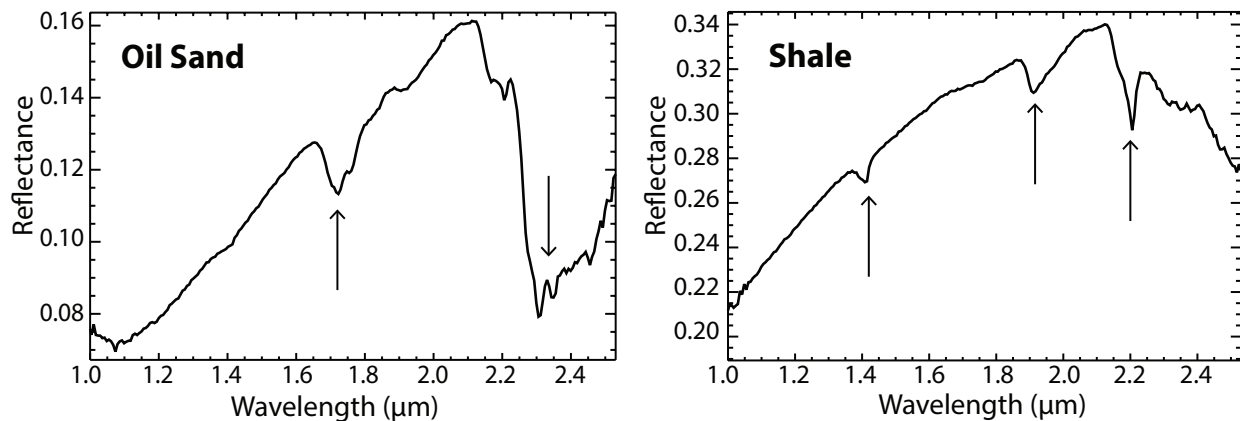


Figure 3.3 Representative reflectance spectra of oil sand and shale. Arrows indicate bitumen absorption features in the oil sand spectrum and clay mineral absorption features in the shale spectrum.

In 2010, Lyder et al. used continuous wavelet analysis to identify which absorption features are most strongly correlated with bitumen content in homogenized oil sands samples. Wavelet transforms are used in hyperspectral data analysis for reducing noise and minimizing non-compositional effects (Rivard et al., 2008). Wavelet analysis involves decomposing a spectrum into a series of linearly additive spectra known as wavelets (Torrence and Compo, 1998). The

width, or scale, of the wavelet base determines the type of spectral feature captured – low scale wavelets capture narrow absorption features and the highest scale wavelets capture the overall shape of the background continuum. The amplitude of the wavelet base required to fit the amplitude of each spectral feature is recorded as the wavelet power. Lyder et al. (2010) identified absorption features from three wavelength regions (1.7 μm , 2.2 μm and 2.3 μm) in the SWIR that were strongly correlated or anti-correlated with bitumen abundance. More details about the features and how they were selected are provided in Lyder et al. (2010).

Rivard et al. (2010) used the features identified by Lyder et al. (2010) to develop several different mathematical models for converting reflectance measurements to an ore grade estimate. Their study utilized a point spectrometer and their models were designed for online conveyor belt monitoring of fresh, crushed oil sands ore. Their most successful model, known as the normalized wavelet five band model, was adapted for use on drill core samples. Adapting the model for imagery of drill core required recalibration to account for bitumen-free zones such as shale beds and man-made materials (e.g. the box, the casing). Spectral interference from other mineral phases must also be considered. Carbonate minerals pose the greatest threat for interference because, like bitumen, they have absorption features in the 2.3-2.5 μm range (Hunt and Salisbury, 1971). This issue is dealt with by defining a carbonate index, where pixels that are recognized to have a value greater than a certain threshold are automatically labeled as 0 wt % bitumen.

The adaptation of Rivard et al's (2010) five band model for the analysis of drill core imagery resulted in the development of two models: broadband and wavelet. The broadband model estimates TBC directly from reflectance data. The model is referred to as "broadband" because the hyperspectral data is resampled, meaning that multiple spectral bands are averaged to give a single broadband reflectance for a given absorption feature. This serves to reduce the dimensionality of the data set and reduce noise. The wavelet model, on the other hand, estimates

TBC from wavelet power spectra, which are obtained by applying continuous wavelet transforms to the original reflectance spectra. Since wavelet analysis de-noises spectra, averaging bands is not necessary. Both models use the 1.7 μm and 2.3 μm bitumen absorption features and the 2.2 μm clay absorption feature. The wavelet model is expected to provide more accurate results than the broadband model because the effects of surface roughness and other non-compositional variables that could affect reflectance will be minimized. However, continuous wavelet transforms are computationally intensive. As a result, the wavelet model has the disadvantage of a significantly longer processing time (minutes vs. seconds per box of 2 inch core). Both models are expected to perform better for predicting TBC in the fresh core than in the dry core because the crushed ores used by Lyder et al. (2010) and Rivard et al. (2010) for the selection of absorption features and the original development of the models were fresh.

3.3.3 Viewing Spectral TBC Results

The spectral models calculate TBC on a pixel scale and these results are displayed in the form greyscale images (Figure 3.4). The greyscale represents the range of pixel values in the image, where black is void of bitumen and white is the highest grade. This imagery provides the opportunity for rapid visual assessment of the quantitative distribution of the oil in the core. Spectral TBC results can also be viewed as a function of depth in the form of vertical core profiles. Figure 3.4 shows an example of this for a 0.75 m long section of dry core. Results can be presented at the pixel scale, as in the example shown, providing highly detailed information on the variability in TBC with depth. Pixels can also be averaged to show broader scale trends in bitumen content. These profiles are a convenient way of presenting ore grade data and allow for easy comparison to petrophysical well log data.

3.3.4 Evaluating Spectral TBC Results

In order to evaluate the performance of the two models, spectral TBC values were compared to Dean-Stark results. However, these two methods calculate TBC at different spatial scales. As

described above, the spectral models calculate TBC on a per-pixel scale. Dean-Stark analysis, on the other hand, provides a single TBC value for sections of core 10-30 cm in length. In order to compare the mm-scale spectral results to Dean-Stark results, mean spectral TBC values were calculated over the same lengths of core that were used for Dean-Stark analysis. Mean spectral TBC can be calculated by drawing a rectangular or linear region of interest (ROIs) over the Dean-Stark sampled interval, as illustrated in Figure 3.4.

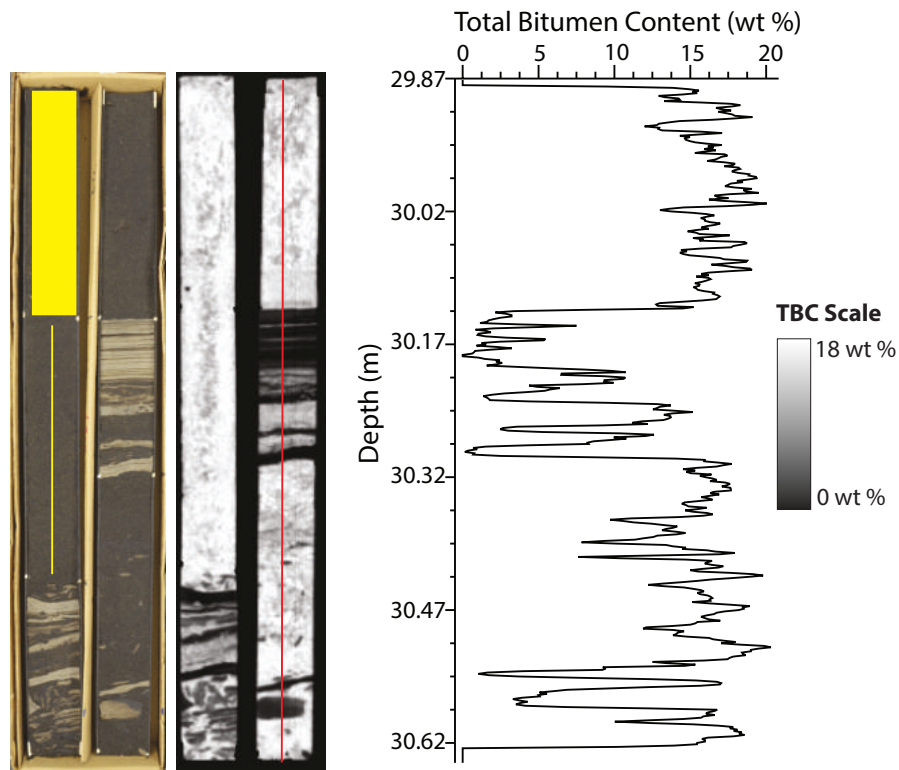


Figure 3.4 Photo of a box from core E (left), its greyscale TBC image (middle) and a vertical TBC profile (right). The greyscale represents the range of pixel values in the image where black means void of bitumen and white means highest grade. The yellow rectangle and line show examples of rectangular and linear region of interests that can be used to calculate mean spectral TBCs for comparison to Dean-Stark values. The vertical TBC profile represents variation in TBC as a function of depth at the mm scale, and is derived from pixel values along the red line shown on the greyscale TBC image. Core diameter = 6 cm.

Depending on the size of the Dean-Stark sample and the diameter of the core, for rectangle ROIs this meant averaging 5000-30,000 pixel spectra. This approach maximizes the number of pixels covered for a Dean-Stark interval, presumably providing the most accurate representation of the

sample. However, this process can be time-consuming and is not practical for core samples that are highly fractured. A faster alternative is drawing lines along the Dean-Stark interval, where 100-600 pixel spectra are averaged. To investigate if there is a significant difference between the mean spectral TBC values obtained using the two methods, both approaches were tested on Core A.

In all cases except for Core E (the dry core), spectral TBC estimates were compared to Dean-Stark values. Although Dean-Stark analysis was completed for Core E, the raw data was not available. Bitumen mass fractions were calculated for Dean-Stark sample intervals using porosity and oil saturation data obtained when the core was fresh. For this calculation, a constant grain density of 2.65 g/cm³ was assumed and fluid volume was assumed to be equal to pore volume. These same assumptions are used in Dean-Stark analysis. The Dean-Stark data and bitumen mass fraction data are collectively referred to as “true TBC” herein.

The relationship between the spectral TBC estimates and the true TBC was evaluated by linear least squares regression analysis. In all cases, regressions were forced through the origin in the interest of evaluating the performance of the model in terms of providing a one to one correlation between spectral TBC and true TBC. The accuracy of the results was evaluated by calculating the root mean square (RMS) error, defined as:

$$RMS = \sqrt{\frac{\sum_{i=1}^n (\hat{y}_i - y_i)^2}{n - 1}}$$

where n is the number of Dean-Stark samples, y is the spectral TBC value and \hat{y} is the TBC value predicted by the regression line.

No information on the margin of error in the Dean-Stark data was available. To the authors' knowledge, there is no published work that provides a rigorous assessment of repeatability and

error in Dean-Stark analysis. From discussions with various industry operators, margins of error ranging from ± 0.5 wt % to ± 1.5 wt % tend to be assumed in Dean-Stark data, but there is little agreement on this. In this study, we assume that any error in the Dean-Stark data is uniform across all samples and all ore grades. We also assume that there is no error due to sub-sampling.

3.4 Results

Spectral TBC values were calculated for Core A using two different methods, as described above. Linear regions of interest covered only $\sim 2\%$ of the pixels encompassed by rectangular regions for each Dean-Stark sample interval. Interestingly, when the mean TBC values calculated from linear ROIs were compared those from rectangular ROIs for each Dean-Stark sample, the results were strongly correlated for both spectral models ($R^2 = 0.99$ for $n = 61$; Figure 3.5). Mean spectral TBCs from both lines and rectangles were also compared to Dean-Stark analysis data. The root mean square error for rectangle ROIs was ± 1.77 wt % for the broadband model and ± 1.48 wt % for the wavelet model. RMS errors for line results were only slightly higher, ± 1.83 wt % and ± 1.55 wt % for broadband and wavelet, respectively. In the interest of minimizing the error, spectral results presented hereafter were calculated using rectangular regions of interest. However, linear ROIs can be expected to give comparable results and this approach may be more convenient in some cases, such as for highly fractured core samples.

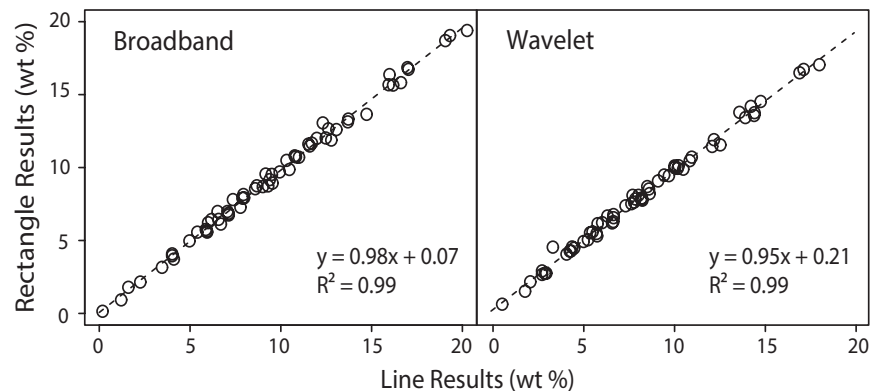


Figure 3.5 Correlation plot showing the relationship between the mean spectral TBC obtained from rectangular regions of interest vs. linear regions of interest for Dean-Stark samples in core A ($n = 61$). Results are shown for both spectral models. The equation of the regression line (dashed) and the coefficient of determination (R^2) is provided on each plot.

The results of linear regression analysis for all five suites of core are shown in Figure 3.6. Broadband model results are presented in the left column and wavelet model results in the right. Fresh cores A, B, C and D are combined in the top row of plots and the dry core E results are presented in the bottom row. The dry core was analyzed independently of the fresh cores for two reasons: 1) the unique dehydrated nature of the sample and 2) the true spectral TBC values being bitumen mass fraction values rather than raw Dean-Stark results. For each plot, true TBC is given on the horizontal axis and the corresponding predicted TBC (mean spectral TBC value) is given on the vertical axis. The number of Dean-Stark samples is given by n. The dashed lines are the regression lines and their equations are provided on each plot along with coefficients of determination (R^2) and RMS errors in units of \pm wt % bitumen.

For the fresh core, the spectral TBC results are very strongly correlated with the Dean-Stark data. Linear regression analysis produced results of $R^2 = 0.97$ for the broadband model and $R^2 = 0.96$ for the wavelet model. The margins of error for the two models were comparable at ± 2.26 and ± 2.22 wt %, respectively. Fresh core results were also analyzed individually by core (Table 3.3).

Table 3.3 Results of linear regression analysis for individual fresh cores for both spectral models. RMS error is given in units of \pm wt % TBC.

Core	Broadband		Wavelet	
	R^2	RMS	R^2	RMS
A	0.97	1.77	0.97	1.48
B	0.97	2.52	0.97	2.58
C	0.99	1.29	0.99	1.31
D	0.98	1.28	0.98	1.39

Interestingly, Core A, C and D performed significantly better than Core B with both spectral models. Although all four suites individually showed very strong correlation between spectral TBC and Dean-Stark ($R^2 = 0.97-0.99$), Cores A, C and D have lower RMS errors. The error for Cores A, C and D ranged from ± 1.28 to 1.77 wt % for the broadband model and from ± 1.31 to 1.48 wt % for wavelet. Core B's RMS errors were nearly double these values: ± 2.52 wt % for

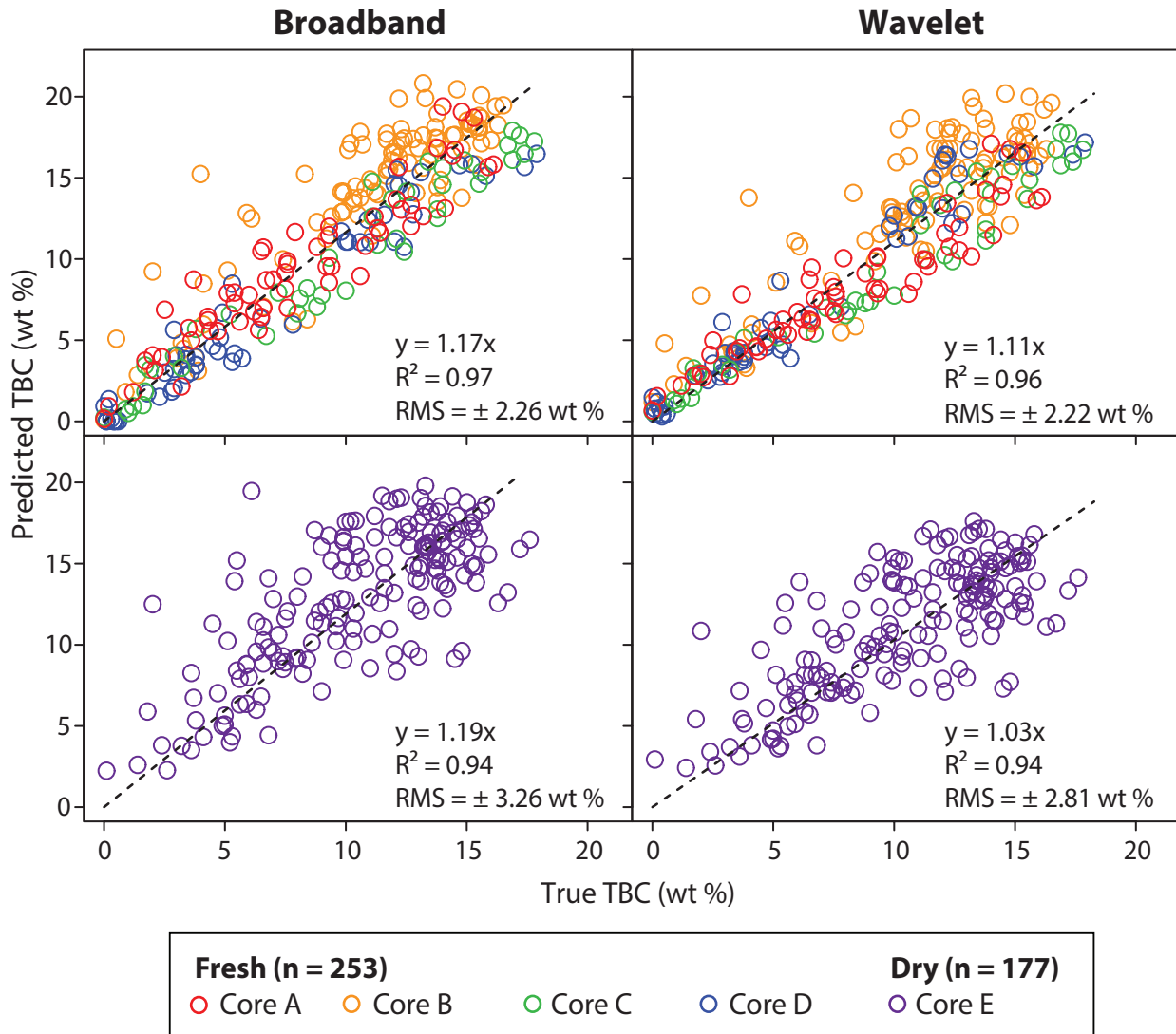


Figure 3.6 Correlation plots showing the linear regression results for all 5 suites of core. Broadband model results are in the left column and wavelet model results are given in the right column. Fresh cores are shown in the top row of plots and the dry core is shown in the bottom row. Regressions were forced through the origin. The equation of the dashed regression line, R^2 , and the RMS error are provided on each plot. The number of Dean-Stark samples is given by n .

broadband and ± 2.58 wt % for the wavelet model. Although the Core B results still reflect a strong correlation between the spectral TBC values and the Dean-Stark values ($R^2 = 0.97$), the distributions of the Core B points in Figure 3.6 indicate that both spectral models had a tendency to overestimate. Regression analysis of the combined data set of Cores A, C and D (not shown) produced $R^2 = 0.98$ and RMS errors of ± 1.58 wt % for broadband and ± 1.53 wt % for wavelet.

For the dry core, a strong correlation between true and predicted TBC was also achieved, with linear regression results of $R^2 = 0.94$ for both spectral models. The margin of error in the dry core results is larger than that observed in the fresh cores. The broadband model in particular had a high RMS error of ± 3.26 wt %, while the wavelet model produced an RMS error of ± 2.81 wt %. Samples in Core E that showed disagreement between the predicted TBC and the true TBC tended to be overestimated, which is consistent with the problematic samples in fresh core B.

3.5 Discussion

3.5.1 Fresh Core

In this study, the wavelet model was expected to provide more accurate results than the broadband model. For Core A, C and D, the difference between the broadband and wavelet results was negligible both in terms of correlation with true TBC (R^2) and RMS error. In these cases, the broadband model would be preferable due to its shorter processing time.

Broadband and wavelet model results were also comparable for Core B, with an RMS error of approximately ± 2.5 wt % for both models. Due to this high error, an analysis of problematic samples, or outliers, was carried out for fresh core B. Outliers were defined as samples where the absolute difference between the true TBC and the mean spectral TBC exceeded twice the standard deviation of the rectangular region of interest used to calculate each mean spectral TBC. Based on this definition, 36 outliers were identified for the broadband model and 24 for the wavelet model in Core B. This represents 38% and 25% of Core B's sample population,

respectively. Being from the same industry operator, Core B was presumably subject to the same preparation and storage conditions as Core A. However, only 5 outliers were identified for Core A for the broadband model (8%) and none for the wavelet.

For all outliers identified in Core B, the spectral models overestimated the TBC relative to the Dean-Stark value. Most of the outlier samples represented continuous sections of consecutive Dean-Stark samples. These sections were classified as one of three types based on their sedimentological characteristics. Type 1 samples consist of high grade (>10 wt %), very fine to fine clean sand. These samples are very well sorted and very tightly consolidated, providing a very smooth surface texture. The samples appear perfectly massive, lacking any visible sedimentary or biogenic structures. Visually, the oil appears evenly distributed. The surfaces of the core sample have little to no fracturing and although they are smooth, they are not slick (i.e. no specular reflectance). Type 2 samples are high grade (>12 wt %), composed of medium to coarse grained sand and appear to be loosely consolidated in that the core appears very porous. The samples show cross-bedding and small-scale fracturing, usually along the bedding surfaces. The rougher surface texture of Type 2 samples, imparted by looser packing of coarser grains as well as the fractures, clearly contrasts the smooth surfaces of Type 1 samples. Type 3 samples are similar to Type 1 in terms of being high grade (>10 wt %), fine grained, well sorted and tightly consolidated; the only difference is that these samples have well-defined cross-bedding. The distribution of the oil does not appear uniform, as the cross-beds appear as alternating dark and light layers. The grain size is constant across the beds, but the sample surface is not as smooth as Type 1 due to the presence of very fine scale fractures running both along and across bedding planes.

It is interesting to note that all three types of outliers are associated with overestimates in high grade ores. On average, low to mid-grade (true TBC <10 wt %) clean sands in Core B performed better than high grade clean sands. High grade samples in Core B that did perform well tended

to be more lithologically heterogeneous. This observation is consistent with the superior results of Core A, which has a large proportion of heterogeneous samples (i.e. highly oil saturated sands with mud intraclast breccia or sections of interbedded shales). From a production perspective, the margin of error in clean, high grade ores that are well above the economic cut-off (~7 wt %) is not of highest concern. Precision is very crucial, however, in mid-grade samples. Of the 36 samples that were identified as outliers for both spectral models in Core B, only one had a true TBC less than 10 wt %.

The cause of overestimation in Type 1 samples is unclear. Concentration of oil along the core surface may occur in high grade ores during slabbing. Although core samples are frozen when slabbed, melting can occur along the saw blade resulting in mobilization of the oil. However, if any smearing of oil has occurred in the problematic sections, it is not readily visible on the samples. A possible source of error in the Type 2 and 3 samples is surface roughness imparted by loosely consolidated grains, bedding and small scale fracturing. Examples of these textures are shown in Figure 3.7. This is consistent with observations by Donkor et al. (1995), who found that roughening the surface of high grade ores (>11 wt %) with a fork resulted in elevated spectral TBC estimates but the same manipulation of the surface lowered the spectral TBC result for low grade ores (<8 wt %). They attributed this to spreading of the continuous phase, which in high grade samples is the bitumen and in low grade samples is clays and water.

It is interesting to note that the Type 2 outlier group included all the coarse grained (>250 μm) samples in Core B. Although the relative proportion of these samples is small (~3 %), these results bring to question the effect of grain size on the spectral TBC estimate. In the SWIR wavelength region, a coarser grain size would be expected to cause decreased volume scattering of the incident light, which would result in a decrease in the total reflectance returned to the sensor and in the spectral contrast (Salisbury et al., 1991). However, exactly how this would affect the performance of the spectral TBC models remains a research preoccupation

and the limited number of coarse grained ($>250\ \mu\text{m}$) samples in the fresh cores precludes any conclusions on this.

3.5.2 Dry Core

Because the spectral models were originally calibrated with fresh ore samples, it was anticipated that the lack of water in the dry core may negatively impact the performance of the models.

The loss of hydrocarbon components from prolonged exposure to ambient conditions was also considered. In spite of these factors, the dry core achieved very strong correlations with true TBC, comparable to that of fresh core. However, the RMS errors were considerably higher for the dry core, particularly for the broadband model. Outlier analysis for dry core E revealed 29 outliers in the broadband results and 15 in the wavelet (16% and 8% of the sample population, respectively). Although the loss of volatiles may be expected to lead to underestimation of TBC in dry core, it is interesting to note that most of the outliers were overestimated by the spectral models. There were only three cases of underestimation; one sample was underestimated by both spectral models and two samples were underestimated by the wavelet model only. Samples that were overestimated by the spectral models were mostly mid- to high grade ($>6\ \text{wt}\ \%$) and showed considerable grain size variability from fine to very coarse sand. Cross-bedding, visually defined both by grain size changes and uneven oil distribution, was observed in the majority of problematic samples. Samples of similar grade that performed well appeared to have more uniform distribution of oil (Figure 3.8). Even in the presence of grain size variability and cross-bedding, uniform oil distribution may provide a smoothing effect for the sample surface at the microscopic scale. All three underestimated samples were very fine grained and highly bioturbated. One sample is visually very low grade, but the other two appear to be mid-grade. The surface of the mid-grade samples is covered in a fine mud or dust giving them a reflective sheen that may be causing specular reflectance. Early work with frozen A-side cores found that specular reflectance from slick surfaces resulted in systematic underestimation of bitumen content by the spectral models. Error in the bitumen mass fraction data may be also be a factor.

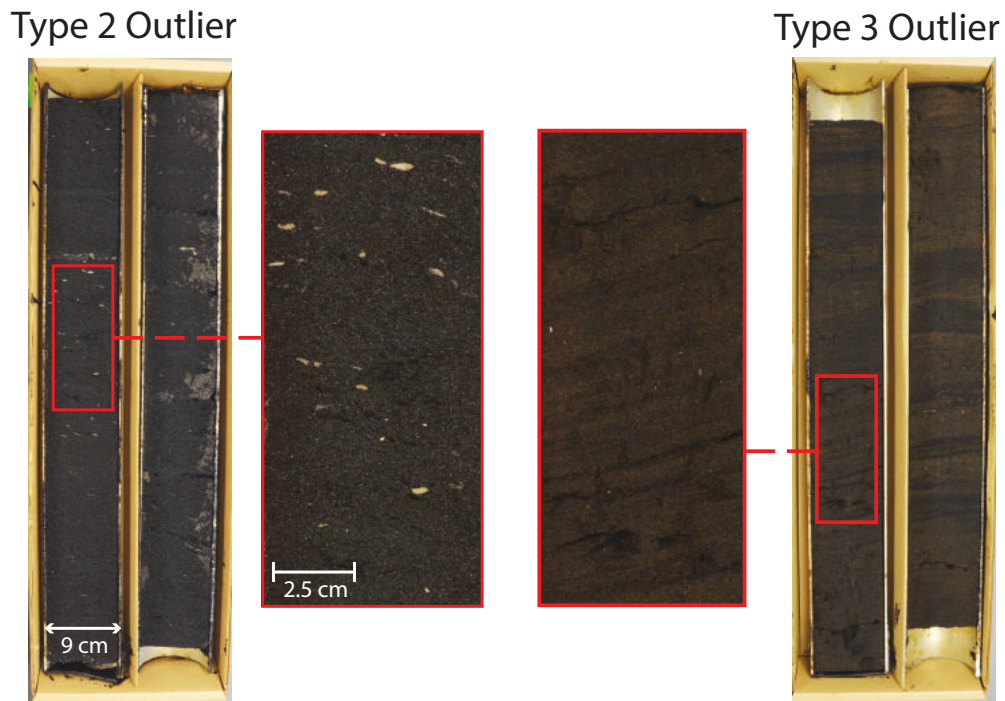


Figure 3.7 Photos of boxes from fresh core B showing rough surface textures that may be a source of error in the spectral results. The left image is an example of a Type 2 problematic sample: coarse grained and loosely consolidated. The right image is a Type 3 problematic sample: fractured surface and cross-bedding with uneven bitumen distribution.

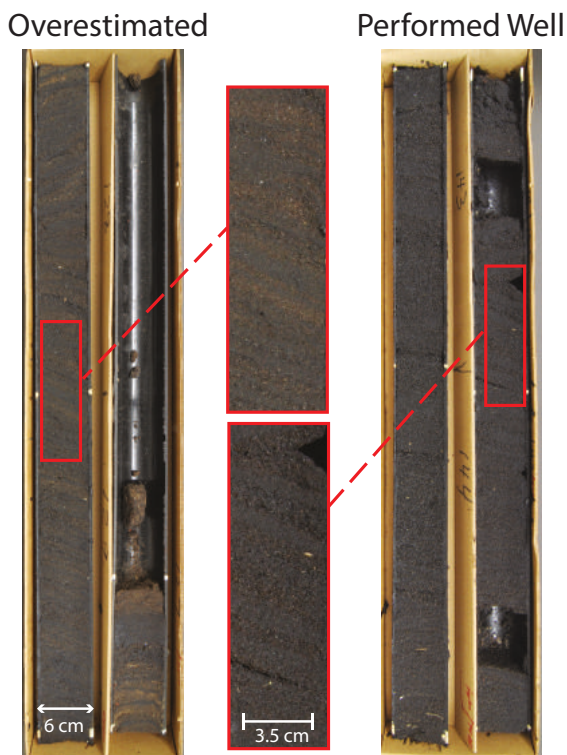


Figure 3.8 Photos showing examples of two boxes from dry core E where one was overestimated and the other performed well. As shown in the inset photos, the overestimated sample shows cross-bedding defined by variable grain size and bitumen distribution. The beds impart a micro-topography to the sample surface where finer grained, oil-rich beds are higher and coarser grained, oil-poor beds are lower. A sample with similar cross-bedding but uniform oil distribution is shown for comparison. In this case, the bedding is clearly visible because of grain size variation, however the bitumen content does not appear to vary between the stripes. This sample has a smoother surface texture as all beds have similar prominence.

Generally speaking, the dry core has a rougher surface texture than the fresh core. This is likely an artefact of dehydration but perhaps also of the generally coarser grain size of this core suite relative to the other cores. Since wavelet transforms minimize the spectral effects of grain size variability in particulate samples, the superior performance of the wavelet model relative to the broadband model in the dry core is consistent with expectations. Interestingly, the wavelet model apparently did not correct for the coarser grain size of Type 2 outlier samples in fresh core B. A possible explanation for this is that the bitumen acts as a continuous phase in the fresh core (pliable) but not the dry core (completely hardened), meaning that the former may not spectrally behave as particulate matter. Because of the strong correlations achieved for the dry core, the results of this study suggest that lack of moisture and loss of hydrocarbons from prolonged dehydration does not negatively impact the performance of the spectral models. These results also suggest that devolatilization does not substantially affect the shortwave infrared properties of bitumen.

3.6 Conclusions

This study investigated the application of hyperspectral imaging, a remote sensing technique, to Athabasca oil sands core samples for the purpose of total bitumen content (TBC) determination. Two spectral models, broadband and wavelet, were tested on fresh and dry B-side cores, where the fresh cores are less than 2 years old, moist and pliable and the dry core is more than 15 years old and completely hardened. For three out of four suites of fresh core, TBC was predicted within ± 1.5 wt % of the Dean-Stark data with both spectral models achieving correlations of $R^2 > 0.97$. Although the wavelet model was expected to perform better than the broadband, these results indicate that the broadband model, nearly ten times faster than the wavelet, is capable of producing results of comparable accuracy. For dry core and the fourth suite of fresh core, a strong agreement with Dean-Stark data was also observed for both models. However, the margin of error was larger, particularly for the dry core broadband results. Analysis of problematic samples revealed a tendency for the spectral models to overestimate TBC in these two suites

of core. Surface roughness due to uneven oil distribution, small scale fracturing and loosely consolidated sediment was identified as a potential source of error in some spectral TBC results. In these cases, the wavelet model may be preferable. Further work is required for understanding the conditions under which over-reporting of TBC by the spectral models occurs. The effect of grain size on the performance of the spectral models requires further investigation in particular.

Hyperspectral imaging provides a number of benefits over existing TBC determination methods. The spectral models produce high resolution greyscale imagery that allows for rapid visual assessment of the quantitative distribution of the oil in the core. Results are produced within minutes and the technique is non-destructive to the core sample. Even if the spectral TBC models may require further validation to be used to obtain absolute TBC values, the strong correlations achieved by the spectral models for all the core samples demonstrate that relative TBC estimates can be made with confidence. This study demonstrates that the spectral models are robust in that they can be applied to fresh or dry cores samples from different locations, depths and operators in the Athabasca deposit, making this technique an attractive potential alternative for bitumen content estimation.

References

- Adams, J., Larter, S., Bennett, B., Huang, H., Westrich, J., Larter, S., Bennett, B., Huang, H., Westrich, J., and van Kruisdijk, C., 2013, The dynamic interplay of oil mixing, charge timing, and biodegradation in forming the Alberta oil sands: Insights from geologic modeling and biogeochemistry, in: Hein, F.J., Leckie, D., Larter, S., and Suter, J.R. (Eds.), *Heavy-oil and Oil-sand Petroleum Systems in Alberta and Beyond*, AAPG Studies in Geology 64, American Association of Petroleum Geologists, p. 23–102.
- Bayliss, P., and Levinson, A.A., 1976, Mineralogical review of the Alberta oil sand deposits (Lower Cretaceous, Mannville Group), *Bulletin of Canadian Petroleum Geology*, v. 24, no. 2, p. 211–224.
- Benyon, C., Leier, A., Leckie, D.A., Webb, A., Hubbard, S.M., and Gehrels, G., 2014, Provenance of the Cretaceous Athabasca oil sands, Canada: Implications for continental-scale sediment transport, *Journal of Sedimentary Research*, v. 84, no. 2, p. 136–143.
- Berbesi, L.A., di Primio, R., Anka, Z., Horsfield, B., and Higley, D.K., 2012, Source rock contributions to the Lower Cretaceous heavy oil accumulations in Alberta: A basin modeling study, *AAPG Bulletin*, v. 96, no. 7, p. 1211–1234.
- Bulmer, J.T., and Starr, J., 1979, *Syn crude Analytical Methods for Oil Sand and Bitumen Processing*, Alberta Oil Sands Technology and Research Authority (AOSTRA), Edmonton, AB, 173 p.
- Carrigy, M.A., 1959, Geology of the McMurray Formation, Pt. III: General geology of the McMurray area, Research Council of Alberta, Geological Division – Memoir 1, 130 p.
- Clark, R.N., 1999, Spectroscopy of rocks and minerals, and principles of spectroscopy, in: A.N. Rencz (Ed.), *Remote Sensing for the Earth Sciences: Manual of Remote Sensing*, John Wiley & Sons, Inc., p. 3–58.
- Cloutis, E., 1989, Spectral reflectance properties of hydrocarbons: Remote-sensing implications, *Science*, v. 245, no. 4914, p. 165–168.
- Donkor, K.K., Kratochvil, B., and Thompson, G.R., 1995, Analysis of Athabasca oil sand by near-infrared-diffuse reflectance spectroscopy, *Analyst*, v. 120, p. 2713–2717.
- Finlay, A.J., Selby, D., and Osborne, M.J., 2012, Petroleum source rock identification of United Kingdom Atlantic Margin oil fields and the western Canadian oil sands using platinum, palladium, osmium and rhenium: Implications for global petroleum systems, *Earth and Planetary Science Letters*, v. 313-314, p. 95–104.
- Flach, P.D., and Hein, F.J., 2001, Outcrop-core correlation of channel and non-channel facies, McMurray Formation, Fort MacKay area, NE Alberta (abs.), CSPG Rock the Foundation Convention Extended Abstracts, June 18-22, 2001, Calgary, AB, p. 132–133.
- Flach, P.D., and Mossop, G.D. 1985, Depositional environment of Lower Cretaceous McMurray Formation, Athabasca oil sands, Alberta, *AAPG Bulletin*, v. 69, no. 8, p. 1195–1207.
- Gao, Z., and Kratochvil, B., 2002, Sampling variance as a function of single-increment size for estimation of bitumen in an oil-sand core, *Canadian Journal of Chemistry*, v. 80, no. 4, p. 440–446.

- Head, I.M., Jones, D.M., and Larter, S., 2003, Biological activity in the deep subsurface and the origin of heavy oil, *Nature*, v. 426, no. 6964, p. 344–352.
- Hein, F.J., and Cotterill, D.K., 2006, The Athabasca oil sands — A regional geological perspective, Fort McMurray area, Alberta, Canada, *Natural Resources Research*, v. 15, no. 2, p. 85–102.
- Hein, F.J., Cotterill, D.K., and Berhane, H., 2000, An atlas of lithofacies of the McMurray Formation Athabasca oil sands deposit, northeastern Alberta: Surface and subsurface, Earth Sciences Report 2000-07, Alberta Geological Survey, Edmonton, AB, 217 p.
- Hunt, G.R., 1977, Spectral signatures of particulate minerals in the visible and near infrared, *Geophysics*, v. 42, no. 3, p. 501–513.
- Hunt, G.R., and Salisbury, J.W., 1970, Visible and near-infrared spectra of minerals and rocks: I. Silicate Minerals, *Modern Geology*, v. 1, p. 283–300.
- Hunt, G.R., and Salisbury, J.W., 1971, Visible and near-infrared spectra of minerals and rocks: II. Carbonates, *Modern Geology*, v. 2, p. 23–30.
- Larter, S., Huang, H., Adams, J., Bennett, B., Jokanola, O., Oldenburg, T., Jones, M., Head, I., Riediger, C., and Fowler, M., 2006, The controls on the composition of biodegraded oils in the deep subsurface – Part II: Geological controls on subsurface biodegradation fluxes and constraints on reservoir-fluid property prediction, *AAPG Bulletin*, v. 90, no. 6, p. 921–938.
- Lyder, D., Feng, J., Rivard, B., Gallie, A., and Cloutis, E., 2010, Remote bitumen content estimation of Athabasca oil sand from hyperspectral infrared reflectance spectra using Gaussian singlets and derivative of Gaussian wavelets, *Fuel*, v. 89, no. 3, p. 760–767.
- Masliyah, J., Czarnecki, J., and Xu, Z., 2011, *Handbook on Theory and Practice of Bitumen Recovery from Athabasca Oil Sands*, Kingsley Knowledge Publishing, 468 p.
- Mossop, G., 1980, Geology of the Athabasca Oil Sands, *Science*, v. 207, no. 4427, p. 145–152.
- Ranger, M., 1994, A basin study of the southern Athabasca oil sands deposit, PhD thesis, University of Alberta, Edmonton, AB, 289 p.
- Ranger, M.J., and Gingras, M.K., 2003, *Geology of the Athabasca Oil Sands: Field Guide & Overview*, I.C.E. 2004: CSPG CHOA CWLS Joint Conference Field Trips & Short Courses, Calgary, AB, Canadian Society of Petroleum Geologists, 123 p.
- Ranger, M.J., and Gingras, M.K., 2008, Stratigraphy and sequence stratigraphic surfaces of the McMurray Formation (abs.), AAPG Hedberg Research Conference - Heavy Oil and Bitumen in Foreland Basins: From Processes to Products, Banff, AB, AAPG Search and Discovery Article #90075, 6 p.
- Rivard, B., Feng, J., Gallie, A., and Sanchez-Azofeifa, A., 2008, Continuous wavelets for the improved use of spectral libraries and hyperspectral data, *Remote Sensing of Environment*, v. 112, no. 6, p. 2850–2862.
- Rivard, B., Lyder, D., Feng, J., Gallie, A., Cloutis, E., Dougan, P., Gonzalez, S., Cox, D., and Lipsett, M.G., 2010, Bitumen content estimation of Athabasca oil sand from broad band infrared reflectance spectra, *The Canadian Journal of Chemical Engineering*, v. 88, p. 830–838.

- Salisbury, J.W., Walter, L.S., Vergo, N., and D'Aria, D.M., 1991, *Infrared (2.1-25 μm) Spectra of Minerals*, The Johns Hopkins University Press, Baltimore, MD, 267 p.
- Selby, D., and Creaser, R.A., 2005, Direct radiometric dating of hydrocarbon deposits using rhenium-osmium isotopes, *Science*, v. 308, no. 5726, p. 1293–1295.
- Shaw, R.C., and Kratochvil, B., 1990, Near-infrared diffuse reflectance analysis of Athabasca oil sand, *Analytical Chemistry*, v. 62, no. 2, p. 167–174.
- Stewart, G.A., and MacCallum, G.T., 1978, *Athabasca Oil Sands Guidebook*, Canadian Society of Petroleum Geologists, Calgary, AB, 33 p.
- Thompson, G.R., 1983, Method and apparatus for on-line monitoring of bitumen content in tar sand, Canada Patent #1139702.
- Torrence, C., and Compo, G.P., 1998, A practical guide to wavelet analysis, *Bulletin of the American Meteorological Society*, v. 79, no. 1, p. 61–78.
- Zhou, S., Huang, H., and Liu, Y., 2008, Biodegradation and origin of oil sands in the Western Canada Sedimentary Basin, *Petroleum Science*, v. 5, no. 2, p. 87–94.

Chapter 4

Shortwave infrared hyperspectral imaging: A novel method for enhancing the visibility of sedimentary and biogenic features in oil-saturated core

This chapter has been accepted for publication as: Speta, M, Gingras, M.K., Rivard, B., Shortwave infrared hyperspectral imaging: A novel method for enhancing the visibility of sedimentary and biogenic features in oil-saturated core, *Journal of Sedimentary Research*, accepted Dec. 13, 2015.

4.1 Introduction

One of the primary goals of sedimentary core logging is to identify sedimentary and biogenic features that are indicative of depositional environment. This is critical for facies classification and further geological interpretation. However, these features can be difficult to observe, particularly to the novice eye. Sedimentary cores can appear homogeneous for a number of reasons, such as fine grain size, high degree of sorting, lack of lithological/mineralogical heterogeneity, or masking of contrast due to oil saturation. Oil sands are an example of such sediments where qualitative core analysis is challenging. Oil sands are a naturally occurring mixture of quartz sand, clay minerals, water and bitumen. Bitumen is an extra-heavy crude oil (8-10° API) characterized by very high viscosity. The world's most developed bitumen deposits are located in northeastern Alberta, Canada and the Athabasca deposit is the largest of three in the province (Figure 4.1). The Lower Cretaceous McMurray Formation is the primary reservoir unit in the deposit. Because the McMurray Formation lacks lateral continuity, drill core sampling is crucial for the investigation of subsurface geology in the Athabasca, and the deposit is renowned for its exceptional drill control (Hein et al., 2000). Oil sands are uncemented; the quartz sand is held together by the high viscosity oil. As a result, drill core must be encased in PVC or aluminum pipe. The core is split longitudinally after drilling to provide a flat surface for viewing. Oil sands are typically well sorted and medium to fine sand grain size, which, in combination with the masking effect of the heavy oil, makes sedimentary and biogenic features

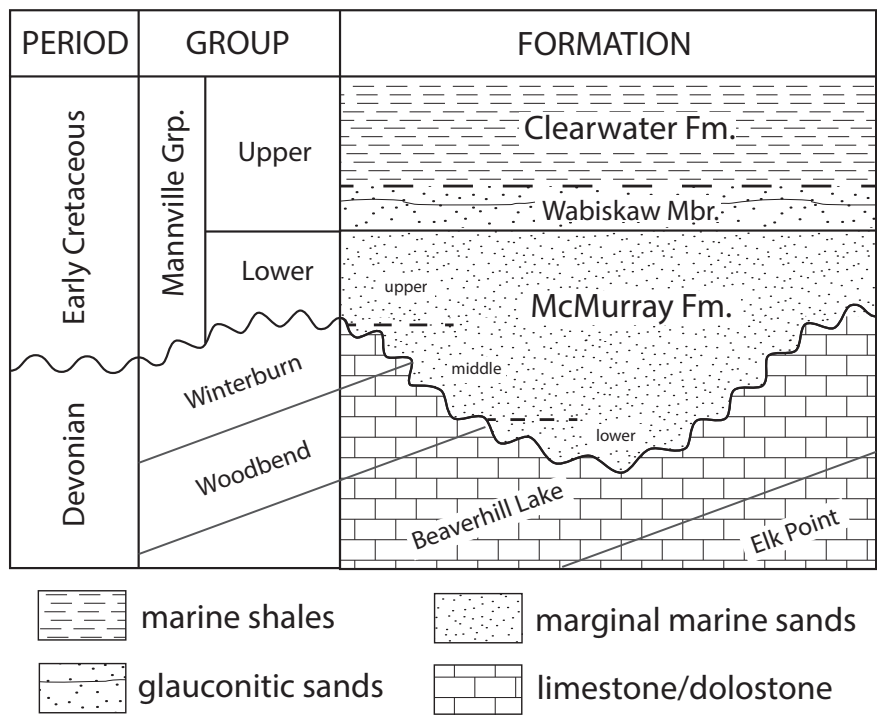
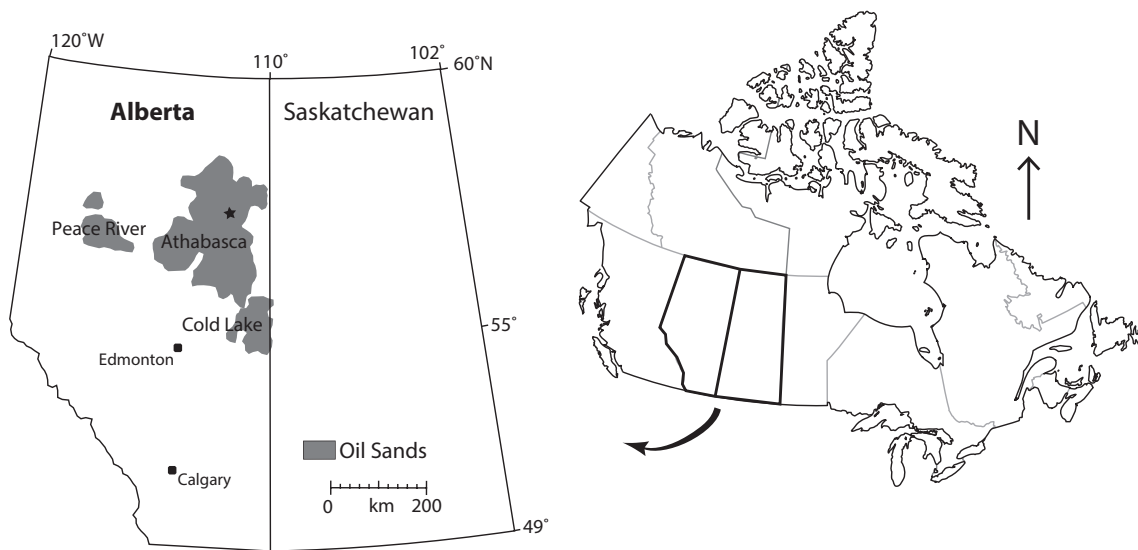


Figure 4.1 The oil sands deposits of northeastern Alberta, Canada, and the stratigraphy of the Athabasca deposit. Star indicates approximate location of drill core used in this study. Map modified from Ranger and Gingras (2003), stratigraphic column modified from Mossop and Flach (1983).

very difficult to see in the bitumen-saturated zones.

A plethora of core imaging techniques has developed over the past several decades for facilitating the visual analysis of sedimentary cores. Rothwell (2006) provides thorough reviews of such methods, including x-ray radiography, x-ray computed tomography (CT) scanning, magnetic resonance imaging (MRI) and confocal macro/microscopy. However, the application of these techniques has focused on deep sea sediments. Significantly less work has been done on improving the visibility of sedimentological features in oil-saturated sediments. Ultraviolet and infrared light photography has been applied to oil sands for the purposes of automating the discrimination and quantification of sand and shale beds (Phillips et al., 1991). X-ray radiography was used to aid the identification of stratification in high-grade oil sands in an unpublished MSc thesis (Fox, 1988), but time and cost were major limiting factors. In the oil and gas industry, most laboratory service providers list “core imaging” as one of their core analysis services. This typically refers to high resolution photography. Core photography is a fundamental part of the core analysis workflow in the oil sands industry; photos are used for everything from core logging to integrating core data with petrophysical well logs. However, photographs do not reveal more than the unaided eye can see, and the challenges in unmasking important sedimentological features in structureless-appearing oil sands core persist.

Hyperspectral imaging is a remote sensing technique that may provide a simple and elegant solution to this problem. Also known as imaging spectroscopy, hyperspectral imaging can be defined as the combination of reflectance spectroscopy with digital imaging. Visible to shortwave infrared reflectance spectroscopy is an established method for the analysis of geological materials, from mineral identification (e.g. Hunt and Salisbury, 1970; Hunt, 1977; Gaffey, 1985; Clark, et al. 1990) and quantification (e.g. Deaton and Balsam, 1991; Kruse, 1996) to rock type classification (e.g. Hunt and Salisbury, 1976; Hunt and Ashley, 1979; Crowley, 1986). The operating principle behind this technique is the fact that light absorption, as a function

of wavelength, is controlled by mineralogy (crystal structure and chemical composition). Geological materials can be identified based on the wavelengths at which absorption features, or troughs, appear in their reflectance spectra (Figure 4.2). The relative intensity or depth of the absorption feature is correlated with the amount of the material present. Traditional spectrometers measure reflectance at a single point on the sample surface. Imaging spectrometers measure reflectance for all possible spatial positions on the target within the sensor's field of view. Accordingly, each pixel of the digital image contains a reflectance spectrum (Figure 4.2). The term "hyperspectral" refers to the fact that reflectance measurements are collected in many narrow, contiguous intervals, known as bands, resulting in the creation of smooth, detailed reflectance spectra (Clark, 1999).

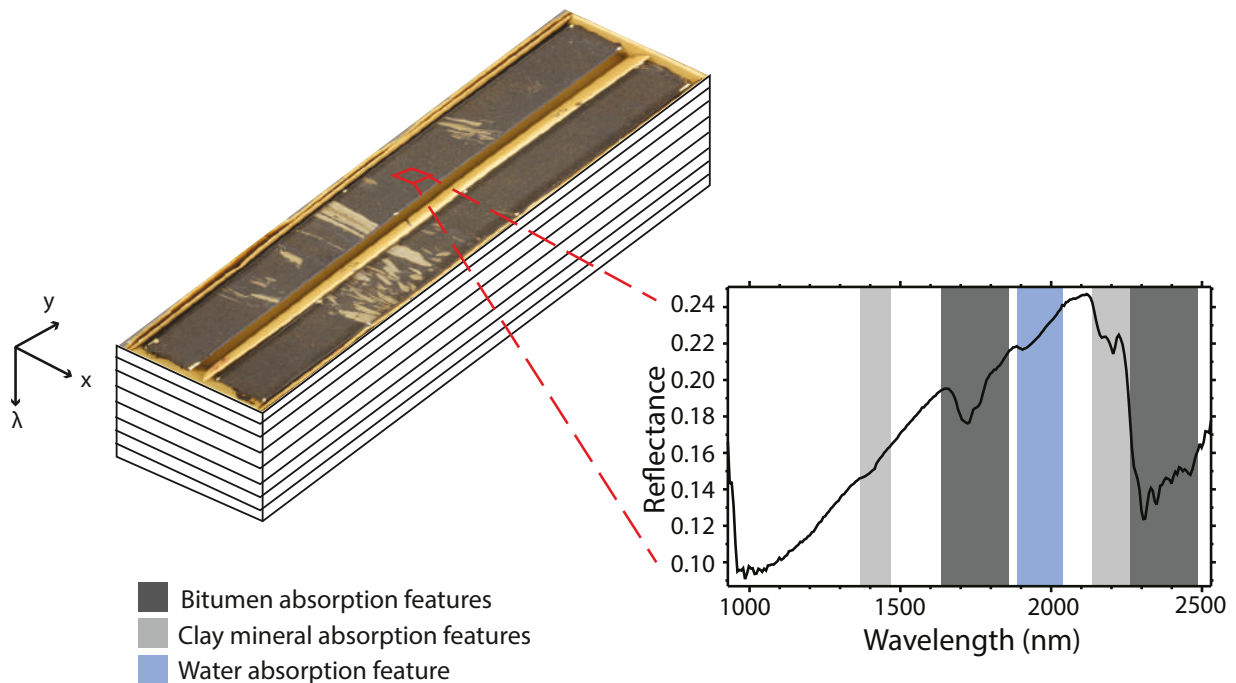


Figure 4.2 Schematic diagram of a hyperspectral data cube for a box of oil sands core. x and y represent the spatial coordinates of the pixels in the digital image and λ represents wavelength. Reflectance measurements are recorded at wavelength intervals known as bands, which are illustrated as layers in the data cube. The red box represents a pixel with its corresponding spectrum shown. Portions of the spectrum are shaded according to the legend to indicate bitumen (1700 nm and 2300 nm; dark gray), clay mineral (1400 nm and 2300 nm; light gray) and water (1900 nm; blue) absorption features.

The shortwave infrared (SWIR, 1000-2500 nm) spectral characteristics of McMurray Formation

oil sands from the Athabasca deposit have been thoroughly investigated by Cloutis (1989) and Cloutis et al. (1995). Oil sands spectra are characterized by bitumen absorption features at 1700 nm and 2300 nm (Figure 4.2), which are caused by aliphatic and aromatic C-H bond vibrations in the oil (Cloutis, 1989; Cloutis et al., 1994). The two main mineralogical constituents of McMurray Formation oil sands are quartz and clay minerals (Bayliss and Levinson, 1976). Clay minerals cause absorptions around 1400 and 2200 nm due to O-H and OH-cation bond vibrations, respectively (Hunt and Salisbury, 1970). The shape (asymmetry, width) and the precise wavelength of maximum band depth of these features varies with clay mineral type (e.g. kaolinite, montmorillonite, illite) and abundance (Clark et al., 1990). The final absorption feature at 1900 nm is caused by H-O-H bending in water (Clark, 1999). This can be due to free water, water adsorbed to clays or structural water in clays, depending on the exact wavelength of the absorption feature (Cloutis, 1989; Cloutis et al., 1995). Fluid inclusions in quartz grains may also cause absorptions at 1400 and 1900 nm. Quartz affects the overall reflectance of the oil sands, but there are no absorption features due to the quartz itself as it is not spectrally active in the SWIR (Hunt and Salisbury, 1970). In this study, hyperspectral imaging is applied for the purposes of aiding the qualitative examination of oil sands core samples. Hyperspectral imagery is investigated at different wavelengths and resolutions for the purposes of improving the visual discrimination and interpretation of sedimentary structures and trace fossils in oil-saturated strata.

4.2 Samples

Hyperspectral imagery was collected for a drill core from the Kears Lake area of the Athabasca deposit (13-17-95-8W4M, Figure 4.1). The total length of this core is approximately 136 m and it spans the entire McMurray Formation, which, in the Athabasca region, is underlain by Devonian carbonates and overlain by the glauconitic sands of the Clearwater Formation's Wabiskaw Member (Figure 4.1). The McMurray Formation is typically 40-60 m thick (Ranger, 1994) but can be <10 m or >100 m (Hein et al., 2000). This core represents a particularly thick interval of

the McMurray Formation at 119 m. The McMurray Formation is commonly informally divided into a lower fluvial member, a middle estuarine member and an upper marine member (Stewart and MacCallum, 1978; Flach and Mossop, 1985), all three of which appear in this core. A full range of bitumen saturations is also represented in this core, with oil sands ranging from 0.1 to 17.6 weight percent (wt %) bitumen. This core was drilled more than 25 years ago and is completely dehydrated and hardened from long-term exposure to ambient conditions.

4.3 Methods

Hyperspectral imagery of the core was collected at the University of Alberta using an instrument known as the SisuROCK core imaging system, which is manufactured by SPECIM, Spectral Imaging Ltd. It is one of several such instruments commercially available around the world that are specifically designed for scanning drill core samples. The main body of the unit at the University of Alberta houses two pushbroom spectral cameras and a set of quartz halogen lamps that provide incident light (Figure 4.3). One spectral camera measures visible to near-infrared reflectance (VNIR; 400-1000 nm) and the other measures shortwave infrared reflectance (SWIR; 1000-2500 nm). Core samples are loaded onto a platform that moves below the cameras at a rate set by the user. Important metadata, such as depth and well identification, is entered into the system by the user prior to scanning. The scanning platform (1.6 m long x 0.65 m wide) can hold samples weighing up to 50 kg. The system can be used in any enclosed environment that maintains an ambient temperature above 0 °C. The SWIR camera can also be removed from the housing for other applications, such as tripod-mounted field surveys.

Data was collected only in the SWIR because bitumen and clay minerals are spectrally active in this wavelength region. Technical specifications of the SWIR camera are provided in Table 4.1. The hyperspectral image is built line-by-line as the camera detects the sample. The SWIR camera is a 16-bit system, which means that radiance is recorded in each pixel as a brightness value ranging from 0 to 65,535 across 256 wavelength bands. Brightness values are converted to

reflectance by normalizing the radiance measurement from the target material against that of a Spectralon™ panel (100% reflectance) at the head of the scanning platform (Figure 4.3). For this study, data was collected at two different spatial resolutions: low (1.2-1.5 mm/pixel) and high (0.20-0.25 mm/pixel). The total time to complete a scan, including calibration measurements, was less than two minutes. For low resolution imaging, up to four boxes of core (6 m) could be scanned at a time. For high resolution, the camera is much closer to the sample and thus the field of view is narrower – approximately the width of a single core. In this case, samples were removed from the box and placed lengthwise on the platform, which allowed 1.5 m of core to be scanned at a time. Image analysis was conducted using the ENVI software package (Exelis VIS Inc.).

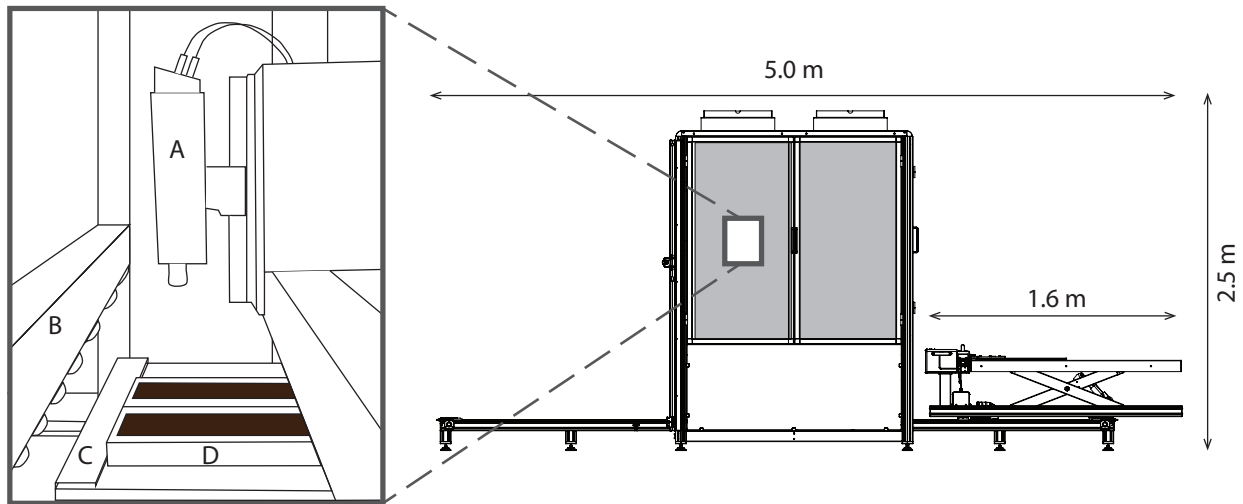


Figure 4.3 A schematic diagram of the hyperspectral imaging system used in this study. The inset shows the interior of the camera housing with the following labelled components: A) SWIR camera, B) quartz lamps, C) Spectralon™ panel, and D) box of core. The spectral camera is fixed and the platform carrying the core sample moves below it at rate set by the user.

Table 4.1 Technical specifications of the SisuROCK shortwave infrared camera and associated hyperspectral imagery.

Spectral Range	Number of Spectral Bands	Spectral Resolution	Pixel Size
970-2500 nm	256	10 nm	0.2-2.0 mm

Hyperspectral imagery of the core was analyzed by viewing single-band images as well as color composite images, which are combinations of three wavelength bands displayed in red,

green and blue (RGB) channels. Viewing different combinations of bands is a basic remote sensing analysis technique for evaluating the spectral diversity in a given image. Selecting different wavelength bands for viewing in the three channels of color allows for the emphasis or suppression of different spectral components in the scene (Mustard and Sunshine, 1999). In order to qualitatively evaluate the degree of visual enhancement of sedimentary structures and trace fossils, hyperspectral images were compared to the core samples themselves (examined visually), to high-resolution photographs of the core, and to a conventional litholog (scale 1:150, Figure 4.4).

4.4 Results

4.4.1 Band Selection

Single-band spectral images are displayed in grayscale, where each pixel is assigned a gray tone that represents the magnitude of the reflectance for that particular wavelength (Figure 4.5). The visibility of sedimentary and biogenic features in oil-saturated sections of the core used in this study was enhanced in single band imagery for all wavelength bands from 1464 nm to 2461 nm. Single-band images convey spectral variability in terms of brightness, while three-band color composites convey it in terms of both brightness and color. Various different combinations of bands were evaluated for building color composite core images. The preferred three-band combination was 2162 nm, 2199 nm and 2349 nm in the red, green and blue channels, respectively (Figure 4.5, D). This combination dramatically enhanced the visibility of sedimentological features while maintaining near-natural colors that are visually intuitive and pleasing to the eye. Comparing single-band and three-band imagery in Figure 4.5 demonstrates the advantage of color composites. Three-band images allow for the discrimination of different lithologies because they capture absorption features at multiple wavelengths, and thus capture compositional differences. Single-band images only capture the overall reflectance, which is not affected solely by mineralogy/chemical composition, but also by properties such as moisture content, grain size or surface roughness.

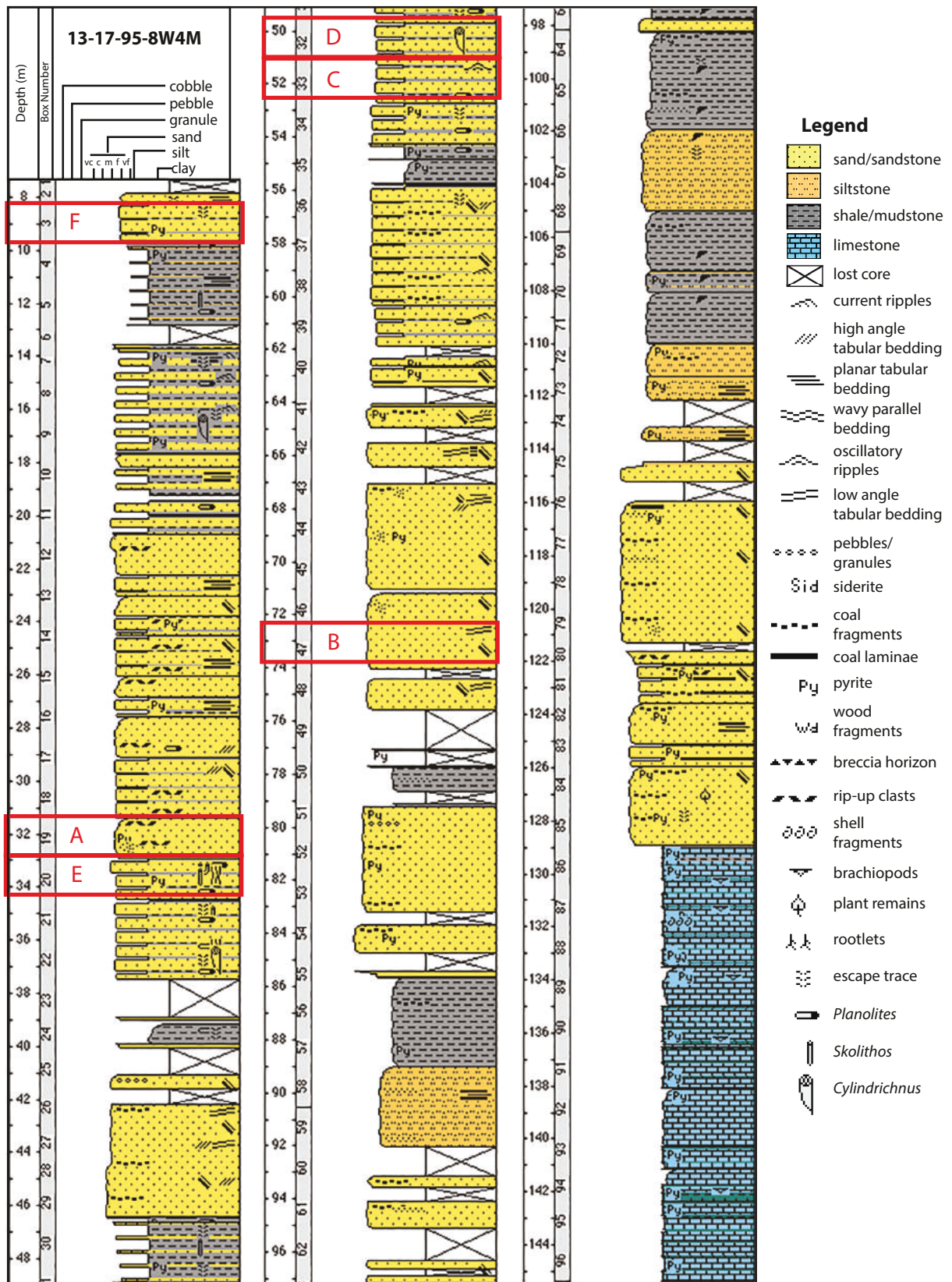


Figure 4.4 Conventional lithology of the core sample used in this study. Core was logged at a scale of 1:150 by C. Ciskowski. Locations of boxes shown in Figure 4.6 are indicated in red.

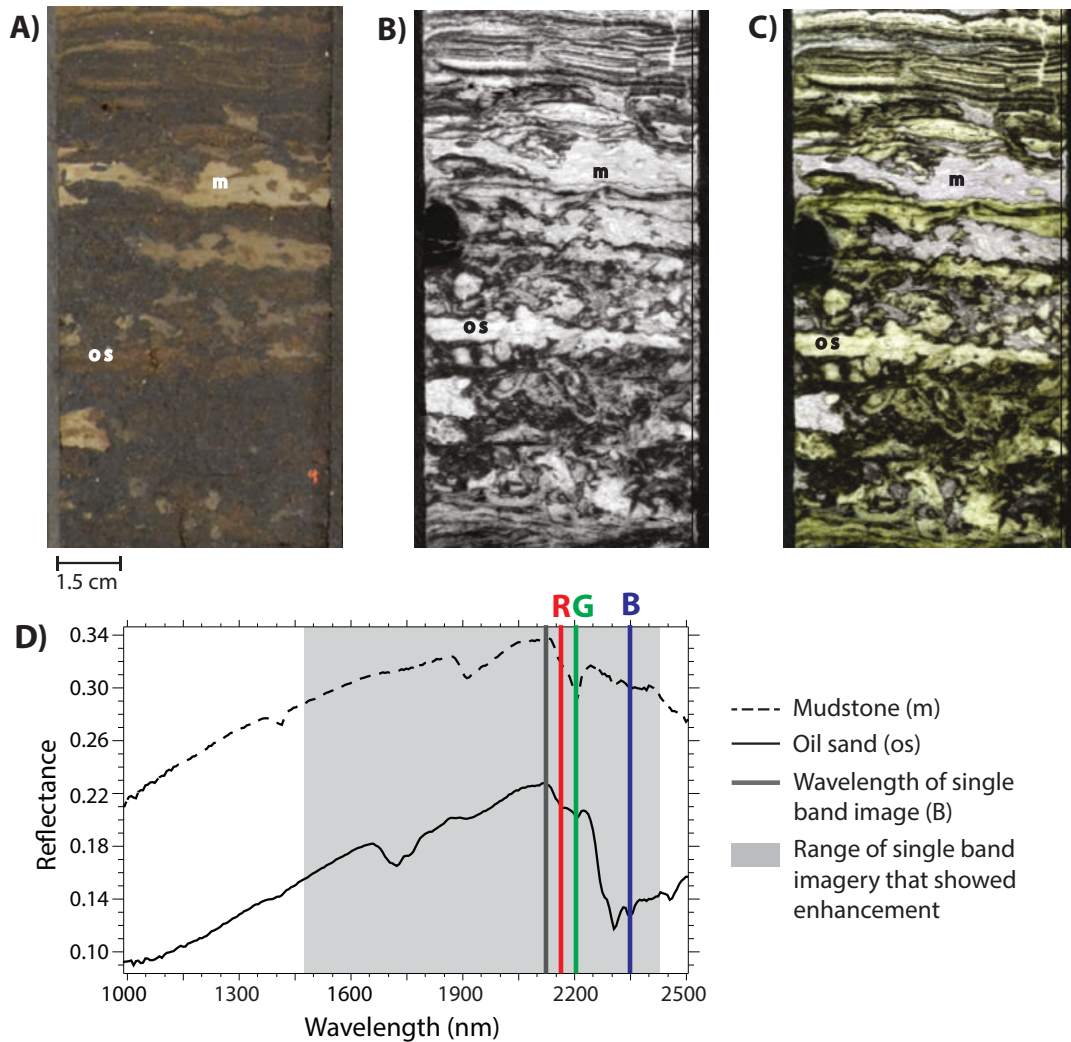


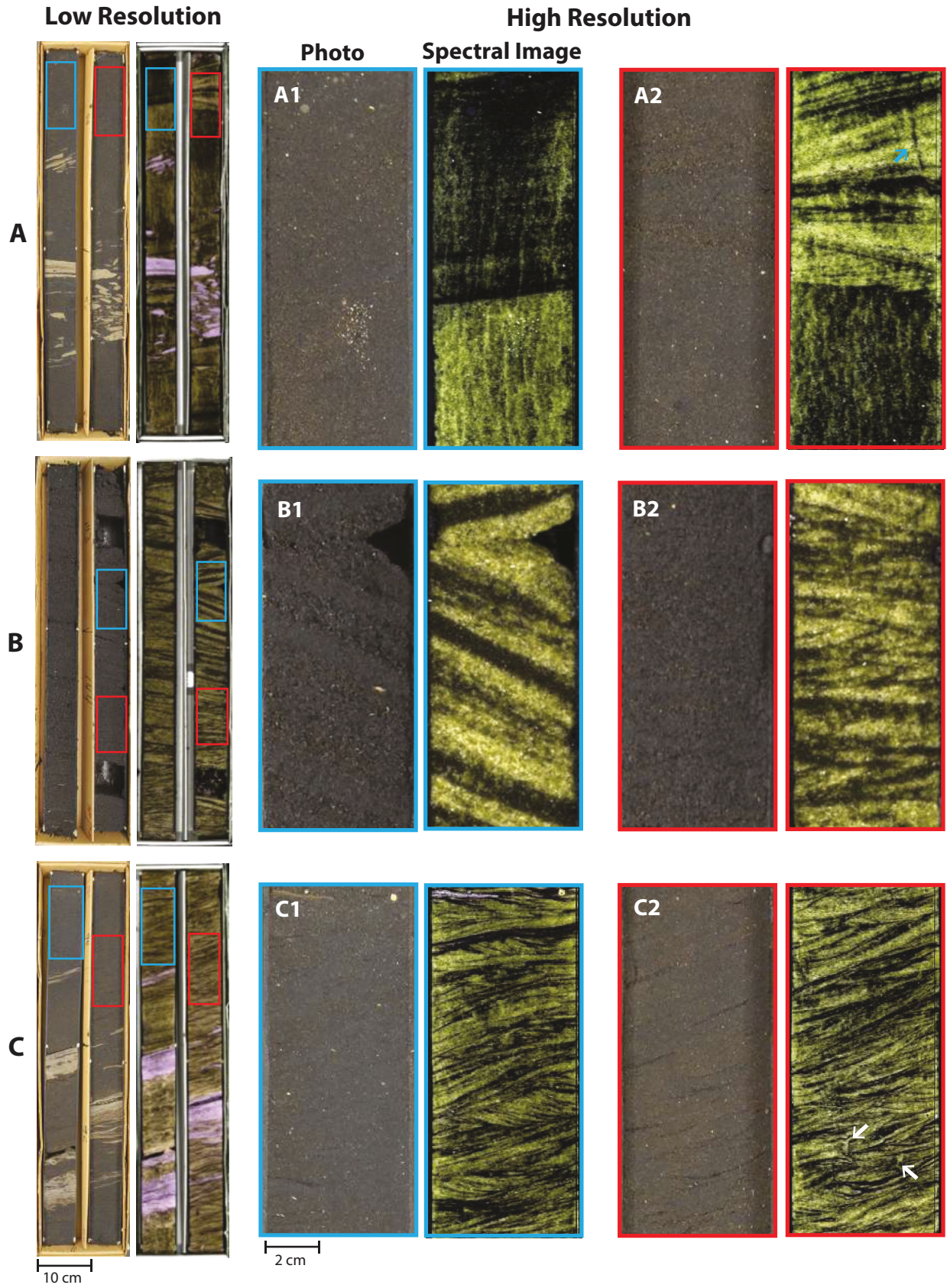
Figure 4.5 Examples of spectral imagery of the same section of core, with a photo (A) for reference. B is a single band grayscale image and C is a three-band color composite image. The reflectance spectra shown (D) are average spectra from the mudstone (dashed line, indicated by “m” on the images) and oil sand (solid line, indicated by “os” on the images) sections of this core. The light gray shaded region of the spectrum represents the range of wavelength bands in which sedimentary features were enhanced in single band imagery. The dark gray band represents the wavelength shown in the single band image. The red, green and blue bands show the three-band combination that was used to make the color composite images presented in this study. While both single-band and three-band images enhance the contrast of sedimentary features, color composites images allow for the discrimination of lithology. In image C, the green tone of the oil sand makes it easy to distinguish from the pale blue-toned mudstone, while in image B, bright sections of oil sand could easily be confused with equally bright mudstone.

4.4.2 Sedimentary Structures

Large-scale sedimentary structures (>1 cm) were clearly enhanced in both low and high resolution spectral imagery of core, and small-scale sedimentary structures (<1 cm) were best enhanced in high resolution imagery (Figure 4.6, A-C). Spectral imagery revealed abrupt contacts between low angle planar-tabular cross-stratification and massive sand (Figure 4.6, A1), and between cross-bedded sand and massive sand (Figure 4.6, A2) where the oil sand appeared entirely structureless. The visibility of bedding was also enhanced in cases where the beds could be discerned from the core and/or photographs due to the presence of grain size variability. For example, cross-stratification in McMurray Formation core is commonly characterized by alternating cm-scale coarse- and fine-grained beds of sand referred to as grain striping (*sensu* Gingras and Rokosh, 2004). The change in grain size provides a textural contrast that makes the beds discernable despite oil-saturation (Figure 4.6, B1). However, in spectral imagery the contrast between beds is greatly enhanced. Dark fine-grained beds stand out against bright coarse-grained beds, clearly showing the individual bed thicknesses as well as changes in bedding dip direction (Figure 4.6, B1). Finer scale features, like current ripple cross-stratification, are especially difficult to see in oil-saturated sand. Ripples can be inferred in the presence of parting planes formed by preferential erosion along foreset bedding surfaces (Figure 4.6, C2) but are difficult to identify when the core surface is smooth (Figure 4.6, B2; C1). Spectral image results are highly detailed, with ripple foresets visible even at low resolution and individual ripple laminae visible at high resolution (Figure 4.6, B2; C1; C2). Many of the features observed in the spectral imagery are not visible in photos, but have significant implications for the interpretation of the depositional environment.

4.4.3 Trace Fossils

The visibility of trace fossils was best enhanced using high resolution spectral imagery of the core (Figure 4.6, D-F). Ichnofossils are abundant in the middle and upper McMurray Formation, which are commonly interpreted as estuarine and marginal marine/embayed depositional



Low Resolution

High Resolution

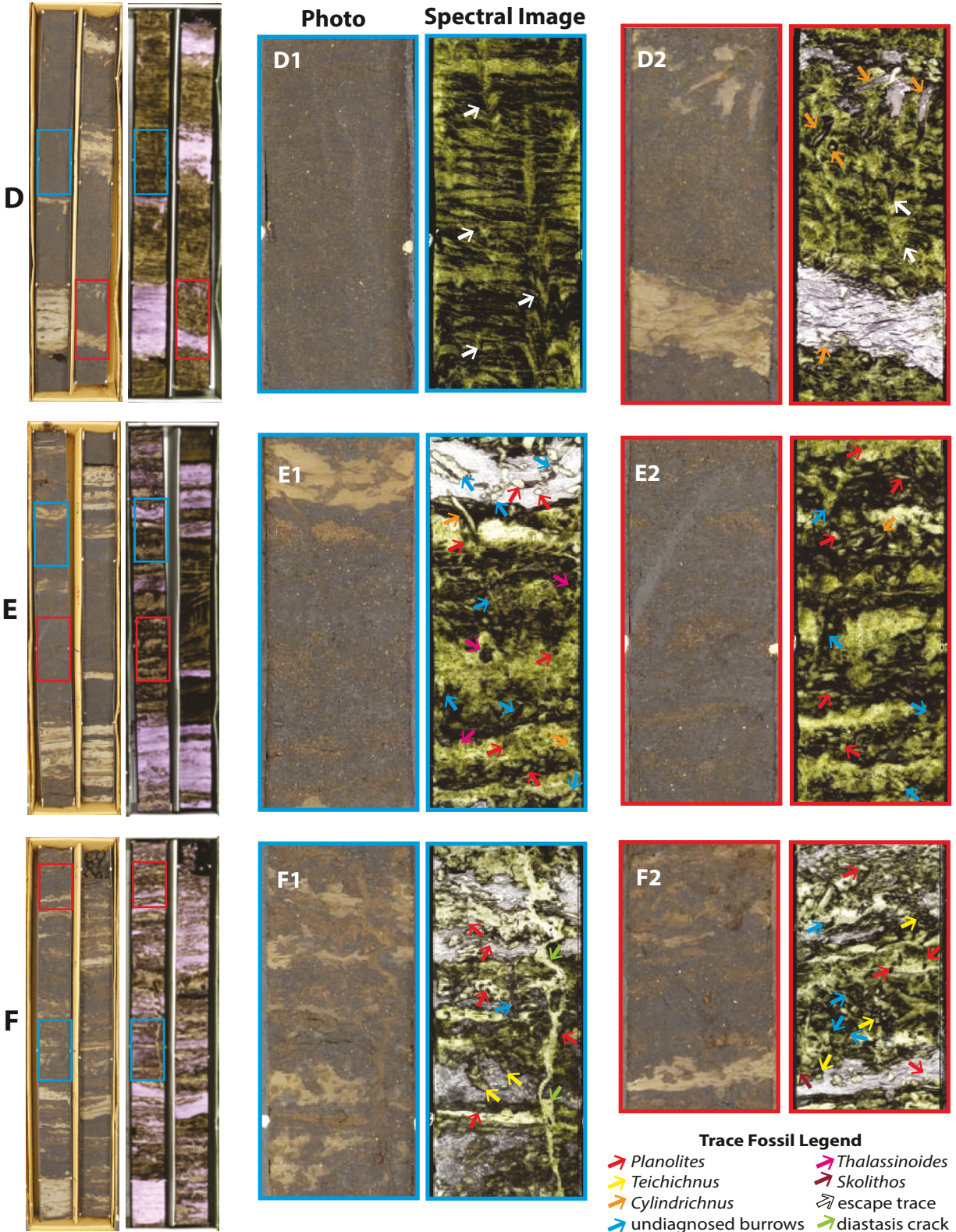


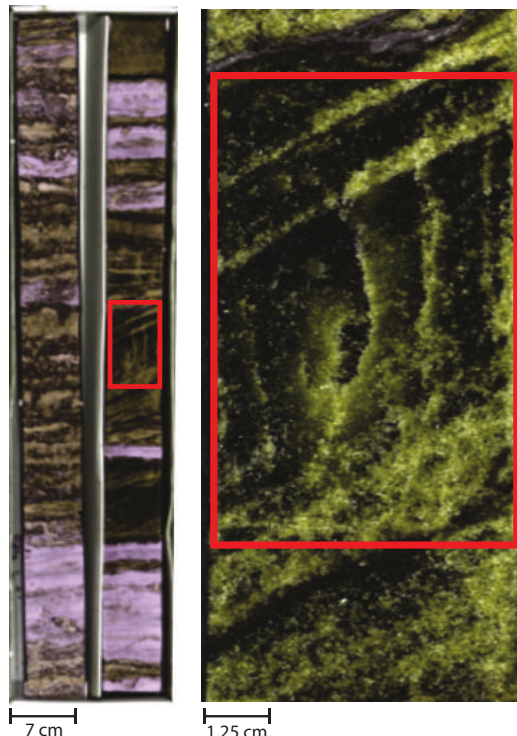
Figure 4.6 Examples of spectral imagery where the visibility of sedimentary structures and trace fossils is enhanced relative to the corresponding photographs, which are shown at the same scale. Low resolution images show the full core box and high resolution images are shown as sections of the sample as indicated with red and blue rectangles. Colored arrows indicate ichnofossils as per the legend. A1) The oil sand looks entirely structureless, but spectral imagery reveals a contact between low angle planar-tabular cross-bedded sand and massive sand. A2) Spectral imagery reveals cross-bedded sand abruptly overlaying massive sand. This contact is clear at both high and low resolution. A vertical burrow is also revealed in the high resolution spectral image. B1) Large-scale cross-stratification can be inferred in the photo due to grain size variability across the beds, but the spectral image clearly differentiates finer grained (125-500 μm) dark stripes from coarser grained (500-1000 μm) bright stripes at both low and high resolution. B2) Without grain size variability, the oil sands appear structureless. However, high resolution spectral imagery reveals current ripples. C1) Current ripples are cryptic in the photo but clearly defined in the high resolution spectral image, which also reveals the climbing nature of the ripples and intercalated sigmoidal bedding. C2) Current ripples can be discerned in the photo when there is erosion along bedding surfaces and parting planes are visible, but the high resolution spectral image reveals details such as individual foreset laminae and mm-scale escape traces. D1) Low degree of bioturbation. No primary sedimentary fabric or ichnofabric is visible in the photos. Spectral imagery reveals current ripples with abundant escape traces. D2) Moderate to high degree of bioturbation. Biogenic disturbance of primary sedimentary fabric can be inferred from the photo but discrete trace fossils are not visible if not mud-filled. Spectral image reveals escape traces as well as *Cylindrichnus* in the oil-saturated sand. E1) Moderate degree of bioturbation. Disturbance of primary sedimentary fabric is clear in mudstone bed, but ambiguous in the oil sand. Spectral image improves visual contrast of trace fossils in both the mudstone and the oil sand sections. *Planolites*, *Thalassinoides* and *Cylindrichnus* can be identified as well as numerous undiagnosed burrows. E2) Moderate degree of bioturbation. Little indication of biogenic disturbance of the sediment can be deduced from the photo. Spectral image reveals *Planolites*, *Cylindrichnus*, and undiagnosed burrows. F1) High degree of bioturbation. The magnitude of biogenic disturbance is evident from the mottled texture of the interbedded mud and sand in the photo. Spectral images reveal the full extent of the bioturbation and facilitate the identification of trace fossils, including *Planolites* and *Teichichnus*. A 17 cm long sand-filled diastasis crack (Cowan and James, 1992) can also be identified. F2) High degree of bioturbation. Abundant *Planolites*, *Teichichnus*, and *Skolithos*, as well as numerous undiagnosed burrows, are clear in the spectral image.

environments, respectively (e.g. Flach and Mossop, 1985; Hein and Cotterill, 2006). The middle McMurray is characterized by brackish water trace fossils such as *Cylindrichnus* or *Thalassinoides*, as well as *Skolithos*, *Planolites*, *Gyrolithes*, *Palaeophycus*, and vertical escape traces (Pemberton et al., 1982; Ranger and Pemberton, 1992; Hein et al., 2000; Lettley et al., 2007). The upper McMurray is host to many of the same trace fossils as the middle McMurray, as well as *Teichichnus*, *Bergaueria*, and *Chondrites*, which are consistent with higher salinities

(Pemberton et al., 1982; Ranger and Pemberton, 1992; Hein et al., 2000; Lettley et al., 2007). Degree of bioturbation can be difficult to estimate in oil sand because the bitumen masks both primary sedimentary fabrics and ichnofabrics. Individual trace fossils, often impossible to see in oil sand, are only identifiable in muddy sections of core. High resolution three-band color composite spectral images increase contrast in both oil-saturated and muddy intervals. Both primary sedimentary fabrics and ichnofabrics can be clearly identified in spectral imagery of oil sands with low to moderate degrees of bioturbation (Figure 4.6, D; E). Individual trace fossils can be clearly identified in oil-saturated sections even if highly bioturbated (Figure 4.6, F).

While low-resolution imagery provides a sufficient level of detail for the enhancement of large-scale sedimentary features, such as contacts between bedded and non-bedded sediments or cm-scale cross-stratification, high resolution imagery is necessary for the identification of trace fossils. In fact, for the novice eye, low resolution imagery has the potential to cause confusion as some insignificant features may become highly visible. For example, fine-scale surficial fractures, which are evident at high resolution, may be confused for vertical burrows at low resolution (Figure 4.7).

Figure 4.7 An example of low resolution spectral imagery that demonstrates why a higher resolution is required for accurate identification of trace fossils. At low resolution (left), the features enclosed in the red rectangle may appear like vertical burrows. At high resolution (right), it becomes clear that these features are merely surficial fractures.



4.5 Discussion

Sedimentary structures and trace fossils are only visible in rocks at the hand sample (cm or dm) scale if a change in grain size or mineralogy visually defines the feature. When contrast is lacking in highly homogeneous sediments, or is masked by oil-saturation, the alignment of mineral grains into beds may be too subtle to observe with the unaided eye. In the SWIR spectral imagery of oil sands core produced in this study, sedimentary and biogenic features are readily perceived because they are visually defined by dark (low reflectance) and bright (high reflectance) domains. In order to investigate the cause of the enhanced visibility of sedimentary and biogenic features in SWIR spectral imagery, the spectral characteristics of bright and dark domains were investigated.

In some samples, the change in reflectance between dark and bright domains corresponded with a visible change in grain size, but in other samples there was no visible grain size change across bright and dark domains. These two cases are referred to as Type 1 and Type 2, respectively.

Type 1 spectral response was observed in fine to coarse sand sized oil sands with large-scale (>1 cm) sedimentary features such as bedding and grain striping (Figure 4.8, A). In Type 1 samples, bright domains in the spectral image correspond to coarse-grained beds (medium to coarse sand) and dark domains correspond to fine-grained beds (fine sand). Bitumen content imagery produced using a spectral model described in Speta et al. (2015) revealed that bitumen saturation is variable across bright and dark domains (Figure 4.8, A). This observation is confirmed by investigating mean spectra of bright and dark domains (Figure 4.9). The Type 1 bright domain spectrum has a deeper bitumen absorption feature in continuum-removed spectra than the Type 1 dark domain (Figure 4.9, B), where depth refers to the intensity of the absorption band as measured from the continuum. This indicates that bright domains have higher degrees of bitumen saturation than dark domains.

Type 2 spectral response was observed in very fine to fine sand sized oil sands and in interbedded

sands and muds (Figure 4.8, B). Bright and dark domains define fine-scale features such as individual current ripple laminae. In Type 2 samples, no grain size change between dark and bright domains can be observed with the unaided eye. Unlike Type 1 samples, features defined by bright and dark domains in Type 2 samples do not appear clearly in the corresponding bitumen content image (Figure 4.8, B). This suggests that bitumen content does not vary between reflectance domains, which is supported by the fact that there is no difference in the depth of the bitumen feature in bright and dark Type 2 spectra (Figure 4.9, B).

The shape of the continuum-removed 2200 nm clay absorption feature varied between Type 1 and 2 samples, but not between bright and dark domains within each type (Figure 4.9, C). This variability could be due to differences in the relative abundances of different clay minerals, and is not surprising considering that Type 1 and 2 samples have different sedimentological characteristics. In Type 2 samples, the depth of the 2200 nm clay feature was deeper for dark domains than bright domains. This suggests variability in clay content, or ratio of clay to quartz, could be a reason for the difference in contrast in Type 2 samples. The difference in clay feature depth between bright and dark domains in Type 1 samples is minor, suggesting that this is not a major factor in the variable reflectance response.

The results of the spectral analysis of bright and dark domains in spectral imagery indicate that the enhanced visibility of sedimentary and biogenic features can be attributed to changes in grain size and bitumen content in the case of Type 1 samples and to changes in relative abundance of clays in Type 2 samples. However, the observed relationships may not necessarily imply simple correlations. In oil sands, variables such as bitumen content, grain size and mineralogy are difficult to investigate independently. As in most clastic sedimentary rocks, grain size changes are often accompanied by mineralogical changes. The ratio of quartz to clay minerals, which influences reflectance response, tends to decrease with decreasing grain size. Bitumen saturation is also related to grain size; Carrigy (1962) found that oil saturation decreases as the

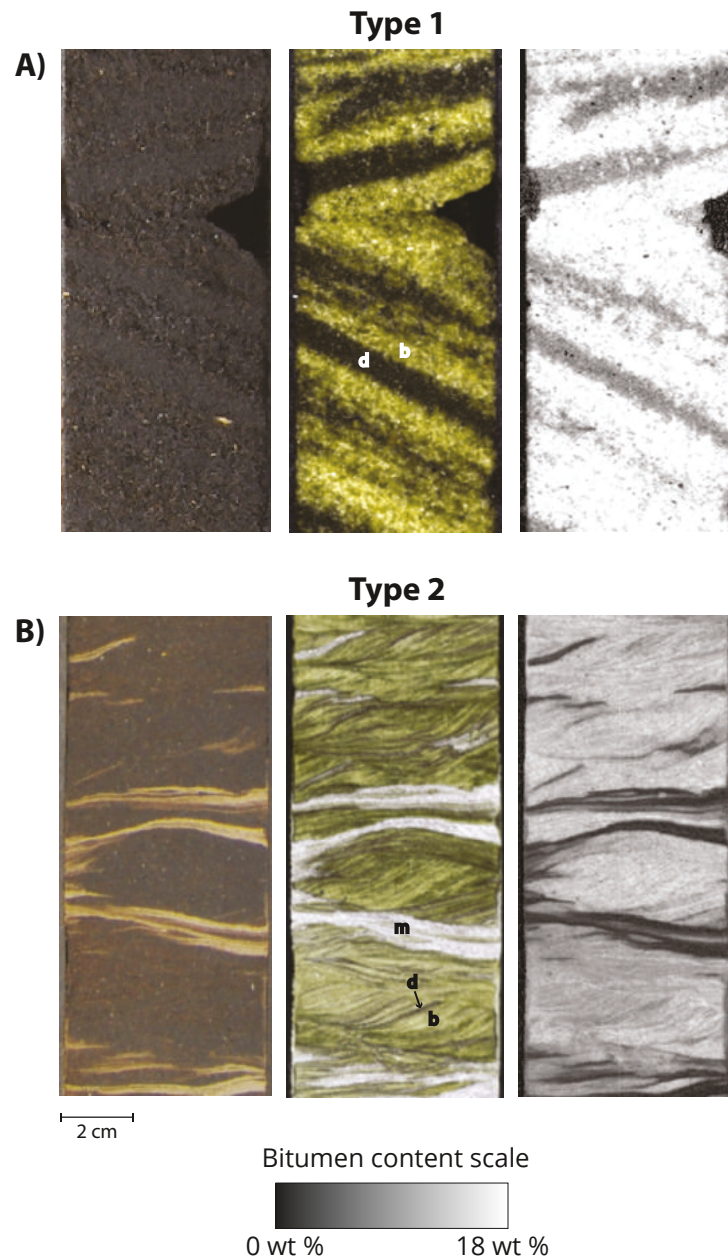


Figure 4.8 From left to right: Photo, color composite spectral image and grayscale bitumen content image of oil sands sections that showed Type 1 (A) and Type 2 (B) spectral response. In the bitumen content images, black represents 0 wt % and white represents 18 wt % oil, as shown in the color bar legend. b = bright domain, d = dark domain, m = mudstone. Bitumen content images were produced using a spectral model described in Speta et al. (2015).

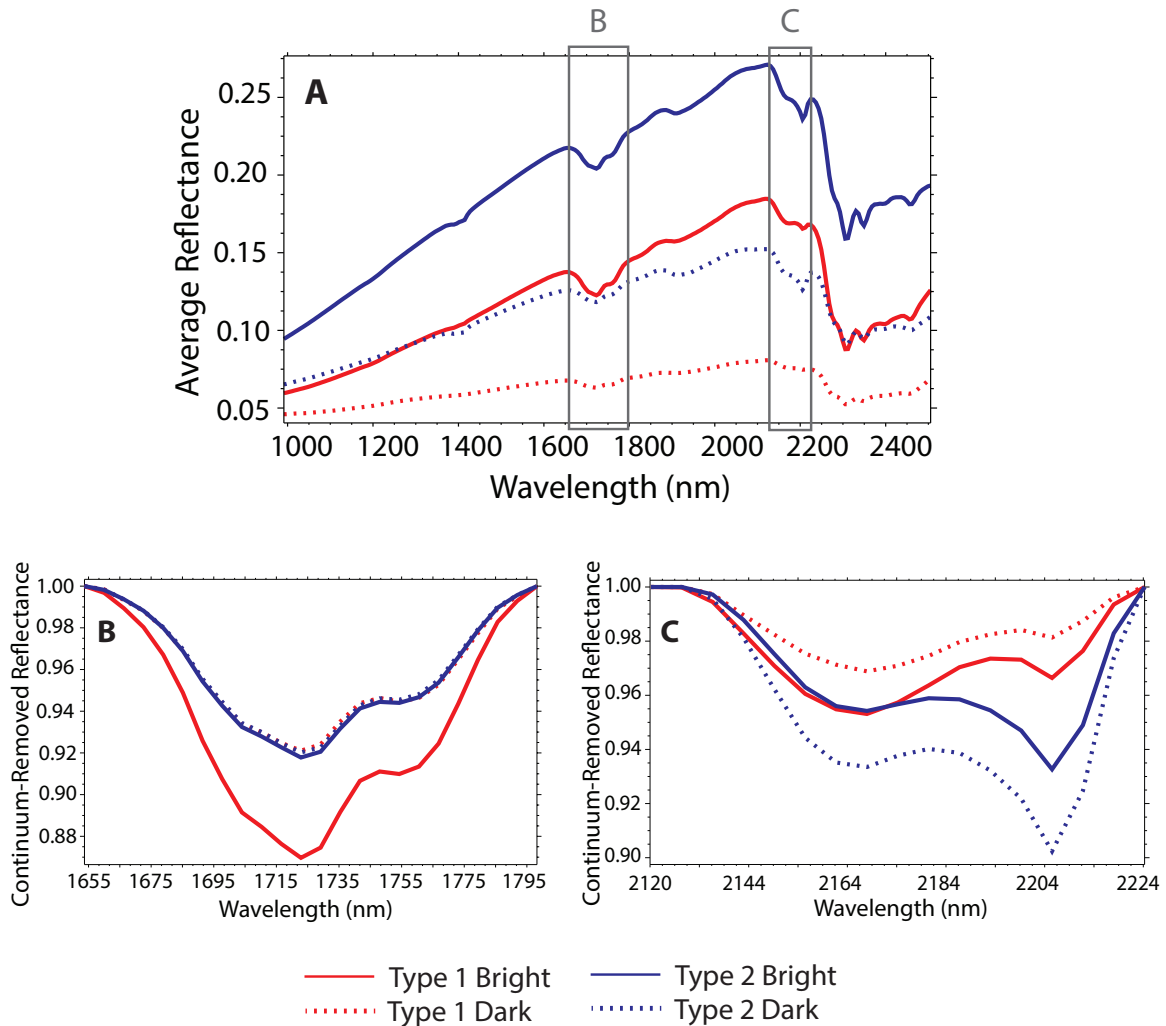


Figure 4.9 Average spectra for bright (solid lines) and dark (dashed lines) domains for Type 1 (red) and Type 2 (blue) samples. Spectra are the average of 4000-6000 pixels collected from multiple sections of core showing each type of spectral response. Plot A shows whole spectra, with gray boxes showing the wavelength ranges to which continuum-removal was applied. Plot B is the continuum-removed view of the 1700 nm bitumen absorption feature and plot C shows the continuum-removed view of the 2200 nm clay absorption feature.

median diameter of grains decreases and the fraction of clay-size particles ($<2 \mu\text{m}$) increases. Although bitumen is known to decrease reflectance, previous studies have demonstrated that there is no direct correlation between bitumen content and the overall reflectance of oil sands (Cloutis, 1989). The enhanced visibility of sedimentological features can be attributed to a combined effect of variability in bitumen content, grain size and mineralogy, but the independent relationships between each of these factors and the reflectance response of oil sands is beyond the scope of this study.

4.6 Advantages of Hyperspectral Imaging

Hyperspectral imaging has several advantages over other imaging techniques that make it attractive for the analysis of sedimentary cores. Hyperspectral imaging is fast, non-destructive, typically requires no sample preparation and imaging spectrometers are easy to use. It is an objective means of acquiring information about the core and could be highly cost-effective on a commercial scale. It provides much higher resolution than what can be obtained through downhole imaging techniques (e.g. micro-resistivity tools). Yet, arguably the greatest advantage of this method is that the spectral data can provide more information than just visual enhancement of sedimentological features. While most other imaging techniques provide data that has a single purpose, the spectral data collected for imaging oil sands core can also be used to predict bitumen content (Rivard et al., 2010; Speta et al., 2015) and automatically classify lithology (Speta et al., 2016). Preliminary results from concurrent research have demonstrated potential for the spectral characterization of clay minerals in core (Entezari et al., 2015). Further geological applications of hyperspectral imaging are emerging as this rapidly developing field of research continues to grow.

4.7 Limitations of the Technique

Unlike penetrative methods, such as x-ray radiography and CT scanning, hyperspectral imaging is a surficial technique. The depth of penetration of the incident light is on the order of tens of

microns, thus only features that are exposed on the surface of the sample can be detected. For the same reason, any damage to the surface of the core and/or the presence of dirt (e.g. from drilling) would decrease the quality of the spectral image results. Features on the sample surface with positive or negative relief, such as fractures, may be out of focus and thus poorly rendered in the spectral imagery. Naturally, this technique should supplement, not replace, traditional core logging by a trained geologist and by no means diminishes the value of looking at the rock itself.

4.8 Conclusions

The identification of sedimentary and biogenic features is one of the primary goals of sedimentary core logging, but these features can be very difficult to see in oil-saturated strata. In this study, shortwave infrared spectral imagery of Athabasca oil sands core samples was analyzed to demonstrate that hyperspectral imaging is a viable method for aiding the visual examination of oil-saturated core. Color composite imagery consisting of the three-band RGB combination of 2162 nm, 2199 nm and 2349 nm was found to enhance the visibility of sedimentary structures and trace fossils that were difficult or even impossible to see with the unaided eye. Features can be more easily perceived because spectral domains differing in overall reflectance provide visual contrast in structureless-appearing oil-saturated sand. The cause of the enhanced contrast appears to vary between samples based on their sedimentological character, with variability in grain size and bitumen content across bright and dark domains in some cases (Type 1 samples) and variability in clay abundance, or clay to quartz ratio, in other cases (Type 2 samples). Low resolution imagery (1.2-1.5 mm/pixel) was suitable for the analysis of large-scale sedimentary structures such as cm-scale bedding. Higher resolution (0.2-0.25 mm/pixel) is necessary for the accurate identification of trace fossils and for visualizing smaller scale structures, such as current ripple cross-lamination.

Spectral imaging technology is advancing rapidly and shortwave infrared spectral cameras are decreasing in cost while increasing in quality. Hyperspectral imaging is fast, non-destructive to

the sample, user-friendly and the system would be easy to integrate into existing core analysis centers. The spectral data is reproducible, could be easily integrated with well log data and can serve multiple purposes in the core analysis workflow. Hyperspectral imaging has the potential to dramatically impact conventional core logging in the oil sands, especially in high throughput facilities where time efficiency is essential. The application of hyperspectral imaging to sedimentary cores is in its infancy and additional work will investigate the broader impact of this technique. Study of core samples from outside the McMurray Formation will allow for the assessment of the applicability of hyperspectral imaging to oil-saturated sediments beyond the Athabasca oil sands.

References

- Bayliss, P., and Levinson, A.A., 1976, Mineralogical review of the Alberta oil sand deposits (Lower Cretaceous, Mannville Group), *Bulletin of Canadian Petroleum Geology*, v. 24, p. 211–224.
- Carrigy, M.A., 1962, Effect of texture on the distribution of oil in the Athabasca oil sands, Alberta, Canada, *Journal of Sedimentary Petrology*, v. 32, no. 2, p. 312–325.
- Clark, R.N., 1999, Spectroscopy of rocks and minerals, and principles of spectroscopy, in: A.N. Rencz (Ed.), *Remote Sensing for the Earth Sciences: Manual of Remote Sensing*, John Wiley & Sons, Inc., p. 3–58.
- Clark, R.N., King, T.V.V., Klejwa, M., and Swayze, G.A., 1990, High spectral resolution reflectance spectroscopy of minerals, *Journal of Geophysical Research*, v. 95, no. B8, p. 12653–12680.
- Cloutis, E., 1989, Spectral reflectance properties of hydrocarbons: Remote-sensing implications, *Science*, v. 245, p. 165–168.
- Cloutis, E., Gaffey, M., and Moslow, T., 1994, Spectral reflectance properties of carbon-bearing materials, *Icarus*, v. 107, p. 276–287.
- Cloutis, E., Gaffey, M., and Moslow, T., 1995, Characterization of minerals in oil sands by reflectance spectroscopy, *Fuel*, v. 74, p. 874–879.
- Cowan, C., and James, N., 1992, Diastasis cracks: Mechanically generated synaeresis-like cracks in Upper Cambrian shallow water oolite and ribbon carbonates, *Sedimentology*, v. 39, no. 6, p. 1101–1118.
- Crowley, J.K., 1986, Visible and near-infrared spectra of carbonate rocks: Reflectance variations related to petrographic texture and impurities, *Journal of Geophysical Research*, v. 91, p. 5001–5012.
- Deaton, B.C., and Balsam, W.L., 1991, Visible spectroscopy - A rapid method for determining hematite and goethite concentration in geological materials, *Journal of Sedimentary Research*, v. 61, p. 628–632.
- Entezari, I., Speta, M., Rivard, B., and Geramian, M., 2015, Hyperspectral characteristics of oil sands clay mineral assemblages (abs.), Cosia/PTAC Oil Sands Clay Workshop & Conference, April 28–29, 2015, Edmonton, AB, 1 p.
- Flach, P. D., and Mossop, G.D., 1985, Depositional environment of Lower Cretaceous McMurray Formation, Athabasca oil sands, Alberta, *AAPG Bulletin*, v. 69, no. 8, p. 1195–1207.
- Fox, A.J., 1988, The Lower Cretaceous McMurray Formation in the subsurface of Syncrude oil sands lease 17, Athabasca oil sands, northeastern Alberta: A physical sedimentological study in an area of exceptional drill core control, MSc thesis, University of Alberta, Edmonton, AB, 245 p.
- Gaffey, S.J., 1985, Reflectance spectroscopy in the visible and near-infrared (0.35–2.55 μm): Applications in carbonate petrology, *Geology*, v. 13, p. 270–273.

- Gingras, M.K., and Rokosh, D., 2004, A brief overview of the geology of heavy oil, bitumen and oil sand deposits (abs.), CSEG National Convention: Great Explorations - Canada and Beyond, Calgary, AB, 3 p.
- Hein, F. J., D. K. Cotterill, and H. Berhane, 2000, An atlas of lithofacies of the McMurray Formation Athabasca oil sands deposit, northeastern Alberta: Surface and subsurface, Earth Sciences Report 2000-07, Alberta Geological Survey, Edmonton, AB, 217 p.
- Hein, F.J., and Cotterill, D.K., 2006, The Athabasca oil sands - A regional geological perspective, Fort McMurray area, Alberta, Canada, *Natural Resources Research*, v. 15, no. 2, p. 85-102.
- Hunt, G.R., 1977, Spectral signatures of particulate minerals in the visible and near infrared, *Geophysics*, v. 42, p. 501–513.
- Hunt, G.R., and Ashley, R.P., 1979, Spectra of altered rocks in the visible and near infrared, *Economic Geology*, v. 74, p. 1613–1629.
- Hunt, G.R., and Salisbury, J.W., 1970, Visible and near-infrared spectra of minerals and rocks: I. Silicate Minerals, *Modern Geology*, v. 1, p. 283–300.
- Kruse, F.A., 1996, Identification and mapping of minerals in drill core using hyperspectral image analysis of infrared reflectance spectra, *International Journal of Remote Sensing*, v. 17, p. 1623–1632.
- Lettley, C.D., Pemberton, S.G., Gingras, M.K., Ranger, M., and Blakney, B.J., 2007, Integrating sedimentology and ichnology to shed light on the system dynamics and paleogeography of an ancient riverine estuary, in: MacEachern, J.A., Bann, K.L., Gingras, M.K., and Pemberton, S.G. (Eds.), *Applied Ichnology*, SEPM (Society for Sedimentary Geology) Short Course Notes Vol. 52, p. 147–165.
- Mossop, G.D., and Flach, P.D., 1983, Deep channel sedimentation in the Lower Cretaceous McMurray Formation, Athabasca oil sands, Alberta, *Sedimentology*, v. 30, p. 493-509.
- Mustard, J.F., and Sunshine, J.M., 1999, Spectral Analysis for Earth Science: Investigations Using Remote Sensing Data, in: A.N. Rencz (Ed.), *Remote Sensing for the Earth Sciences: Manual of Remote Sensing*, John Wiley & Sons, Inc., p. 251–306.
- Pemberton, S.G., Flach, P.D., and Mossop, G., 1982, Trace fossils from the Athabasca oil sands, Alberta, Canada, *Science*, v. 217, p. 825–827.
- Phillips, C., DiFoggio, R., and Burleigh, K., 1991, Extracting information from digital images of core, SCA Conference Paper #9125, Society of Core Analysts 5th Technical Conference, p. 1–20.
- Ranger, M., 1994, A basin study of the southern Athabasca oil sands deposit, PhD thesis, University of Alberta, Edmonton, AB, 289 p.
- Ranger, M.J., and Gingras, M.K., 2003, *Geology of the Athabasca Oil Sands: Field Guide & Overview*, I.C.E. 2004: CSPG CHOA CWLS Joint Conference Field Trips & Short Courses, Calgary, AB, Canadian Society of Petroleum Geologists, 123 p.
- Ranger, M.J., and Pemberton, S.G., 1992, The sedimentology and ichnology of estuarine point bars in the McMurray Formation of the Athabasca oil sands deposit, northeastern Alberta, Canada, in: Pemberton, S.G. (Ed.), *Applications of Ichnology to Petroleum Exploration: A*

Core Workshop, SEPM (Society for Sedimentary Geology), p. 401–421.

Rivard, B., Lyder, D., Feng, J., Gallie, A., Cloutis, E., Dougan, P., Gonzalez, S., Cox, D., and Lipsett, M.G., 2010, Bitumen content estimation of Athabasca oil sand from broad band infrared reflectance spectra, *The Canadian Journal of Chemical Engineering*, v. 88, p. 830–838.

Rothwell, R.G., 2006, *New Techniques in Sediment Core Analysis*, Geological Society Special Publication No. 267, London, 266 p.

Speta, M., Rivard, B., Feng, J., Lipsett, M., and Gingras, M.K., 2015, Hyperspectral imaging for the determination of bitumen content in Athabasca oil sands core samples, *AAPG Bulletin*, v. 99, no.7, p. 1245–1259.

Speta, M., Rivard, B., and Feng, J., 2016, Longwave infrared (8-12 μm) spectral imaging for the automated mapping of lithofacies in Athabasca oil sands core (abs.), AAPG Annual Convention & Exhibition, June 19-21, 2016, Calgary, AB, 1 p.

Stewart, G.A., and MacCallum, G.T., 1978, *Athabasca Oil Sands Guidebook*, Canadian Society of Petroleum Geologists, Calgary, AB, 33 p.

Chapter 5

Automated lithological mapping of McMurray Formation oil sands core with shortwave (1.0-2.5 μm) and longwave infrared (8-12 μm) hyperspectral imaging

5.1 Introduction

Drill core sampling is one of the principal methods for investigating subsurface geology in the petroleum industry. Whole core sampling provides a complete record of the reservoir rock and cores are used to develop facies schemes and calibrate petrophysical well log data. Cores are also sub-sampled for the determination of mineralogical characteristics and key reservoir properties. Collecting and analyzing core is especially critical for reservoir characterization in formations that are geologically complex and lack lateral continuity, such as the McMurray Formation of the Athabasca oil sands deposit in Alberta, Canada. Oil sands are a naturally occurring mixture of quartz sand, clay minerals, water and an extra-heavy oil known as bitumen. The McMurray Formation experienced little to no post-depositional diagenesis resulting in a general lack of mineral cement, and its sands are either bitumen-saturated (oil sands) or water-saturated (barren sands) (Mossop, 1980a; 1980b). Because of the lack of cementation, the distribution of bitumen in the formation is considered a direct function of the depositional history (Mossop, 1980b; Wightman and Pemberton, 1997). The oil-saturated sands, commonly interpreted as estuarine channel deposits, typically occur as narrow, vertically stacked units segregated by impermeable shales (e.g. Mossop and Flach, 1983). The resulting complex reservoir architecture requires a high degree of drill control and makes core analysis an indispensable part of oil sands industry operations.

The first step of core analysis is recording a detailed lithological description of the rock in the form of a strip log, or litholog. Core logging is an important but time- and labour-intensive task. Traditionally done manually by geologists with a pencil and paper, core logging in the industry

today is completed digitally. High-resolution photographs of core are used in conjunction with borehole imagery and petrophysical well logs to create digital lithologs using software programs such as AppleCORE (Ranger, 2010). This so-called digital core logging has many benefits, making the process less tedious, more efficient and allowing for core logging to be done anywhere, even without direct access to the core sample itself. It also creates a digital record of the core that can be accessed from anywhere in conjunction with associated petrophysical data. However, a significant degree of manual labour and expert knowledge is still required. Core logging is inherently subjective and the quality of the results inevitably depends on the experience of the logger.

Hyperspectral imaging is a remote sensing technique that is highly relevant to drill core analysis. Also known as imaging spectroscopy, hyperspectral imaging can be defined as reflectance spectroscopy in the spatial context of digital imaging. For a given wavelength range, a high resolution digital image is obtained and a reflectance measurement, or spectrum, is collected in every pixel of the digital image. Because the absorption of light in such data is largely controlled by the target material's chemical composition, geological materials like minerals and oil can be identified based on the wavelengths at which absorption features appear in their reflectance spectra. Quantitative information can also be obtained as the relative intensity of the absorption features is directly correlated with the abundance of the material. The application of hyperspectral imaging for the analysis of drill core has been a growing field since the early work of Kruse (1996), who demonstrated proof of concept for the mapping of a variety of minerals in spectral imagery of Cu-Au porphyry core. This method has since been applied for the classification of minerals and rocks in various types of cores, including sulfide-bearing igneous and metamorphic rocks (Feng et al., 2011; Kruse et al., 2012), iron oxide-copper-gold deposits (Huntington et al., 2006; Tappert et al., 2011), rare earth element deposits (Turner et al., 2014), and kimberlites (Tappert et al., 2015). In the mineral resources industry, hyperspectral imaging is also becoming a means of creating digital core databases. For example, in 2014 the Geological

Survey of Sweden began a project that will see 200 km of the institution's archive core scanned and digitized (Geological Survey of Sweden, 2014).

The application of hyperspectral imaging to sedimentary cores and to research problems in the petroleum industry is not at the same stage of development. Lang et al. (1990) demonstrated that reflectance spectra collected from sedimentary drill core could be used to characterize both the mineralogy and the lithology of the sample. Recent studies have investigated the application of hyperspectral imaging to oil sands core for the purposes of determining bitumen saturation and mapping the spatial distribution of the oil (Speta et al., 2015), and spectral imagery has been shown to enhance the visibility of sedimentary structures and trace fossils in oil-saturated sediments (Speta et al., in press). However, hyperspectral imaging has yet to be applied for rock type classification in oil sands cores. This study aims to evaluate the potential of hyperspectral imaging for the automated mapping of lithological units in McMurray Formation drill core. Two wavelength ranges are investigated, the shortwave infrared (SWIR, 1.0-2.5 μm) and the longwave infrared (LWIR, 8-12 μm), in order to capture the absorption features of all the major components of the McMurray Formation. If different sedimentary lithologies can be discriminated based on their reflectance spectra, and an automatic classification technique can be used to identify them in hyperspectral imagery of core, efficiency could be increased and subjectivity decreased in routine logging operations. This study is a primary investigation that ultimately aims to contribute to the broader goal of developing a robust, accurate and efficient method for the automated detection and mapping of lithological units in oil sands core.

5.2 Oil Sands Reflectance Spectroscopy

The application of hyperspectral imaging for geological mapping hinges on the interpretation of rock and mineral reflectance spectra. A reflectance spectrum of a rock is the combination of the reflectance spectra of its constituent minerals. Absorption features in the reflectance spectra of minerals are caused either by electronic processes at the atomic level or by vibrational processes

at the molecular level. Electronic absorption features, caused by the migration of electrons in response to incoming radiant energy, are typical of transition metal-bearing minerals. These absorption features occur primarily in the visible to near infrared (0.4-1.0 μm) portion of the electromagnetic spectrum and appear as troughs in reflectance spectra (Hunt and Salisbury, 1970; Hunt, 1977). Vibrational absorption features, caused by bond vibrations that induce a change in the dipole moment of the molecule, occur as troughs in the shortwave infrared (SWIR, 1.0-2.5 μm) but primarily induce reflectance peaks in the longwave infrared (LWIR, 8-12 μm) (Hunt and Salisbury, 1970; Hunt, 1977; Salisbury et al., 1991).

Bitumen, water and McMurray Formation minerals like clays and siderite are all spectrally active in the SWIR. Absorption features in clay minerals are caused by O-H and cation-OH bond vibrations. All clay minerals will show hydroxyl absorptions around 1.4 μm and 2.2 μm , but the width, symmetry and wavelength of maximum band depth of the features varies with the type of clay and the presence of substituting cations (Clark et al., 1990; Bishop et al., 2008). An absorption feature around 1.9 μm due to H-O-H stretching and bending of water molecules is also common in clays, either due to structural water in swelling clays, or adsorbed water in non-swelling clays (Hunt and Salisbury, 1970). This feature can also appear due to the presence of free water, or water inclusions in minerals such as quartz (Hunt and Salisbury, 1970). Siderite spectra are characterized by the combination of a broad electronic absorption feature at 1.0-1.2 μm due to iron and a vibrational feature caused by the carbonate anion at 2.53 μm (Hunt and Salisbury, 1971; Hunt, 1977). Clay, water and siderite absorption features can be observed in oil sands spectra even in the presence of bitumen, which decreases both overall reflectance and spectral contrast (Cloutis et al., 1995). Bitumen itself causes absorption features at 1.7 μm and 2.3 μm due to C-H bond vibrations (Cloutis, 1989).

Quartz, the main mineralogical component of the McMurray Formation, is not spectrally active in the SWIR. Quartz is spectrally active in the LWIR where Si-O bond vibrations cause strong

reflectance peaks (Hunt and Salisbury, 1975). Quartz is characterized by a distinctive doublet peak at 9.2 μm caused by asymmetric Si-O-Si stretching (Salisbury et al., 1991; Clark, 1999). Clay minerals and siderite are also spectrally active in the LWIR. In clays, Si-O stretching causes peaks around 9-10 μm , the exact wavelength and number of peaks varying with clay type (Michalski et al., 2006; Bishop et al., 2008). Substitution of metal cations (e.g. Al, Fe) for Si may shift these features to longer wavelengths, up to 12 μm (Michalski et al., 2006; Bishop et al., 2008). Absorption features also appear in the 10-12 μm region due to cation-OH bending vibrations in clays (Bishop et al., 2008). Carbonate minerals, including siderite, display a reflectance peak near 11.4 μm due to C-O bending (Salisbury et al., 1991; Lane and Christensen, 1997). Bitumen, like other hydrocarbons, is not spectrally active in the LWIR (Lammoglia and Filho, 2011). The SWIR and LWIR absorption features of bitumen and McMurray Formation minerals are summarized in Table 5.1.

Table 5.1 SWIR and LWIR absorption features typical of the McMurray Formation rocks investigated in this study.

	Absorption Feature (μm)	Description	References
Bitumen	1.7	troughs; C-H bond vibrations	Cloutis (1989)
	2.3		
Clay minerals	1.4	trough; O-H bond vibrations	Clark et al. (1990), Bishop et al. (2008)
	1.9	trough; H-O-H bending	
	2.2	trough; cation-OH vibrations	
	9-10	peak(s); Si-O stretching	Bishop et al. (2008)
	11-12	troughs; O-H bending	
Siderite	1.0-1.2	broad trough; Fe electronic absorption	Hunt (1977), Hunt & Salisbury (1971)
	2.5	trough; C-O vibration	
	11.4	peak; C-O bending	Salisbury et al. (1991), Lane & Christensen (1997)
Quartz	8.2-9.2	doublet peak; asymmetric Si-O-Si stretching	Salisbury et al. (1991), Clark (1999)

5.3 Study Area & Samples

5.3.1 Geological Context

The Lower Cretaceous McMurray Formation is the main reservoir unit in the Athabasca oil sands, which is the largest of three oil sands deposits in northeastern Alberta, Canada (Figure 5.1). The McMurray Formation makes up the lower subdivision of the Mannville Group, underlain by Devonian carbonates and overlain by the shales of the Lower Cretaceous Clearwater Formation. The top of the McMurray Formation is defined by the appearance of glauconite in the Wabiskaw Member, which is the sandy basal unit of the Clearwater Formation that is also oil-saturated in much of the Athabasca (Carrigy, 1959; 1963). The McMurray Formation is commonly divided into three informal units consisting of a lower fluvial member, middle estuarine member and upper marine member (Stewart and MacCallum, 1978; Flach and Mossop, 1985). The main lithology of the McMurray Formation is uncemented quartz sand with lesser amounts of siltstone and mudstone/shale (Carrigy, 1963). Other phases that are commonly encountered in the McMurray Formation include siderite, coal (laminae or fragments), pyrite, wood fragments and paleosol horizons. The McMurray Formation sands are mineralogically mature (95% quartz, 5% clay minerals, feldspar and lithic fragments), predominantly very fine to fine grained (62.5-250 μm) and moderately well-sorted (Bayliss and Levinson, 1976; Mossop, 1980a). Bitumen saturation can be up to 18 weight percent (wt %); greater than 10 wt % is considered high grade ore, 6-10 wt % moderate grade and less than 6 wt % low grade ore (Mossop, 1980a).

5.3.2 Samples

A drill core from the northern end of the Athabasca deposit (13-17-95-8W4M) that spans the entire McMurray Formation was selected for this study (Figure 5.2). This particular core was chosen because of its lithological and sedimentological heterogeneity. It displays oil sands ranging in grain size from very fine sand to very coarse sand, interbedded sands and muds, inclined heterolithic stratification (IHS), intraclast breccia, barren sands, silts and muds, siderite

clasts and gravel beds. A complete range of bitumen saturation (0.1-17.6 wt %) is represented in the ~100 m thick section of McMurray Formation represented in this core. Individual boxes are made of cardboard and each box contains 1.5 m of core encased in black ABS plastic tubing that has been longitudinally split to provide a flat, clean surface for viewing. The core is completely dehydrated through long-term exposure (>25 years) to ambient conditions. This study focuses on five rock types: oil sand, barren sand, siltstone, mudstone, and siderite. The four siliciclastic lithologies comprise the majority of the McMurray Formation and siderite is a common accessory phase. In addition to the drill core, spectral measurements for this study were also collected from a sample of pure quartz sand (medium to coarse sand size, 350-1000 μm) obtained from the University of Alberta museum collection.

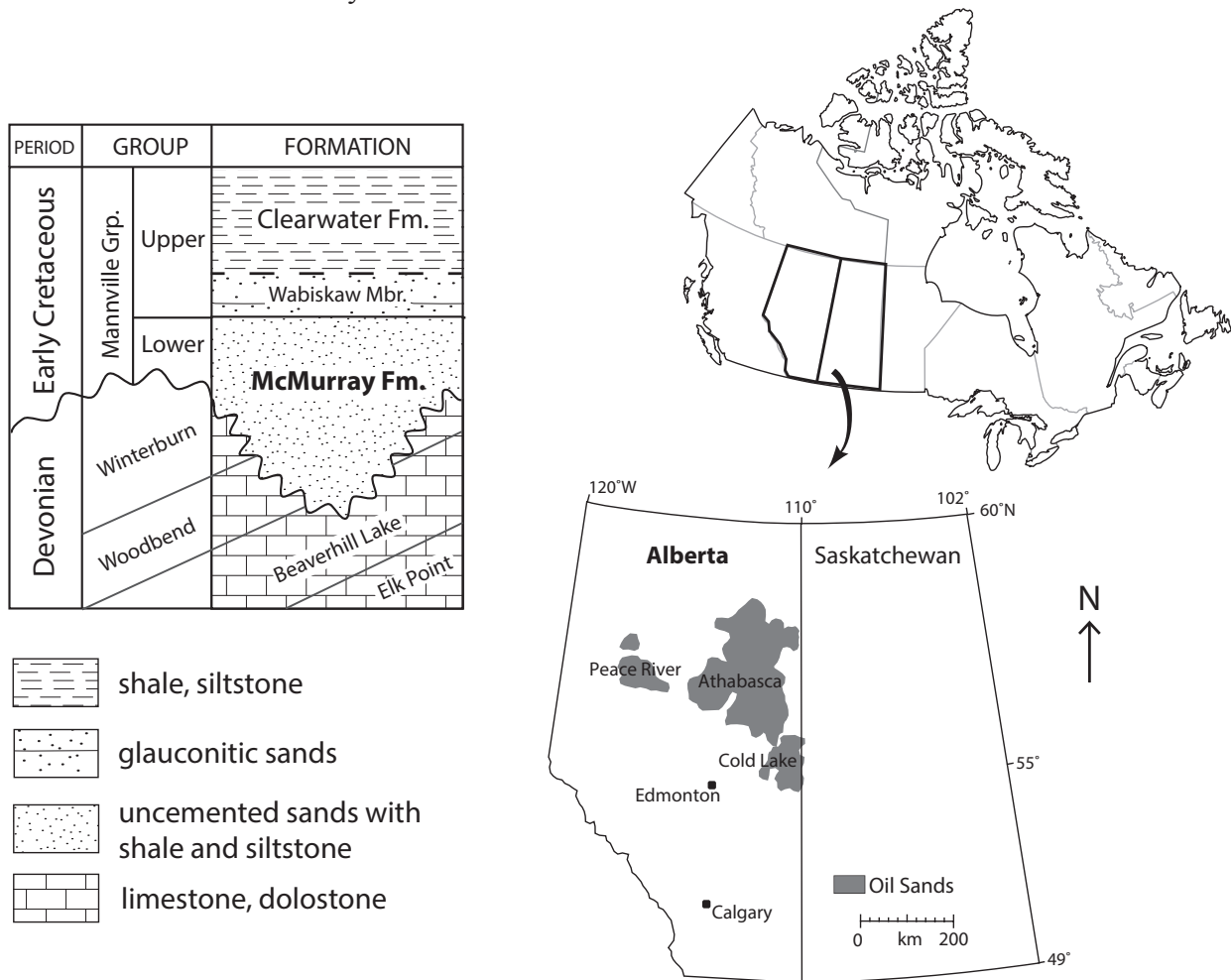


Figure 5.1 The oil sands deposits of northeastern Alberta, Canada, and the stratigraphy of the Athabasca deposit. Map modified from Ranger and Gingras (2003), stratigraphic column modified from Mossop and Flach (1983).

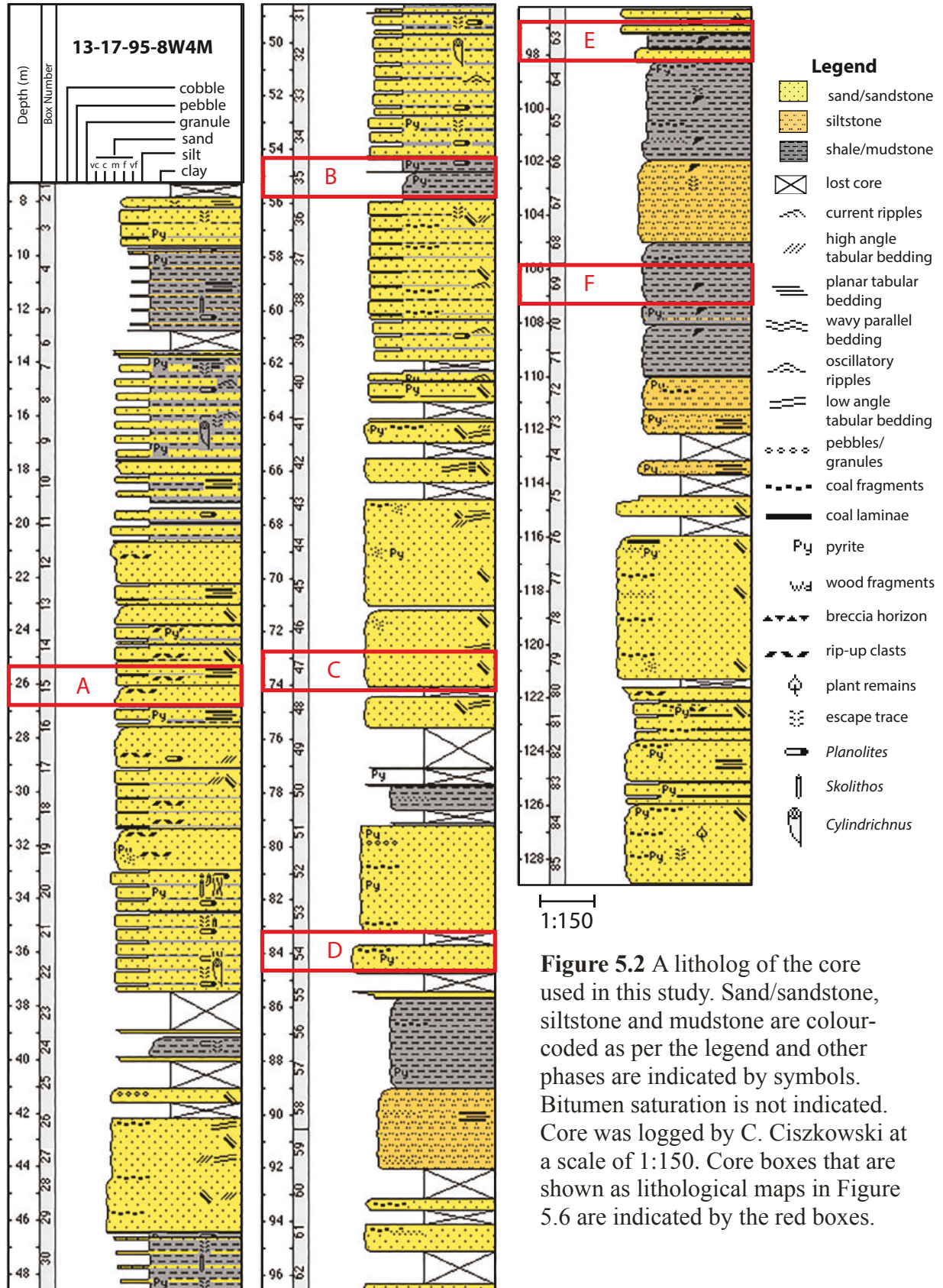


Figure 5.2 A litholog of the core used in this study. Sand/sandstone, siltstone and mudstone are colour-coded as per the legend and other phases are indicated by symbols. Bitumen saturation is not indicated. Core was logged by C. Ciszkowski at a scale of 1:150. Core boxes that are shown as lithological maps in Figure 5.6 are indicated by the red boxes.

5.4 Methods

5.4.1 Data Collection

5.4.1.1 LWIR and SWIR Spectral Imagery

LWIR and SWIR spectral imagery was collected for the drill core as well as the pure quartz sand. The LWIR imaging spectrometer used in this study is an instrument at the University of Alberta manufactured by SPECIM, Spectral Imaging Ltd. This instrument consists of a stand-alone frame that supports a spectral sensor, a radiation source, a calibration target and a height adjustable platform upon which samples are placed. The platform moves the samples under a set of glow bars that emit thermal energy. The energy is reflected from the sample back to the sensor, where a radiance value is recorded. Radiance values are converted to reflectance by normalization against a calibration measurement that is collected for each sample and a background measurement of ambient radiation. A sand-blasted aluminum panel at the head of the platform is used for the calibration measurements. The panel is uniformly rough and approximates 100% reflectance of the LWIR radiation. Background ambient radiation is determined by recording a measurement at the blackbody box, which sits next to the calibration panel. The blackbody box emulates a perfect absorber such that none of the incident radiant energy is reflected back to the sensor, so any measured radiance represents ambient background. The spectral range of the instrument is 7.3 μm to 12.3 μm , encompassed by 35 bands. The spatial resolution of the imagery collected in this study is 0.9 mm/pixel.

The same procedure was repeated in the SWIR. The SWIR imaging platform used in this study is known as the SisuROCK core scanning system and is also manufactured by SPECIM. Similar to the LWIR scanner, the SWIR system consists of a stand-alone frame that houses a pushbroom spectral sensor, a set of quartz halogen lamps (the radiation source), a calibration panel and a moving platform upon which samples are placed. The SWIR camera has a spectral range of 1.0-2.5 μm encompassing 256 bands. Dark current, or background, measurements are collected at the beginning of each scan while the sensor shutter is closed. After dark current subtraction, the

sample radiance value in each band is normalized against that of a Spectralon™ panel (~100% reflectance) to give reflectance results. Imagery was collected at a spatial resolution of 1.2 mm/pixel.

5.4.1.2 FTIR Point Spectra

High spectral resolution point spectra were collected from the pure quartz sand and from selected sections of core to aid the interpretation of the lower resolution LWIR image spectra. A hand-held Agilent 4100 Exoscan Fourier Transform infrared (FTIR) spectrometer with a diffuse reflectance sampling interface/probe was used. The Agilent 4100 FTIR has a spectral range of 2.5-15 μm , but reflectance was measured from 7.3 μm to 12.3 μm to match the range available for the LWIR imagery. This spectral range encompasses 294 wavelength bands in the FTIR spectra, compared to only 35 bands in LWIR image spectra. FTIR measurements were collected by holding the tip of the probe in contact with the sample. A background measurement from a diffuse gold disk was collected between each sample measurement. The instrument records radiance from the sample for a number of scans set by the user. The maximum number of 64 scans was used in this study. Radiance is converted to reflectance by normalizing against the background measurement, and the output is a single reflectance spectrum that is the mean of all the scans. The diameter of the measurement spot for the diffuse reflectance probe is 2 mm when focused. Multiple spot measurements were collected for each lithology from type sections on the core that were selected visually. Type sections were >1 cm wide along the length of the core to ensure that the measured reflectance was from a single rock type. The pure quartz sand was measured by pouring a sample onto wax paper and smoothing the top to create a flat surface. A final spectrum for each rock type and the quartz sand was obtained by averaging all the spot measurements for that lithology (Table 5.2).

5.4.1.3 Rietveld Analysis

Quantitative x-ray diffraction data were collected to corroborate the spectral interpretations of

barren sand, siltstone and mudstone. Rietveld analysis, also known as Rietveld refinement, is a method of processing x-ray diffraction data to obtain highly accurate quantitative results. Data collection and analyses were completed at the X-ray Diffraction Facility at the University of British Columbia. Approximately 5 g samples were collected using a small Dremel tool from one type section of each of the three rock types listed above. The samples were shipped to the University of British Columbia where they were ground to <10 µm grain size under ethanol in a vibratory McCrone Micronizing Mill for ten minutes. X-ray powder diffraction data were collected over the range of 3-80° 2θ with CoKα radiation on a Bruker D8 Advance Bragg-Brentano diffractometer. The long fine-focus Co x-ray tube was operated at 35 kV and 40 mA with a take-off angle of 6°. X-ray diffractograms were analyzed using the International Centre for Diffraction's PDF-4 database. Rietveld refinement of the x-ray powder diffraction data was carried out using the Bruker AXS Rietveld refinement program Topas 4.2.

Table 5.2 Number of spot measurements averaged for each representative spectrum.

Sample	Number of Spot Measurements
Oil Sand	21
Barren Sand	11
Siltstone	6
Mudstone	11
Siderite	3
Pure Quartz Sand	3

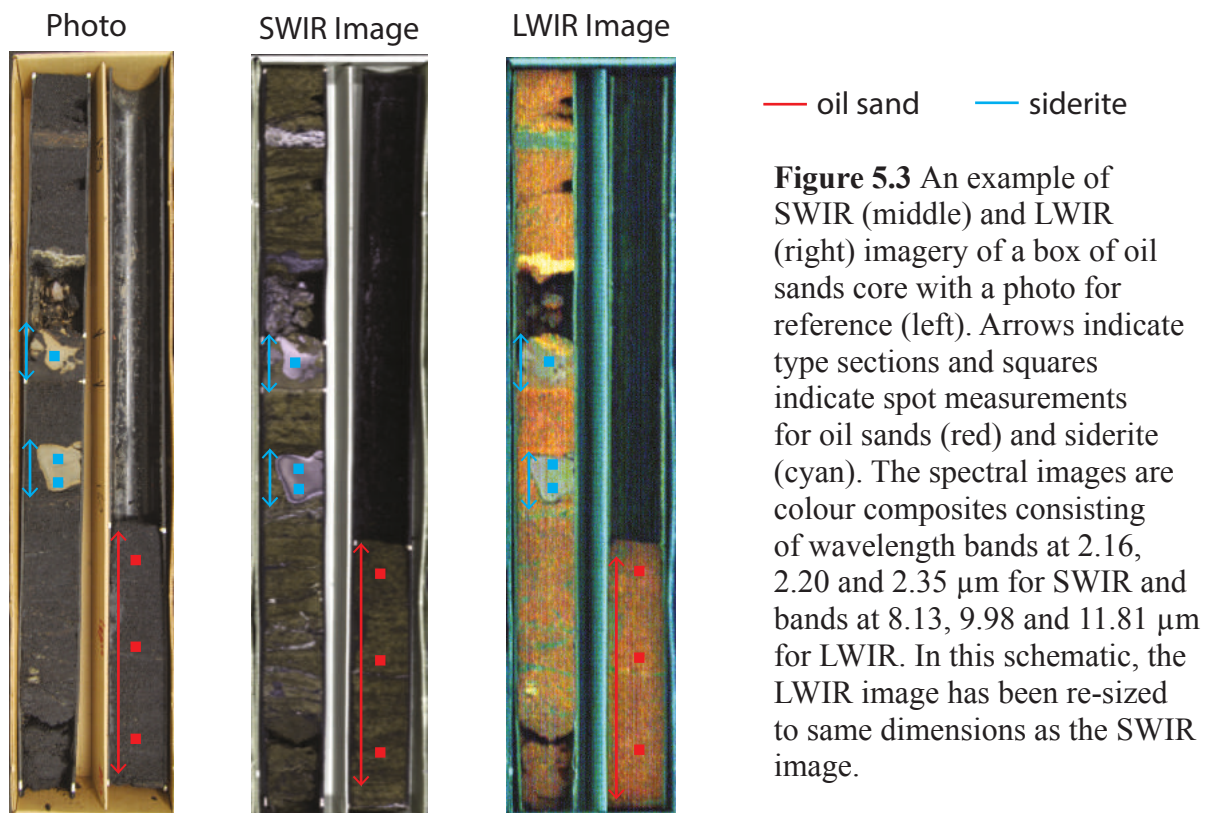
5.4.2 Data Analysis

5.4.2.1 Processing Spectral Data

In order to investigate the spectral characteristics of the five rock types, average spectra for each rock type were obtained from the LWIR and SWIR imagery from the same parts of the core as where FTIR spot measurements were made (Figure 5.3). Mean image spectra for each spot measurement were the average of 80-90 pixels. To allow direct comparison of the two longwave infrared data sets, FTIR spectra were resampled to the spectral resolution of the LWIR image spectra (294 bands to 35 bands) and both groups of spectra were mean normalized. Mean

normalization is a spectral analysis technique that allows for the direct comparison of absorption features between different data sets by minimizing differences in overall brightness (Wu, 2004; Zhang et al., 2005). The normalized reflectance value of each band is calculated by dividing it by the mean reflectance of all bands in the spectrum. Mean normalization accounts principally for the fact that the FTIR spectra and LWIR image spectra were measured against different backgrounds (i.e. diffuse gold for FTIR, diffuse aluminum for LWIR imagery). It also accounts for any illumination geometry effects in the LWIR image data, such as irregularities in the core surface and disparities in viewing and illumination geometries between image and point spectra.

The procedures described above resulted in four datasets of representative spectra for the five rock types (oil sand, barren sand, siltstone, mudstone, and siderite): FTIR point spectra, resampled FTIR point spectra, LWIR image spectra and SWIR image spectra. The first dataset also includes a mean spectrum for pure quartz sand. These data were fundamental for the generation of lithological maps as described in the next section.



5.4.2.2 *Generating Lithological Maps*

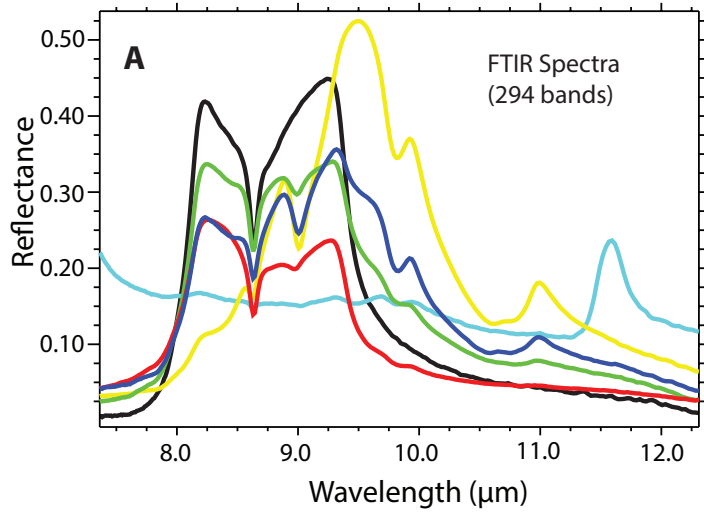
The spatial distribution of the five rock types in the core was mapped in SWIR and LWIR imagery using a classification tool known as the Spectral Angle Mapper (SAM; Kruse et al., 1993). SAM projects reflectance spectra as vectors in n -dimensional space where n is the number of input bands. The direction of the vector is a function of the shape of the spectrum and the length of the vector is proportional to the magnitude of the reflectance. Spectra of unknown materials are compared to known reference spectra, also known as end-members, and if the angle between a pair of such vectors is smaller than a user-defined threshold, the algorithm classifies it as a match. SAM thus classifies spectra based on their shape, not their overall reflectance. Applied to spectral imagery, SAM classifies spectra on a per-pixel scale. The spectrum of each pixel is compared to the end-member spectra and matched pixels are displayed in a colour-coded output image. Pixels that are not matched to any of the end-members are referred to as unclassified and are assigned a single colour on the output image. The lower the threshold angle the greater the accuracy of the results, but the greater the number of pixels that will be left unclassified.

In this study, the end-members are the representative rock type spectra collected from the LWIR and SWIR imagery as described above. A single threshold angle was applied for all five end-members in each case: 0.15 radians (rad) for the SWIR imagery and 0.30 rad for the LWIR imagery. The full spectral range of the data sets was used for SAM input in both cases. Spectral mapping results were evaluated by visual comparison to the core samples as well as a conventional litholog (Figure 5.2). Since bitumen is not spectrally active in the LWIR, the SWIR imagery is expected to provide more accurate results for mapping the spatial distribution of oil sand. Conversely, since quartz is not spectrally active in the SWIR, the LWIR imagery is expected to provide more accurate results for the classification of barren sand, siltstone and mudstone.

5.5 Results

5.5.1 FTIR & LWIR Rock Type Spectra

All five of the representative rock type FTIR point spectra have a unique shape or distinct spectral features (Figure 5.4a). Interpretation of the rock spectra is aided by comparison to that of the pure quartz sand. The pure quartz sand spectrum shows the prominent Si-O vibration doublet, centered at 8.7 μm and peaking in reflectance at 9.2 μm . Of the four siliciclastic rock types, the oil sand and barren sand spectra bear the most similarities to the pure quartz spectrum, both showing a similar strong doublet peaking at 9.2 μm . The main difference between these two spectra and that of the pure quartz sand is the presence of a trough at ~ 8.9 μm in the second lobe of the Si-O doublet for oil sand and barren sand. This splitting of the quartz peak is attributed to the development of the 9.4 μm Si-O clay band. The presence of clay becomes increasingly dominant for the siltstone and then the mudstone, as seen in their respective spectra. While the quartz doublet is still visible in the siltstone spectrum, the clay trough at 8.9 μm is much deeper. The right lobe of the doublet has broadened significantly and the maximum reflectance has shifted to 9.3 μm . The mudstone spectrum is dominated by a strong single peak with maximum reflectance at 9.4 μm . The quartz doublet no longer appears. The presence of quartz as a minor component can be inferred by the small peak at 8.8 μm on the shoulder of the main clay peak. Whereas the pure quartz and oil sand spectra are relatively featureless beyond 9.2 μm , small peaks at 9.9 μm and 10.9 μm appear in the siltstone and mudstone spectra. Weak peaks can be observed at these wavelengths for barren sand as well. Based on comparison to spectra of pure kaolinite, illite and montmorillonite from the Johns Hopkins Spectral Library (Salisbury et al., 1991), these small peaks are attributed to clay minerals. Oil sand has a lower overall reflectance than the barren sand, which is likely due to the bitumen. The siderite spectrum is featureless with the exception of a prominent peak at 11.6 μm . Although this peak appears at a slightly longer wavelength than what has been reported in the literature, we interpret this as the C-O bending band.



- oil sand
- barren sand
- siltstone
- mudstone
- siderite
- pure quartz sand

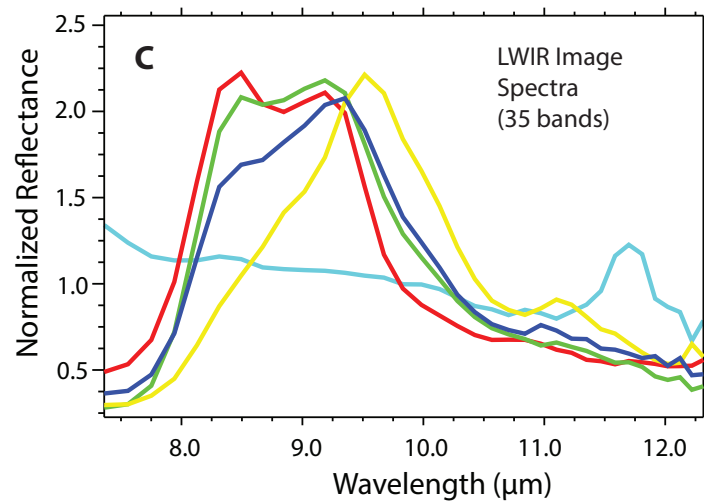
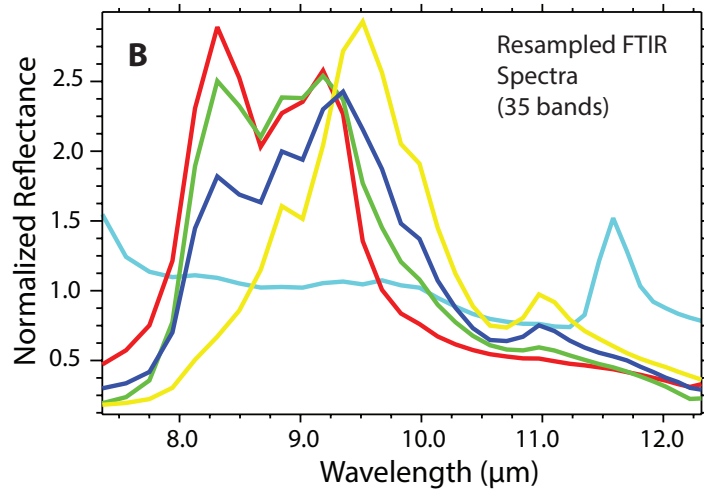


Figure 5.4 LWIR spectra of the five rock types investigated in this study, colour-coded as per the legend. A) Full resolution FTIR point spectra (294 bands). Spectra shown are the average of all point spectra collected for each rock type. A pure quartz sand spectrum is also shown for comparison. B) Resampled, mean normalized FTIR point spectra (35 bands). Full resolution FTIR results were resampled to the same spectral resolution as the LWIR spectral imagery to allow direct comparison of the two data sets. C) Mean normalized LWIR image spectra (35 bands). Spectra shown are the average of all spot spectra collected for each rock type from the LWIR imagery.

Resampling the FTIR spectra reveals that the unique shape of each rock type spectrum and the strongest spectral features are preserved even when the spectral resolution is decreased by a factor of eight (Figure 5.4b). The resampled FTIR spectra are very similar to the LWIR image spectra in terms of overall shape (Figure 5.4c). Some weaker absorption features, such as the 8.9 μm trough, do not appear in the LWIR image spectra. In both datasets, oil sand and barren sand have well developed quartz peaks with maximum reflectance at 9.2 μm , mudstone has a prominent clay peak at 9.4 μm and siltstone is in between the two with a broad doublet and peak reflectance at 9.3 μm . The 11.6 μm peak of the siderite spectrum is the only spectral feature observed beyond 11 μm . Barren sand, siltstone, mudstone and siderite have uniquely shaped end-member spectra, which suggests that the SAM technique is suitable for the classification of these rock types in LWIR spectral imagery. The greatest potential for class confusion in LWIR imagery is between barren sand and oil sand, which are the two most similar end-members. However, their spectra do have a subtle difference in shape at 9.5-10 μm , where the reflectance of barren sand is higher and the slope of its spectrum less steep than that of oil sand. This difference may be due to a higher clay mineral content in barren sand, and may be sufficient for the discrimination of the two classes by SAM.

5.5.2 Rietveld Analysis

A possible explanation for the change in LWIR spectral character moving from barren sand to siltstone to mudstone is a decreasing ratio of quartz to clay minerals. These three rock types are defined by their grain size, but in sedimentary rocks grain size and mineralogy are closely related. Fine-grained sediments (<44 μm) are typically composed of minerals that are less resistant to weathering, such as clays, and coarser grained sediments are often composed of harder minerals like quartz. However, quartz is known to compose a significant portion of the silt-sized fraction (2-44 μm) of the McMurray Formation (55-70% by weight, Osacky et al., 2013). Rietveld analysis was carried out to determine if the relative abundances of quartz and clay minerals in barren sand, siltstone and mudstone are consistent with what the spectral results

suggest.

Rietveld analysis results show decreasing quartz to total clay ratio moving from barren sand to siltstone and to mudstone, respectively (Table 5.3). The complete modeled modal mineralogies of the three samples and the Rietveld refinement plots are provided in Appendix A. Although Rietveld analysis is a quantitative technique, these results should be considered semi-quantitative due to the presence of minor interstratified illite-smectite and kaolinite-smectite, which cannot be measured, as well as the fact that both the illite-muscovite and kaolinite measured in the samples are disordered. Nonetheless, these results support the hypothesis that a decrease in the ratio of quartz to total clays moving from barren sand to siltstone to mudstone is responsible for the unique LWIR spectral characteristics of the three McMurray Formation rocks.

Table 5.3 Quartz and clay mineral content (in wt %) of barren sand, siltstone and mudstone as determined by Rietveld analysis.

	Barren Sand	Siltstone	Mudstone
Illite/Muscovite	13	22	33
Kaolinite	6	18	30
Total Clays	19	40	63
Quartz	79	54	34
Quartz to Total Clay Ratio	4.2	1.4	0.5

5.5.3 SWIR Rock Type Spectra

In the SWIR, the spectral signatures of barren sand, siltstone and mudstone are more alike than they are in the LWIR (Figure 5.5a). The three spectra differ in terms of overall reflectance, but have a similar overall shape displaying absorption features at 1.4, 1.9 and 2.2 μm . The spectrum of mudstone displays a sharper decrease in reflectance and steeper spectral slope beyond 1.7 μm than that of barren sand and siltstone. This is expected to facilitate the discrimination of mudstone from barren sand and siltstone in the SAM mapping results. A closer look at the shapes and intensities of the three absorption features is obtained by continuum-removal, a spectral

analysis technique that allows for the direct comparison of absorption features by removing the background shape of the spectrum (Clark, 1999). Continuum-removal reveals differences in the shape of the 2.2 μm feature between the three rock types (Figure 5.5d). Mudstone has the deepest absorption feature in all three bands, which is consistent with this rock type having the highest clay mineral content (Figure 5.5b-d). Siltstone and barren sand have the same band depths for the hydroxyl features at 1.4 and 2.2 μm and display only a small difference in the 1.9 μm water feature depth. Combined with the similarity of their overall spectra, these results suggest potential for class confusion between siltstone and barren sand using SAM with the SWIR image dataset.

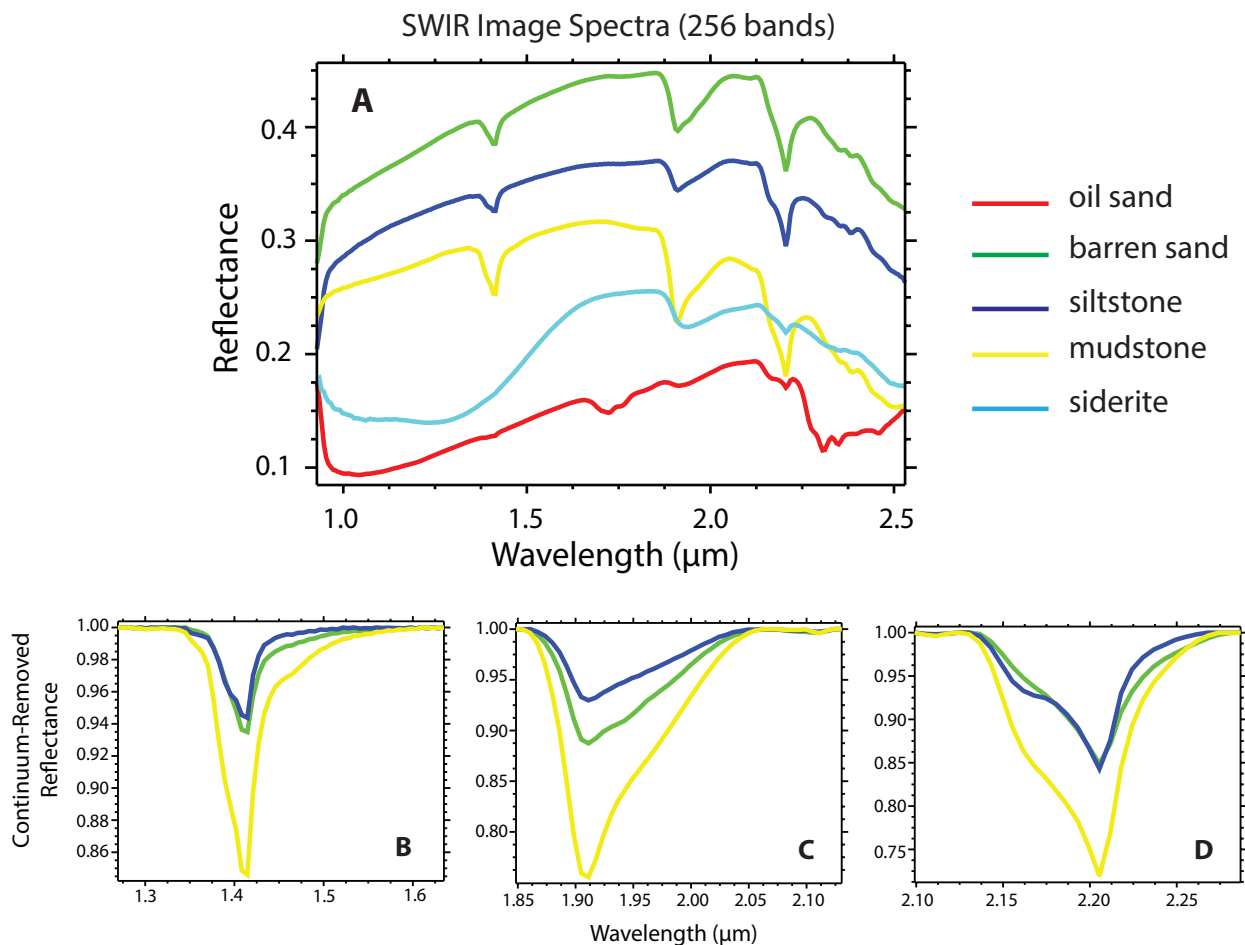


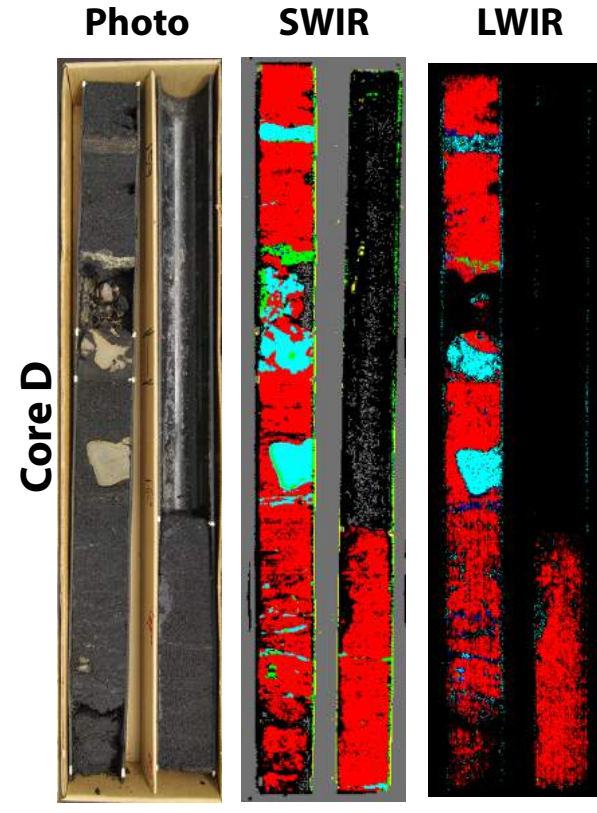
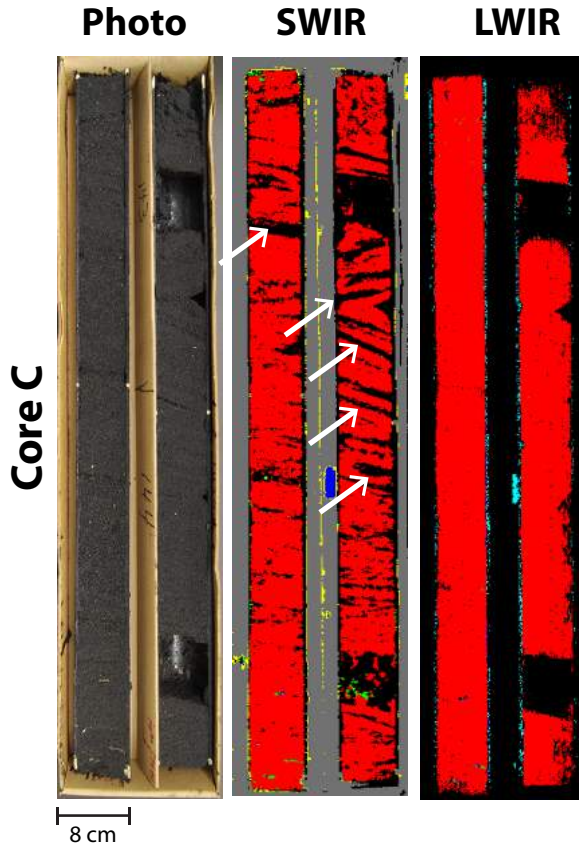
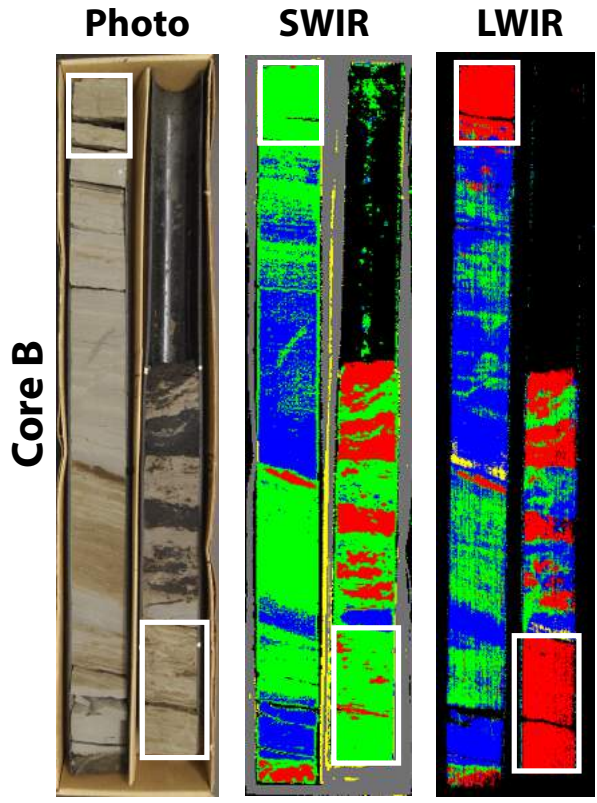
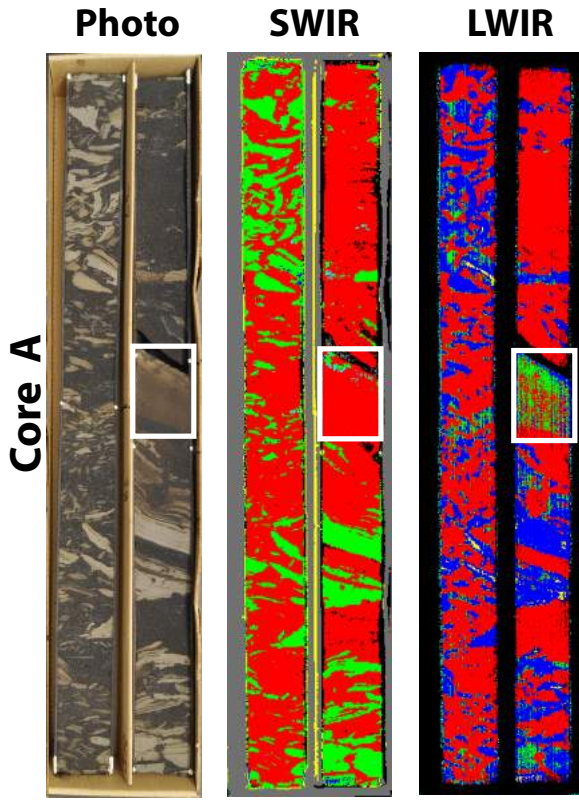
Figure 5.5 A) SWIR spectra (256 bands) of the different rock types investigated in this study, colour-coded as per the legend. B), C), and D) show the continuum-removed views of the 1.4, 1.9 and 2.2 μm features, respectively, for barren sand, siltstone and mudstone.

Oil sand and siderite are spectrally distinct from the other three rock types (Figure 5.5a). The siderite spectrum shows the expected broad trough at 1.0-1.2 μm due to its iron content. The decrease in reflectance at the far end of the spectrum is the start of the C-O vibration band at 2.5 μm , the whole feature being beyond the spectral range of the sensor. Oil sand has the lowest overall reflectance due to bitumen. The shape of the oil sand spectrum is unique due to bitumen absorptions at 1.7 μm and 2.3 μm . Weak clay and water features at 1.4, 1.9 and 2.2 μm can also be observed.

5.5.4 Lithological Core Maps

The SAM classification tool outputs colour-coded images, where each colour represents a single rock type. Six boxes of core were selected as examples to showcase SWIR and LWIR mapping results over a range of different sedimentological properties (Figure 5.6). SWIR maps have an additional colour-coded unit representing cardboard. Preliminary results with the SWIR dataset showed significant interference from cardboard, meaning that the core box was classified as one of the five rock types. An end-member for cardboard (Speta et al., 2013) was added to the SAM classification process to prevent this. This was not necessary for the LWIR dataset as cardboard is not spectrally active in this wavelength range, thus these pixels were left unclassified.

Core A shows an example of intraclast breccia with a matrix of high-grade oil sand. In the SWIR map, the breccia clasts are all classified as barren sand. In the LWIR map, the majority of the clasts are classified as siltstone, which is consistent with visual analysis of the core. Clasts are correctly classified even in the presence of bitumen staining. For example, a ~5 cm bed that grades from silty barren sand at the top, to bitumen-stained sand in the middle, to bitumen-saturated at the bottom is mapped as such in the LWIR results (Figure 5.6a, white box). This same section is classified as part of the oil sand matrix in the SWIR. Because of the unique spectral signature of bitumen in the SWIR, sections that are oil-stained are classified with those that are oil-saturated even though the former is not oil sand from an economic perspective. This



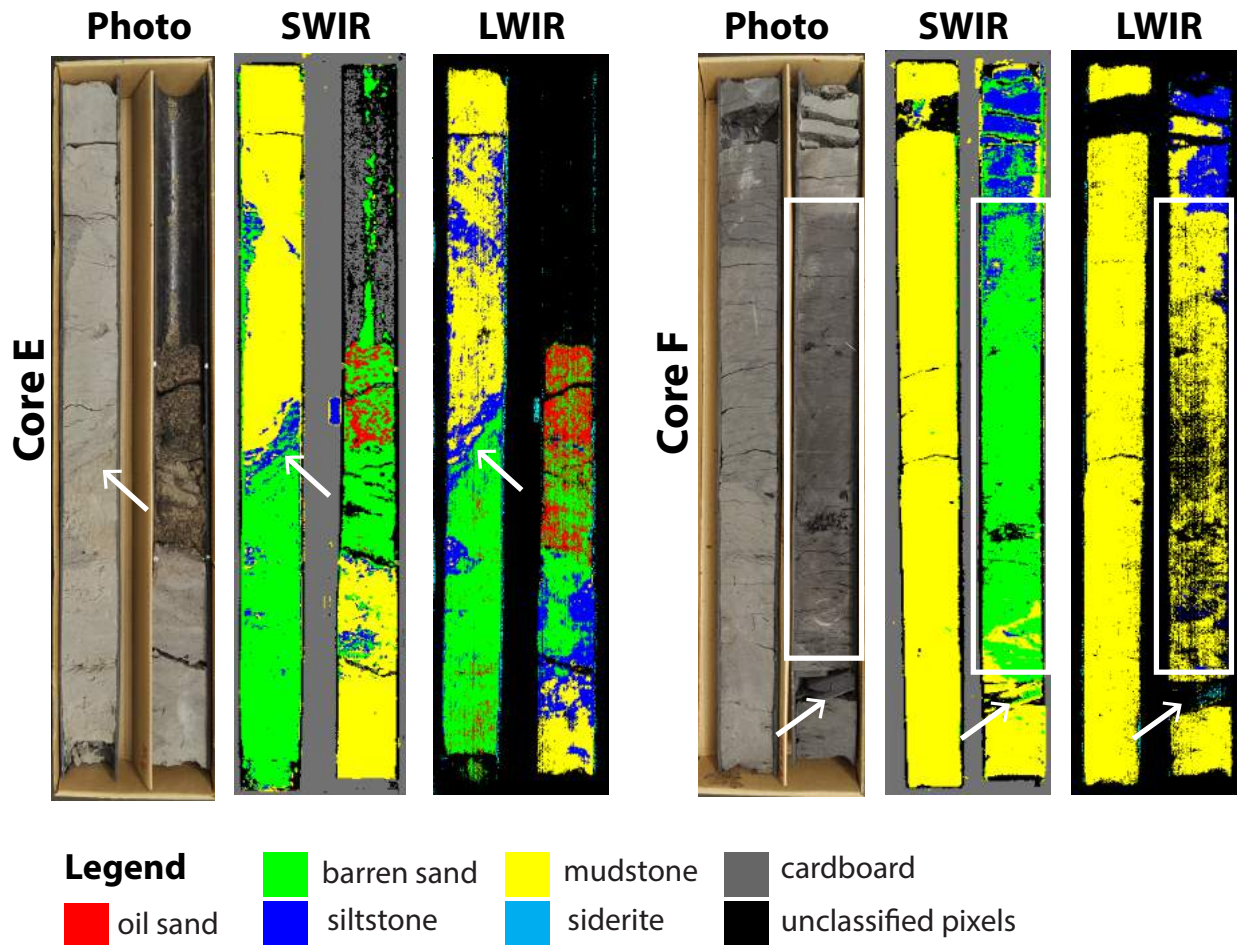


Figure 5.6 Examples of SWIR and LWIR mapping results. SWIR maps have an additional colour-coded unit (grey) representing cardboard. These pixels are unclassified in the LWIR maps because cardboard is not spectrally active in this wavelength range. A) Intraclast breccia with a matrix of high-grade oil sand. A bitumen-stained clast is classified as part of the oil sand matrix in the SWIR, but correctly mapped as barren sand in the LWIR (white box). B) Interbedded sandstone and siltstone with varying degrees of bitumen saturation in the sands. SWIR and LWIR results are comparable with the exception of two barren sand sections that incorrectly classified as oil sand in the LWIR map (white boxes). Spectral mapping results are consistent with visual inspection of the core, both of which disagree with the classification of this core on the conventional litholog (Figure 5.2). C) Oil sand with grain striping. The whole core is correctly classified as oil sand for both datasets. Unclassified beds in the SWIR map (white arrows) correspond to fine grained stripes. D) Oil sand with siderite clasts. Siderite is correctly classified in both maps, as is the oil sand. The grainy appearance of the LWIR map is likely due to lower signal to noise ratio in the LWIR data relative to the SWIR data. E) An example of a mudstone-rich core where the SWIR and LWIR results are comparable. A contact between mudstone and barren sand that is difficult to discern visually is clearly defined in both maps (white arrow). F) An example of a mudstone-rich core where mudstone is misclassified as barren sand in the SWIR results (white box). A coal seam (white arrow) is misclassified as mudstone in the SWIR. Since a coal end-member was not included in the SAM classification, coal would be expected to remain unclassified as in the LWIR map.

is a function of the threshold angle used in the SAM classification, which resulted in pixels with any amount of bitumen being assigned to a single class.

Core B is an example of interbedded sandstone and siltstone with various degrees of bitumen saturation in the sands.¹ The SWIR results are consistent with the visual appearance of the core; high-grade sections are classified as oil sand and sections of the core with little or no bitumen staining are classified as barren sand. The SWIR and LWIR mapping results for core B are comparable, with the exception of two barren sand sections that are incorrectly classified as oil sand in the LWIR map (Figure 5.6b, white boxes). Investigation of the LWIR spectra from these misclassified sections shows that these barren sections are spectrally more similar to the oil sand end-member spectrum than the barren sand end-member (Figure 5.7).

Core C shows a box of high-grade oil sand that shows grain striping, a common form of bedding in the McMurray Formation that is characterized by alternating “stripes” of coarse-grained sand and fine-grained sand. The distribution of bitumen across the grain stripes is uniform based on visual inspection. This box of core is correctly mapped as being entirely composed of oil sand in both the SWIR and the LWIR maps. However, in the SWIR map there are numerous sections of oil sand that are unclassified (Figure 5.6c, white arrows). These unclassified sections correspond to fine-grained stripes. Investigation of mean spectra from the grain stripes (Figure 5.8) reveals that fine-grained beds have significantly lower spectral contrast than coarse-grained beds. This could be due to a decrease in spectral contrast at finer grain sizes because of increased photon interaction with bitumen. In a split core where the surface has been sliced, bitumen may form a more continuous coating over fine-grained quartz than coarser grain sizes. Lowering the spectral angle threshold for the oil sand end-member could help capture the lower contrast oil sand spectra from fine-grained stripes.

¹ It is interesting to note that core B was classified as mudstone on the conventional litholog (Figure 5.2). This is an example of the types of subjective errors that can occur in traditional core logging.

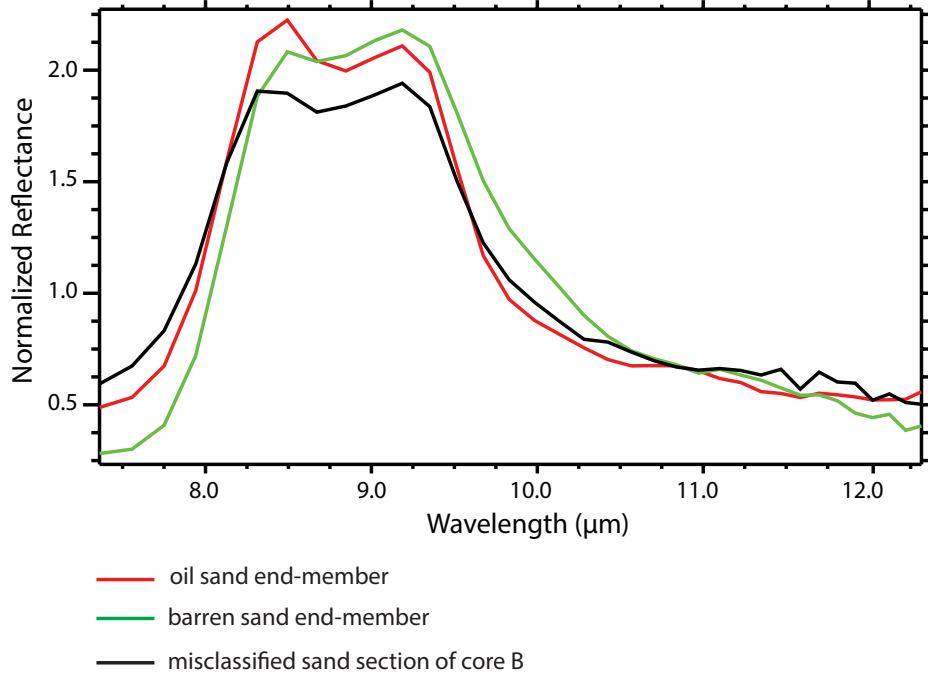


Figure 5.7 Mean spectrum of the problematic section in the LWIR map of core B. This section of barren sand is misclassified as oil sand. Comparison to the end-member spectra of oil sand and barren sand clearly show the spectral similarity of the misclassified section to the oil sand end-member.

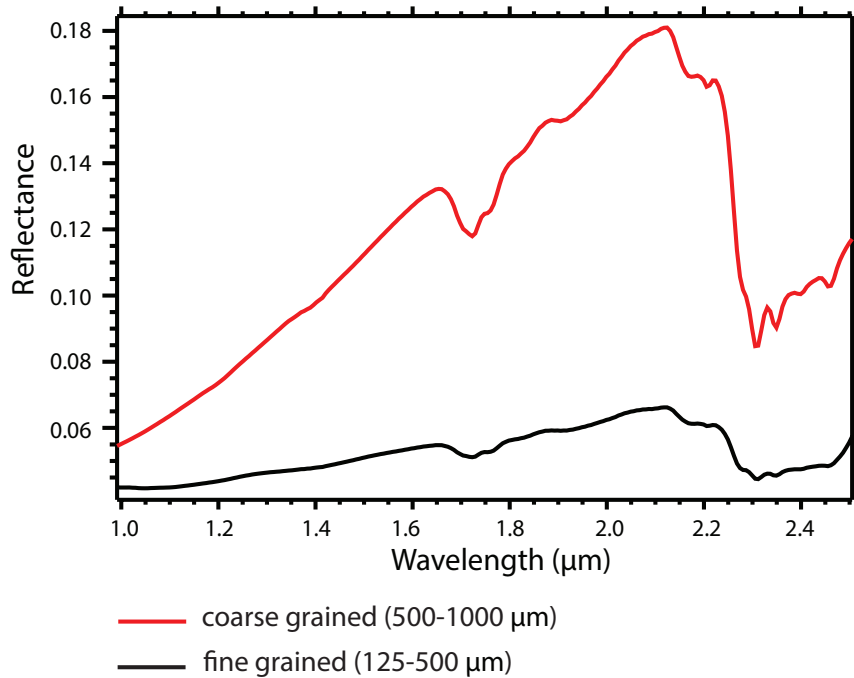


Figure 5.8 Mean spectra of coarse (red) and fine (black) grain stripes from a high resolution (0.25 mm/pixel) SWIR image of core C (not shown). Each spectrum is the mean of ~10,500 pixels. Fine-grained stripes have much lower spectral contrast than coarse-grained stripes, which may explain why they are not matched to the oil sand end-member by the SAM tool.

Core D shows an example of a box of core that contains siderite clasts. The clasts are correctly mapped in both the SWIR and LWIR results, as is the surrounding oil sand. The LWIR map has more unclassified pixels than the SWIR, giving it a grainy appearance. This can also be observed in several of the other examples in Figure 5.6, and is attributed to the lower spectral resolution and lower signal to noise ratio of the LWIR data relative to the SWIR.

Cores E and F are predominantly mudstone with lesser siltstone and barren sand. A sharp contact between mudstone and barren sand is present in core E (Figure 5.6e, white arrow). This contact is difficult to discern visually, but appears clearly in both maps. Both methods also correctly map a small section of very low grade, coarse-grained oil sand. For core E, the SWIR and LWIR results are very comparable. On the other hand, in core F, a large section of mudstone is incorrectly classified as barren sand in the SWIR map (Figure 5.6f, white box). The same section is correctly classified as mudstone in the LWIR map, but there is an abundance of unclassified pixels. The unclassified pixels may be caused by the fact that this particular section of mudstone is very dark (organic-rich), leading to a loss of spectral contrast that may also require an adjustment of the SAM threshold for improved mapping results. Adding a new separate end-member for organic-rich mudstone would be another possible solution. Misclassification of this section of core in the SWIR could also be due to the low spectral contrast, or it could be because of the spectral similarity of barren sand and mudstone in this wavelength range. Core F has a ~3 cm thick coal (Figure 5.6f, white arrow) that is misclassified as mudstone in the SWIR and unclassified in the LWIR. This could be corrected by adding an end-member for coal to the SAM classification process.

5.6 Discussion

The results of this study demonstrate that with a simple methodology (i.e. SAM applied to the full spectral range of the image with a single threshold angle for all end-members) both SWIR and LWIR spectral imagery can be used for the automated mapping of oil sand, barren sand,

siltstone, mudstone, and siderite in McMurray Formation core. In most cases, the core maps produced by the two methods were very similar, despite the spectral similarities of the non-oil-saturated siliciclastic rocks in the SWIR, and of barren sand and oil sand in the LWIR. In cases of disagreement between the two mapping results, the SWIR imagery was more accurate for the classification of oil sand than the LWIR. In the LWIR, bitumen is not spectrally active and the ratio of quartz to clay is the variable that differentiates oil sand and barren sand as spectral end-members. An inverse relationship between bitumen content and clay content is well known in the McMurray Formation, but this is for clays as a grain size fraction rather than a mineral group (Carrigy, 1962). Although clay minerals make up the majority of the clay size fraction (<2 μm) in the McMurray Formation, quartz is also present in quantities as high as 18 wt % (Osacky et al., 2013). This implies that while the quartz to clay ratio may often be a good indicator of bitumen distribution, the relationship does not always hold. For the range of core examined, the use of a single LWIR oil sands end-member spectrum did capture most of the oil sand distribution in the core but, as shown in Figure 5.7, non-oil-saturated sands can show the same spectral signature.

The LWIR imagery was superior for the discrimination of barren sand, siltstone and mudstone. These three rock types have unique spectral signatures in the LWIR, but display considerably less contrast in the SWIR, which negatively impacted the latter SAM mapping results. This problem can be addressed by working with a spectral subset rather than the whole spectral range, as this accentuates finer scale variability in the spectra. For example, in the continuum-removed view of the 2.2 μm clay absorption feature (Figure 5.5d), the shapes of barren sand, siltstone and mudstone are clearly distinct. As shown in Figure 5.9, using the spectral subset of 2.099 μm to 2.286 μm for SAM input facilitates the discrimination of barren sand from siltstone. Siderite and oil sand have similar spectral shapes in this wavelength range, but if the former is not included as a SAM end-member, oil sand is correctly mapped using this approach.

A necessary consideration for mapping the spatial distribution of oil sand is the threshold level

of bitumen saturation required for classification as such. To address this issue, a new method was tested which involved the use of a published spectral model for the estimation of total bitumen content (TBC) from SWIR spectra (Rivard et al., 2010; Speta et al., 2015). When applied to SWIR imagery, the output of the model is a greyscale image of the core that shows TBC on a per-pixel scale. This image can be manipulated to identify pixels with a TBC above or below a certain threshold value, which can then be transferred to the SWIR or LWIR image. In this case, oil sands pixels mapped in the TBC imagery were transferred to the corresponding LWIR image and SAM was applied to map the other four rock types from the remaining pixels. Examples of maps for TBC threshold values of 3 wt %, 6 wt % and 10 wt % are shown in Figure 5.10.

Using this particular method corrected errors in the classification of oil sand in the LWIR imagery while maintaining the accurate discrimination of non-oil saturated rock types. It also correctly mapped oil sand pixels that were left unclassified in some SWIR results due to loss of spectral contrast (e.g. Figure 5.6c). This is likely due to the fact that the spectral TBC model used to detect the oil sand involves a continuous wavelet transform. Wavelet analysis is a technique for minimizing the spectral effects of grain size variability, surface roughness and other non-compositional factors that can affect reflectance response (Rivard et al., 2008), and thus may eliminate the decrease in contrast observed in fine-grained sections. A potential disadvantage of this mapping method is the need for access to both SWIR and LWIR imagery. The need for LWIR data can be a deterrent for practical use given the greater current availability and lower cost of SWIR imaging spectrometers.

Other ways to enhance the mapping results include exploring the use of a greater end-member set (e.g. organic-rich mudstone), including more accessory phases. Preliminary results from concurrent research indicate that coal can be detected in LWIR imagery (Hauf et al., 2016). Other phases of interest may include wood, pyrite and calcite. Defining different spectral angle thresholds for different end-members will also likely show improvements.

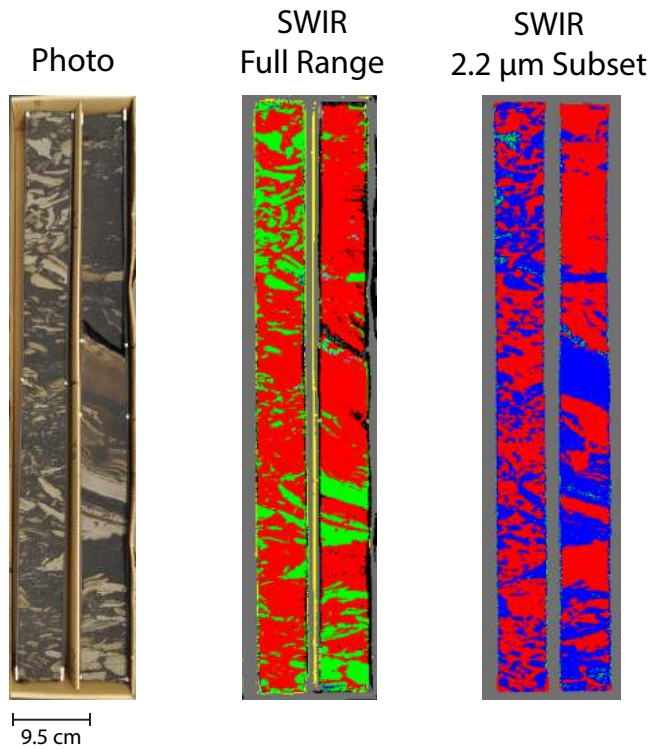


Figure 5.9 Core A mapped in the SWIR using a spectral subset of 2.099 μm to 2.286 μm . The original SWIR map, where the entire spectral range of 1.0-2.5 μm was used, is shown for comparison. Breccia clasts, mapped incorrectly as barren sand when using the whole spectral range, are correctly classified as siltstone using the spectral subset.

Legend

- oil sand
- mudstone
- barren sand
- cardboard
- siltstone
- unclassified pixels

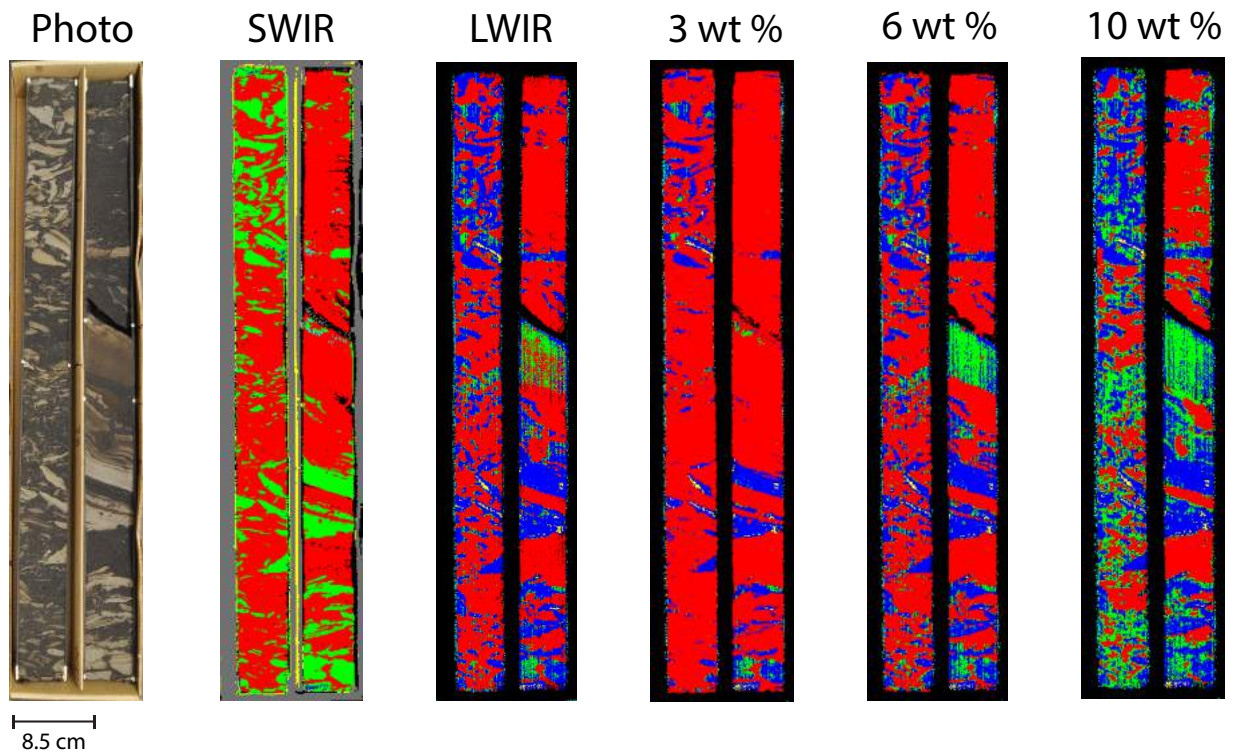


Figure 5.10 Core A as mapped in the SWIR, LWIR and using both datasets together. A spectral model for total bitumen content (TBC) was applied to the SWIR imagery to map oil sand with threshold values of 3 wt %, 6 wt % and 10 wt % TBC. Pixels mapped as oil sands were transferred to LWIR imagery and SAM was used to map the remaining rock types.

5.7 Conclusions

The objective of this study was to investigate the feasibility of using SWIR (1.0-2.5 μm) and LWIR (8-12 μm) hyperspectral imaging for the automated mapping of oil sand, barren sand, siltstone, mudstone and siderite in McMurray Formation oil sands core. Investigation of the spectral properties of these five rock types revealed that barren sand, siltstone, and mudstone are spectrally distinct in the LWIR. Rietveld analysis confirmed that differences in their spectral responses can be attributed to a decreasing ratio of quartz to total clay minerals. Barren sand and oil sand are spectrally similar in the LWIR because bitumen is not spectrally active in this wavelength range. In the SWIR, quartz is not spectrally active, and end-member spectra of barren sand, siltstone and mudstone are spectrally similar. The oil sand end-member is spectrally distinct in the SWIR. Siderite has a unique spectral signature in both wavelength ranges.

A simple mapping methodology using the SAM tool resulted in the successful production of lithological maps that closely compared to the results of careful logging. In cases where there was disagreement between the SWIR and LWIR results, the SWIR was more accurate for the mapping of oil sand, while the LWIR facilitated the discrimination of barren sand, siltstone and mudstone. Map results were enhanced by using the two datasets together with a spectral model for bitumen content estimation, which allowed for the definition of different threshold levels of bitumen saturation for the mapping of oil sand. Improved map results were also attained by applying the simple modification of using a spectral subset for SAM input. Other misclassifications that were observed in this study are very likely to be surmounted with further advances in the mapping methodology, which lies in the context of future work. To the authors' knowledge, this is the first application of hyperspectral imaging for automating the process of logging lithology in oil sands core. The results of this study demonstrate the potential for the development of a robust mapping technology for this purpose. Combined with the other types of information that can be obtained from hyperspectral data, this technology could greatly facilitate the process of routine oil sands core logging.

References

- Bayliss, P., and Levinson, A.A., 1976, Mineralogical review of the Alberta oil sand deposits (Lower Cretaceous, Mannville Group), *Bulletin of Canadian Petroleum Geology*, v. 24, no. 2, p. 211–224.
- Bishop, J.L., Lane, M.D., Dyar, M.D., and Brown, A.J., 2008, Reflectance and emission spectroscopy study of four groups of phyllosilicates: Smectites, kaolinite-serpentines, chlorites and micas, *Clay Minerals*, v. 43, p. 35–54.
- Carrigy, M.A., 1959, Geology of the McMurray Formation, Pt. III: General geology of the McMurray area, Research Council of Alberta, Geological Division – Memoir 1, 130 p.
- Carrigy, M.A., 1962, Effect of texture on the distribution of oil in the Athabasca oil sands, Alberta, Canada, *Journal of Sedimentary Petrology*, v. 32, no. 2, p. 312–325.
- Carrigy, M.A., 1963, Criteria for differentiating the McMurray and Clearwater Formations in the Athabasca oil sands, Research Council of Alberta, Geological Division - Bulletin 14, 32 p.
- Clark, R.N., 1999, Spectroscopy of rocks and minerals, and principles of spectroscopy, in: A.N. Rencz (Ed.), *Remote Sensing for the Earth Sciences: Manual of Remote Sensing*, John Wiley & Sons, Inc., p. 3–58.
- Clark, R.N., King, T.V.V., Klejwa, M., and Swayze, G.A., 1990, High spectral resolution reflectance spectroscopy of minerals, *Journal of Geophysical Research*, v. 95, no. B8, p. 12653–12680.
- Cloutis, E., 1989, Spectral reflectance properties of hydrocarbons: Remote-sensing implications, *Science*, v. 245, p. 165–168.
- Cloutis, E., Gaffey, M., and Moslow, T., 1995, Characterization of minerals in oil sands by reflectance spectroscopy, *Fuel*, v. 74, p. 874–879.
- Feng, J., Rivard, B., Gallie, A., and Sanchez-Azofeifa, A., 2011, Rock type classification of drill core using continuous wavelet analysis applied to thermal infrared reflectance spectra, *International Journal of Remote Sensing*, v. 32, no. 16, p. 4489–4510.
- Flach, P. D., and Mossop, G.D., 1985, Depositional environment of Lower Cretaceous McMurray Formation, Athabasca oil sands, Alberta, *AAPG Bulletin*, v. 69, no. 8, p. 1195–1207.
- Geological Survey of Sweden, 2014, Drill Core Scanning at SGU, Retrieved from: <http://www.sgu.se/en/mineral-resources/geological-information-for-mineral-exploration/drill-core-collection/drill-core-scanning-at-sgu>, on Dec. 28, 2015.
- Hauf, P., Rivard, B., Stancliffe, S., and Speta, M., 2016, Application of hyperspectral imaging for the detection of coal in oil sand drill core (abs.), AAPG Annual Convention & Exhibition, June 19-21, 2016, Calgary, AB, 2 p.
- Hunt, G.R., 1977, Spectral signatures of particulate minerals in the visible and near infrared, *Geophysics*, v. 42, p. 501–513.
- Hunt, G.R., and Salisbury, J.W., 1975, Mid-infrared spectral behaviour of sedimentary rocks,

- Report TR-75-0356, Air Force Cambridge Research Laboratories, 49 p.
- Hunt, G.R., and Salisbury, J.W., 1970, Visible and near-infrared spectra of minerals and rocks: I. Silicate Minerals, *Modern Geology*, v. 1, p. 283–300.
- Hunt, G.R., and Salisbury, J.W., 1971, Visible and near-infrared spectra of minerals and rocks: II. Carbonates, *Modern Geology*, v. 2, p. 23–30.
- Huntington, J.F., Mauger, A.J., Skirrow, R.G., Bastrakov, E.N., Connor, P., Mason, P., Keeling, J.L., Coward, D.A., Berman, M., Phillips, R., Whitbourn, L.B., and Heithersay, P.S., 2006, Automated mineralogical core logging at the Emmie Bluff iron oxide-copper-gold prospect, *MESA Journal*, v. 41, p. 38–44.
- Kruse, F.A., 1996, Identification and mapping of minerals in drill core using hyperspectral image analysis of infrared reflectance spectra, *International Journal of Remote Sensing*, v. 17, no. 9, p. 1623–1632.
- Kruse, F.A., Lefkoff, A.B., Boardman, J.W., Heidebrecht, K.B., Shapiro, A.T., Barloon, P.J., and Goetz, A.F.H., 1993, The spectral image processing system (SIPS) interactive visualization and analysis of imaging spectrometer data, *Remote Sensing of Environment*, v. 44, p. 145–163.
- Kruse, F.A., Bedell, R.L., Taranik, J.V., Peppin, W.A., Weatherbee, O., and Calvin, W.M., 2012, Mapping alteration minerals at prospect, outcrop and drill core scales using imaging spectroscopy, *International Journal of Remote Sensing*, v. 33, no. 6, p. 1780–1798.
- Lammoglia, T., and Filho, C.R.S., 2011, Spectroscopic characterization of oils yielded from Brazilian offshore basins: Potential applications of remote sensing, *Remote Sensing of Environment*, v. 115, no. 10, p. 2525–2535.
- Lane, M.D., and Christensen, P.R., 1997, Thermal infrared emission spectroscopy of anhydrous carbonates, *Journal of Geophysical Research*, v. 102, no. E11, p. 25,581–25,592.
- Lang, H.R., Bartholomew, M.J., Grove, C.I., and Paylor, E.D., 1990, Spectral reflectance characterization (0.4 to 2.5 and 8.0 to 12.0 μm) of Phanerozoic strata, Wind River Basin and Southern Bighorn Basin Areas, Wyoming, *Journal of Sedimentary Petrology*, v. 60, no. 4, p. 504–524.
- Michalski, J.R., Kraft, M.D., Sharp, T.G., Williams, L.B., and Christensen, P.R., 2006, Emission spectroscopy of clay minerals and evidence for poorly crystalline aluminosilicates on Mars from Thermal Emission Spectrometer data, *Journal of Geophysical Research: Planets*, v. 111, no. E3, p. 1–14.
- Mossop, G.D., 1980a, Geology of the Athabasca Oil Sands, *Science*, v. 207, no. 4427, p. 145–152.
- Mossop, G.D., 1980b, Facies control on bitumen saturation in the Athabasca oil sands, in: Miall, A.D. (Ed.), *Facts and Principles of World Petroleum Occurrence*, CSPG Memoir 6, Canadian Society of Petroleum Geologists, Calgary, AB, p. 609–632.
- Mossop, G.D., and Flach, P.D., 1983, Deep channel sedimentation in the Lower Cretaceous McMurray Formation, Athabasca Oil Sands, Alberta, *Sedimentology*, v. 30, p. 493–509.
- Osacky, M., Geramian, M., Ivey, D.G., Liu, Q., and Etsell, T.H., 2013, Mineralogical and

- chemical composition of petrologic end members of Alberta oil sands, *Fuel*, v. 113, p. 148–157.
- Ranger, M., 2010, AppleCORE (software), GeoMEM Ltd.
- Rivard, B., Feng, J., Gallie, A., and Sanchez-Azofeifa, A., 2008, Continuous wavelets for the improved use of spectral libraries and hyperspectral data, *Remote Sensing of Environment*, v. 112, no. 6, p. 2850–2862.
- Rivard, B., Lyder, D., Feng, J., Gallie, A., Cloutis, E., Dougan, P., Gonzalez, S., Cox, D., and Lipsett, M.G., 2010, Bitumen content estimation of Athabasca oil sand from broad band infrared reflectance spectra, *The Canadian Journal of Chemical Engineering*, v. 88, p. 830–838.
- Salisbury, J.W., Walter, L.S., Vergo, N., and D’Aria, D.M., 1991, *Infrared (2.1–25 μm) Spectra of Minerals*, The Johns Hopkins University Press, Baltimore, MD, 267 p.
- Speta, M., Rivard, B., Feng, J., Lipsett, M., and Gingras, M., 2013, Hyperspectral imaging for the characterization of Athabasca oil sands drill core (abs.), IEEE Xplore: Proceedings of 2013 International Geoscience and Remote Sensing Symposium (IGARSS), July 21–26, 2013, Melbourne, p. 2184–2187.
- Speta, M., Rivard, B., Feng, J., Lipsett, M., and Gingras, M.K., 2015, Hyperspectral imaging for the determination of bitumen content in Athabasca oil sands core samples, *AAPG Bulletin*, v. 99, no. 7, p. 1245–1259.
- Speta, M., Gingras, M.K., Rivard, B., in press, Shortwave infrared hyperspectral imaging: A novel method for enhancing the visibility of sedimentary and biogenic features in oil-saturated core, *Journal of Sedimentary Research*, accepted Dec. 13, 2015.
- Stewart, G.A., and MacCallum, G.T., 1978, *Athabasca Oil Sands Guidebook*, Canadian Society of Petroleum Geologists, Calgary, AB, 33 p.
- Tappert, M., Rivard, B., Giles, D., Tappert, R., and Mauger, A., 2011, Automated drill core logging using visible and near-infrared reflectance spectroscopy: A case study from the Olympic Dam IOCG deposit, South Australia, *Economic Geology*, v. 106, p. 289–296.
- Tappert, M.C., Rivard, B., Fulop, A., Rogge, D., Feng, J., Tappert, R., and Stalder, R., 2015, Characterizing kimberlite dilution by crustal rocks at the Snap Lake diamond mine using SWIR (1.90–2.36 μm) and LWIR (8.1–11.1 μm) hyperspectral imagery collected from drill core, *Economic Geology*, v. 110, no. 6, p. 1375–1387.
- Turner, D.J., Rivard, B., and Groat, L.A., 2014, Visible and short-wave infrared reflectance spectroscopy of REE fluorocarbonates, *American Mineralogist*, v. 99, no. 7, p. 1335–1346.
- Wightman, D.M., and Pemberton, S.G., 1997, The Lower Cretaceous (Aptian) McMurray Formation: An overview of the Fort McMurray area, northeastern Alberta, in: Pemberton, S.G. and James, D.P. (Eds.), *Petroleum Geology of the Cretaceous Mannville Group, Western Canada*, CSPG Memoir 18, Canadian Society of Petroleum Geologists, p. 312–344.
- Wu, C., 2004, Normalized spectral mixture analysis for monitoring urban composition using ETM+ imagery, *Remote Sensing of Environment*, v. 93, no. 4, p. 480–492.

Zhang, J., Rivard, B., and Sánchez-Azofeifa, A., 2005, Spectral unmixing of normalized reflectance data for the deconvolution of lichen and rock mixtures, *Remote Sensing of Environment*, v. 95, no. 1, p. 57–66.

Chapter 6

Conclusions

6.1 Summary & Contributions

This research investigated the application of hyperspectral imaging for the characterization of Athabasca oil sands drill core samples. Three specific research avenues were explored in this thesis: 1) the spectral determination of the total bitumen content (TBC) of oil sands core; 2) enhancing the visibility of sedimentary structures and trace fossils in oil-saturated sections of core; and 3) the automated lithological mapping of oil sands core using a spectral classification method. The principal contributions of this research are summarized below.

1. Bitumen content determination

Ore grade, or total bitumen content (TBC), is one of the primary variables controlling the economic recovery of bitumen from oil sands reservoirs. The current industry standard method for ore grade determination, Dean-Stark analysis, is slow, labour-intensive, and destructive to the sample. Cores must be frozen immediately after drilling, which complicates transport and storage, in order to prevent the loss of volatiles for accurate Dean-Stark results. Previously, Rivard et al. (2010) developed a number of spectral models for the rapid determination of bitumen content from point measurements of crushed oil sands ore. Their most accurate model was adapted for application to drill core, resulting in the development of two different models referred to as broadband and wavelet. In this study, these models were applied to shortwave infrared (SWIR, 1.0-2.5 μm) hyperspectral imagery of core samples from different locations and depths in the Athabasca deposit. Four suites of fresh core, drilled less than 2 years ago and still moist and pliable, were tested as well as one dry core, which was more than 15 years old and completely hardened. The wavelet model was expected to provide more accurate results than the broadband because it involves a continuous wavelet transform, which reduces noise and the effects of non-compositional variables (e.g. grain size) in the reflectance response (Rivard et al.,

2008). However, the wavelet model is computationally intensive. The broadband model, nearly ten times faster than the wavelet, was tested to determine if similar quality results could be produced in a fraction of the time.

The spectral models produce greyscale imagery that shows bitumen content on a per-pixel scale, allowing for rapid visual assessment of the distribution of the oil in the core. Mean spectral bitumen content values were calculated for the same intervals of the core as where Dean-Stark sampling was carried out. For three out of four suites of fresh core, TBC was predicted within ± 1.5 wt % of the Dean-Stark data with both spectral models achieving correlations of $R^2 > 0.97$. In these cases, the broadband model produced results of comparable accuracy to that of the wavelet model. For the dry core and the fourth suite of fresh core, a strong agreement with Dean-Stark data was also observed for both models ($R^2 = 0.94-0.97$), but the margins of error were larger ($\pm 2.5-3.3$ wt %). Analysis of problematic samples revealed a tendency for both models to overestimate TBC in high grade (>10 wt %) samples in these two suites of core. Surface roughness due to uneven oil distribution, small scale fracturing and loosely consolidated sediment was identified as a possible source of error in the overestimated samples. In these cases, the wavelet model may perform better than the broadband.

2. Visual enhancement of sedimentological features

One of the main objectives of core logging is the identification of sedimentary structures and trace fossils. This is important for facies analysis and geological modeling. However, it can be challenging in oil sands because these important features are difficult to see in fine-grained, well-sorted, oil-saturated sediments. SWIR hyperspectral imaging was investigated as a method for enhancing the visibility of sedimentary and biogenic features in oil sands core. Spectral imagery can be viewed as greyscale single band images or as three-band colour composite images. Viewing different combinations of wavelength bands is a basic spectral analysis technique that allows for the emphasis or suppression of different components of the image (Mustard and

Sunshine, 1999). The three-band combination of 2.162 μm , 2.199 μm , and 2.349 μm was found to dramatically enhance the visibility of sedimentary structures and trace fossils in massive-appearing bitumen-saturated sand. In many cases, these features were impossible to see with the unaided eye. Low resolution imagery (1.2-1.5 mm/pixel) was suitable for the detection of large-scale sedimentary structures such as cm-scale bedding. Higher resolution (0.2-0.25 mm/pixel) is necessary for the accurate identification of trace fossils and for visualizing smaller scale structures (<1 cm) such as current ripple cross-lamination.

The visibility of sedimentary and biogenic features is enhanced in spectral imagery because domains differing in overall reflectance provide visual contrast in the massive-appearing oil sand. The cause of the variable reflectance can be attributed to a number of factors based on the sedimentological character of the sample. Variability in grain size and bitumen content was observed between bright and dark domains in fine to coarse grained oil sand, while variability in clay abundance across bright and dark domains was found in very fine to fine sand sections.

3. Automated lithological mapping

The first step of core logging is recording a detailed lithological description of the core (a litholog). This is done manually by a trained geologist and is a time-intensive task. This study investigated the automated mapping of five common rock types (oil sand, barren sand, siltstone, mudstone and siderite) in SWIR and LWIR (longwave infrared, 8-12 μm) hyperspectral imagery of oil sands core using a classification tool known as the spectral angle mapper (SAM; Kruse et al., 1993). Investigation of the spectral properties of these rock types revealed that barren sand, siltstone, and mudstone are spectrally distinct in the LWIR. Differences in their spectral response is attributed to a decreasing ratio of quartz to total clay minerals in these three samples, respectively, as confirmed by Rietveld analysis. Barren sand and oil sand are spectrally similar in the LWIR because bitumen is not spectrally active in this wavelength range. The opposite was found in the SWIR, where barren sand, siltstone and mudstone are spectrally similar and oil sand

is spectrally distinct from the other rock types. Siderite has a unique spectral signature in both wavelength ranges.

Lithological mapping of the SWIR and LWIR imagery was conducted using the SAM tool with spectral angle thresholds of 0.15 rad and 0.3 rad, respectively. Both spectral ranges performed well for the classification of the five rock types, producing results that were consistent with visual inspection of the core. In cases where there was disagreement between the SWIR and LWIR results, the SWIR was more accurate for the mapping of oil sand, while the LWIR was more effective for the discrimination of barren sand, siltstone and mudstone. Mapping results were enhanced through the use of bitumen content imagery, which allowed for the classification of oil sands at different levels of bitumen saturation. Using a spectral subset of the SWIR dataset also improved the accuracy of the map results. This study is the first application of hyperspectral imaging for automating the process of logging lithology in oil sands core and the results demonstrate the immense potential for the future development of a robust spectral mapping technique.

The combined results of this thesis demonstrate the potential of hyperspectral imaging for facilitating routine core analyses in the oil sands industry. Hyperspectral imaging provides a number of benefits over existing methods for oil sands core analysis. For TBC determination, the spectral models provide the opportunity for rapid visual assessment of the spatial distribution of the oil in the core. Results are produced within minutes and the technique is non-destructive to the core sample. Furthermore, while Dean-Stark analysis is only effective for fresh oil sand cores that have not undergone loss of volatiles, the results of this study demonstrate that hyperspectral imaging could be used to obtain relative, if not absolute, estimates of ore grade even in completely dehydrated cores. High resolution SWIR imagery facilitates qualitative examination of core by dramatically enhancing the visibility of sedimentary fabrics. Both SWIR and LWIR imagery can be used for automating the process of litho-logging, which is currently

done manually. Spectral imaging technology is advancing rapidly and spectral cameras are decreasing in cost while increasing in quality. Hyperspectral imaging is fast, non-destructive to the sample, and the instrumentation would be easy to integrate into existing core analysis centers. The spectral data is reproducible, facilitates integration of core data and well log data and can serve multiple purposes in the core analysis workflow. Hyperspectral imaging has the potential to dramatically impact conventional core logging in the oil sands, especially in high throughput facilities where time efficiency is essential.

6.2 Future Work

For total bitumen content estimation, further work is required for understanding the conditions under which over-reporting of the TBC by the spectral models occurs. The effect of grain size on the performance of the spectral models requires further investigation in particular. In order to advance our understanding of using SWIR imagery for enhancing sedimentological features in core, a follow up study is warranted to investigate the independent effects of grain size, bitumen content and clay abundance on oil sands reflectance. The application of hyperspectral imaging for mapping lithological units in drill core could be furthered by adding other end-members to the classification, such as coal or wood. Future work in this area will also investigate ways to expedite the joint use of the SWIR and LWIR datasets, as well as more ways to improve the mapping results using the datasets individually. Outlined below are several avenues for future work that are beyond the scope of this study.

6.2.1 Clay Characterization

Clay mineralogy is an important area of research in the oil sands. In the Athabasca deposit, clay minerals that are typical of the McMurray Formation include kaolinite, illite, and montmorillonite, as well as mixed-layer species (Bayliss and Levinson, 1976). Detailed knowledge about clay mineralogy is important in the oil sands because of the detrimental effects clays can have during ore processing. Swelling clays are a group of phyllosilicate minerals that

undergoes changes in volume in response to changing moisture conditions. Montmorillonite, a clay with high swelling potential, has been demonstrated to impede bitumen recovery even if as little as 1 wt % is present in the ore (Kasongo et al., 2000; Liu et al., 2004). Similar effects have been reported for illites, which have an intermediate swelling potential (Ding et al., 2006). The current oil sands industry standard for the identification of swelling clays is the methylene blue index (MBI) test (Hang and Brindley, 1970). MBI analysis is carried out on the dry, extracted (bitumen-free) clay fraction (<2 μm) of oil sands solids. Despite being the most common method used in the industry, MBI is susceptible to large margins of error because it is prone to interference from residual organics and iron oxides and is highly operator sensitive (Kaminsky et al., 2009).

The characterization of clay minerals in oil sands is an interesting research problem for the application of hyperspectral imaging. Pure clay mineral species have been thoroughly characterized by reflectance spectroscopy with in-depth studies beginning in the 1970s and continuing to present day. Reflectance spectroscopy has been successfully applied for detailed studies of clay chemistry in pure mineral separates (e.g. Bishop et al., 2008) and for the prediction of clay swelling potential in soils (e.g. Kariuki et al., 2003; 2004). However, working with oil sands poses new challenges for spectral clay analysis due to both physical mixtures of clays and mixed-layer clay minerals. The swelling behaviour of Athabasca oil sands has been shown to be primarily caused by smectitic interstratification in kaolinite and illite, rather than by discrete montmorillonite (Omotoso and Mikula, 2004). An additional challenge with core samples is the presence of free water and organic matter (i.e. bitumen), both of which are known to have a major masking effect on clay absorption bands (Kariuki et al., 2004). A preliminary spectral study of pure clay mineral samples from the Clay Minerals Society repository successfully separated low swelling potential clays (kaolinites) from moderate to high swelling potential clays (illite-smectites and pure montmorillonites) (Speta et al., 2013). Further work on bitumen-extracted oil sands solids found correlations between clay type and absorption feature

depth, asymmetry and wavelength position (Entezari et al., 2015). The latter work was supported by quantitative XRD data.

6.2.2 Beyond the McMurray Formation

All of the existing published work on the application of reflectance spectroscopy and hyperspectral imaging to oil sands has studied samples from the McMurray Formation of the Athabasca deposit. The McMurray Formation is only one of several bitumen reservoirs in Alberta and is mineralogically and sedimentologically distinct from other formations in the province. For example, the Grand Rapids Formation, which is the main bitumen-saturated unit in the westernmost portion of the Athabasca (also known as Athabasca West or the Wabasca A deposit), is far more feldspar and lithic-rich than the quartz-dominant McMurray Formation (Kramers, 1974; 1980). Mineralogical variability will affect the reflectance response of the sediment and the methods demonstrated in this study may need to be adjusted accordingly. The application of hyperspectral imaging to oil sands outside of the McMurray Formation is an important area for future research as industry operations expand beyond the Athabasca deposit.

References

- Bayliss, P., and Levinson, A.A., 1976, Mineralogical review of the Alberta oil sand deposits (Lower Cretaceous, Mannville Group), *Bulletin of Canadian Petroleum Geology*, v. 24, no. 2, p. 211–224.
- Bishop, J., Madejová, J., Komadel, P., and Fröschl, H., 2002, The influence of structural Fe, Al and Mg on the infrared OH bands in spectra of dioctahedral smectites, *Clay Minerals*, v. 37, no. 4, p. 607–616.
- Ding, X., Repka, C., Xu, Z., and Masliyah, J., 2006, Effect of illite clay and divalent cations on bitumen recovery, *The Canadian Journal of Chemical Engineering*, v. 84, p. 643–650.
- Entezari, I., Speta, M., Rivard, B., and Geramian, M., 2015, Hyperspectral characteristics of oil sands clay mineral assemblages (abs.), Cosia/PTAC Oil Sands Clay Workshop & Conference, April 28-29, 2015, Edmonton, AB, 1 p.
- Hang, P.T., and Brindley, G.W., 1970, Methylene blue absorption by clay minerals: Determination of surface areas and cation exchange capacities (Clay-organic studies XVIII), *Clays and Clay Minerals*, v. 18, p. 203–212.
- Kaminsky, H., Etsell, T.H., Ivey, D.G., and Omotoso, O., 2009, Distribution of clay minerals in the process streams produced by the extraction of bitumen from Athabasca oil sands, *The Canadian Journal of Chemical Engineering*, v. 87, no. 1, p. 85–93.
- Kariuki, P.C., van der Meer, F., and Verhoef, P.N.W., 2003, Cation exchange capacity (CEC) determination from spectroscopy, *International Journal of Remote Sensing*, v. 24, no. 1, p. 161–167.
- Kariuki, P.C., Woldai, T., and van der Meer, F., 2004, Effectiveness of spectroscopy in identification of swelling indicator clay minerals, *International Journal of Remote Sensing*, v. 25, no. 2, p. 455–469.
- Kasongo, T., Zhou, Z., Xu, Z., and Masliyah, J., 2000, Effect of clays and calcium ions on bitumen extraction from Athabasca oil sands using flotation, *The Canadian Journal of Chemical Engineering*, v. 78, p. 674–681.
- Kramers, J.W., 1980, Diagenetic features of Grand Rapids Formation, north-central Alberta, Canada (abs.), AAPG Annual Convention & Exhibition, Denver, CO, p. 735.
- Kramers, J.W., 1974, Geology of the Wabasca A oil sand deposit (Grand Rapids Formation), in: Hills, L. (Ed.), *Oil Sands: Fuel of the Future*, Memoir 3, Canadian Society of Petroleum Geologists, p. 68–83.
- Kruse, F.A., Lefkoff, A.B., Boardman, J.W., Heidebrecht, K.B., Shapiro, A.T., Barloon, P.J., and Goetz, A.F.H., 1993, The spectral image processing system (SIPS) interactive visualization and analysis of imaging spectrometer data, *Remote Sensing of Environment*, v. 44, p. 145–163.
- Liu, J., Xu, Z., and Masliyah, J., 2004, Role of fine clays in bitumen extraction from oil sands, *AIChE Journal*, v. 50, no. 8, p. 1917–1927.
- Masliyah, J., Zhou, Z.J., Xu, Z., Czarnecki, J., and Hamza, H., 2004, Understanding water-

based bitumen extraction from Athabasca oil sands, *The Canadian Journal of Chemical Engineering*, v. 82, p. 628–654.

Mustard, J.F., and Sunshine, J.M., 1999, Spectral Analysis for Earth Science: Investigations Using Remote Sensing Data, in: A.N. Rencz (Ed.), *Remote Sensing for the Earth Sciences: Manual of Remote Sensing*, John Wiley & Sons, Inc., p. 251–306.

Omotoso, O., and Mikula, R.J., 2004, High surface areas caused by smectitic interstratification of kaolinite and illite in Athabasca oil sands, *Applied Clay Science*, v. 25, no. 1-2, p. 37–47.

Petit, S., Madejova, J., Decarreau, A., and Martin, F., 1999, Characterization of octahedral substitutions in kaolinites using near infrared spectroscopy, *Clays and Clay Minerals*, v. 47, no. 1, p. 103–108.

Rivard, B., Feng, J., Gallie, A., and Sanchez-Azofeifa, A., 2008, Continuous wavelets for the improved use of spectral libraries and hyperspectral data, *Remote Sensing of Environment*, v. 112, no. 6, p. 2850–2862.

Rivard, B., Lyder, D., Feng, J., Gallie, A., Cloutis, E., Dougan, P., Gonzalez, S., Cox, D., and Lipsett, M.G., 2010, Bitumen content estimation of Athabasca oil sand from broad band infrared reflectance spectra, *The Canadian Journal of Chemical Engineering*, v. 88, p. 830–838.

Speta, M., Entezari, I., and Rivard, B., 2013, Exploring hyperspectral imaging for the characterization of clay minerals in oil sands core (abs.), CONRAD 3rd Oil Sands Clay Conference & Workshop, Feb. 20-21, 2013, Edmonton, AB, 2 p.

Appendix A

Detailed Rietveld analysis results

Table A1. Results of quantitative phase analysis (modal mineralogy, wt %)

Mineral	Ideal Formula	Barren Sand	Siltstone	Mudstone
Anatase	TiO ₂	0.4	0.7	1
Ankerite?	Ca(Fe ²⁺ ,Mg,Mn)(CO ₃) ₂	0.1	0.3	0.4
Illite/Muscovite 2M1	~K _{0.65} Al _{2.0} Al _{0.65} Si _{3.35} O ₁₀ (OH) ₂ / KAl ₂ (AlSi ₃ O ₁₀)(OH) ₂	13	22	33
Kaolinite 1A	Al ₂ Si ₂ O ₅ (OH) ₄	6	18	30
Pyrite	FeS ₂	0.3	0.3	0.7
Quartz low	SiO ₂	79	54	34
Rutile	TiO ₂	0.7	1	0.6
Siderite, calcian	(Fe ²⁺ ,Ca,Mg)CO ₃		4	
Total		100	100	100

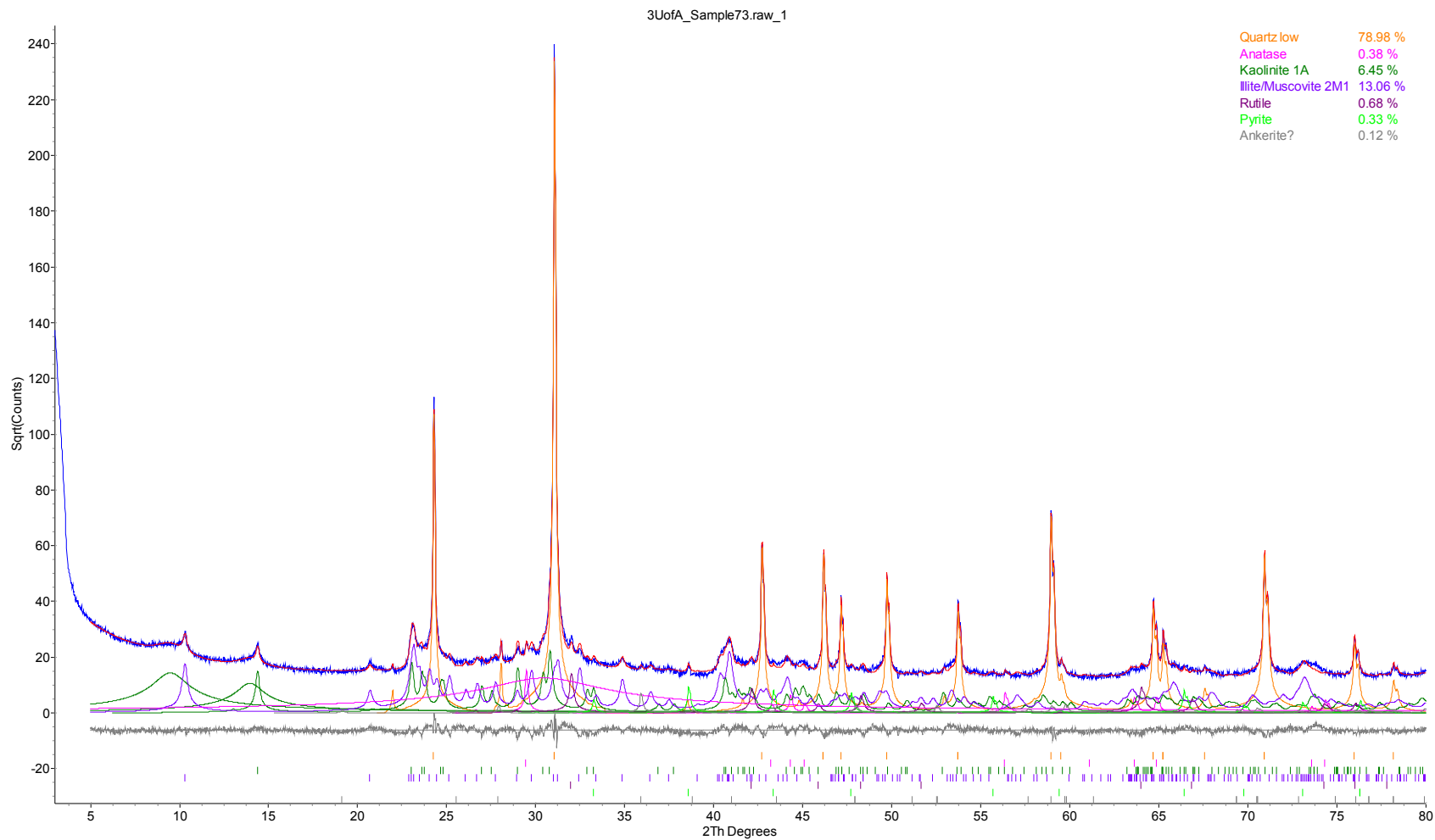


Figure A1. Rietveld refinement plot of sample **Barren Sand** (blue line - observed intensity at each step; red line - calculated pattern; solid grey line below - difference between observed and calculated intensities; vertical bars - positions of all Bragg reflections). Coloured lines are individual diffraction patterns of all phases.

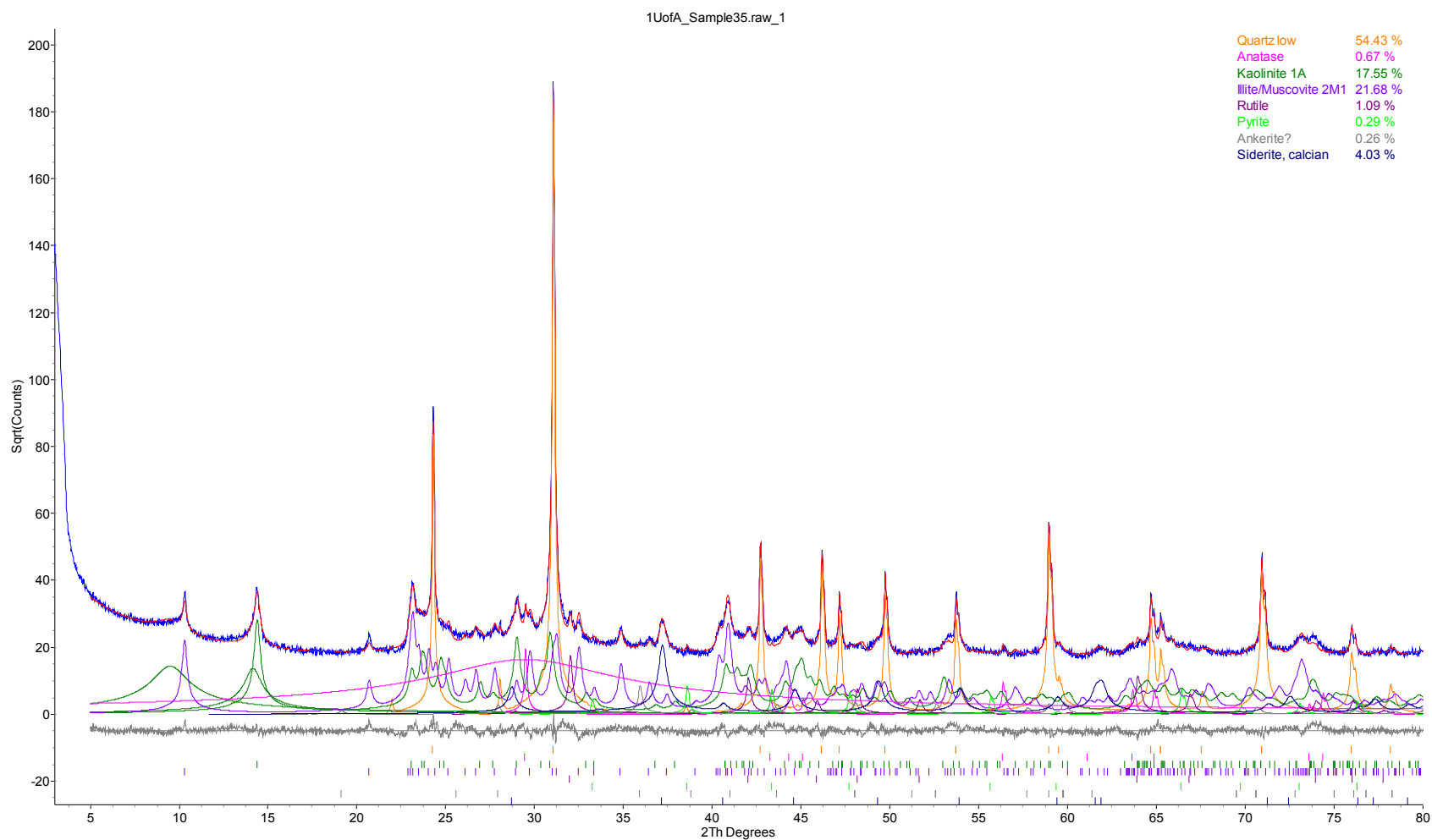


Figure A2. Rietveld refinement plot of sample **Siltstone** (blue line - observed intensity at each step; red line - calculated pattern; solid grey line below - difference between observed and calculated intensities; vertical bars - positions of all Bragg reflections). Coloured lines are individual diffraction patterns of all phases.

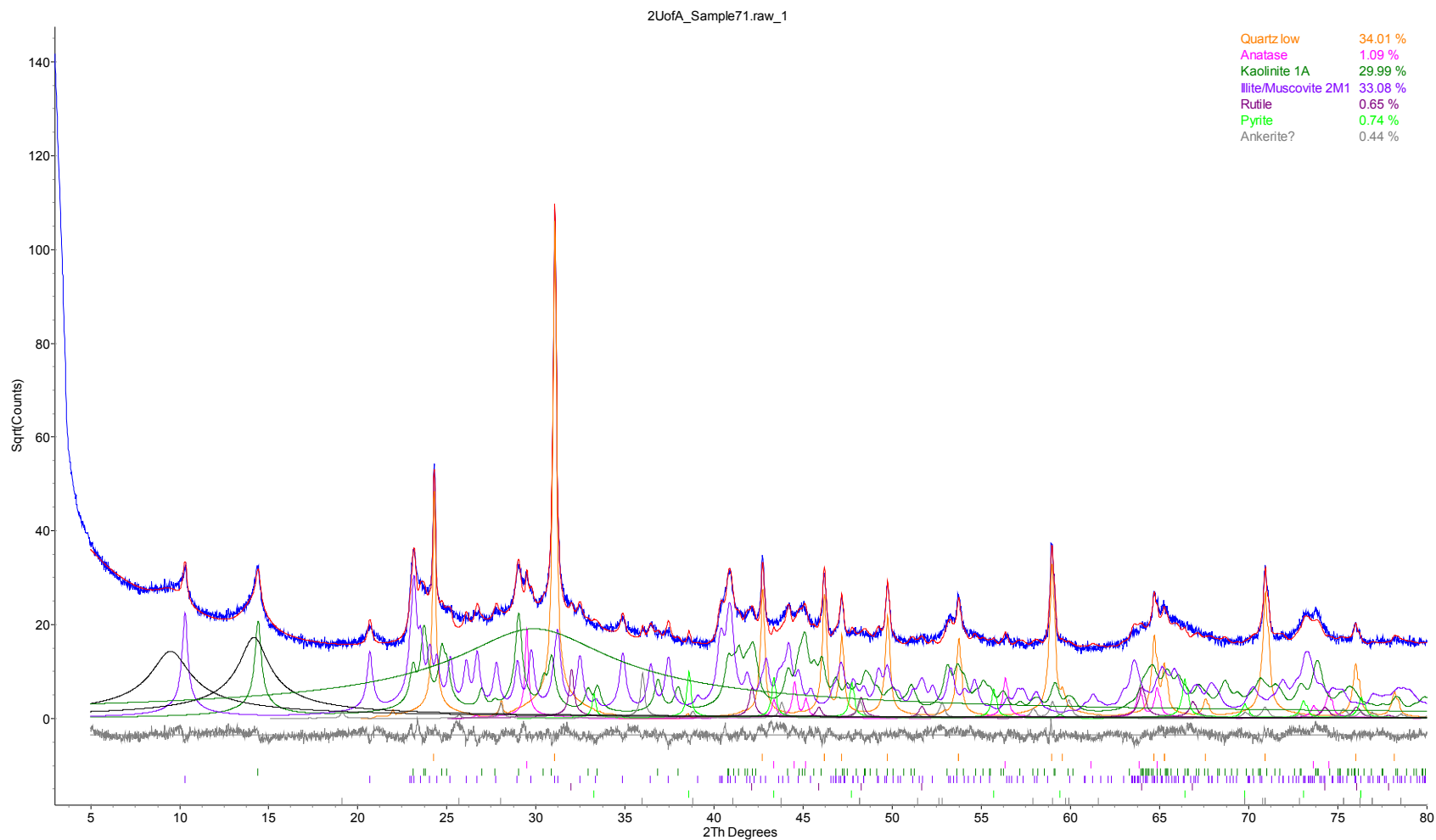


Figure A3. Rietveld refinement plot of sample **Mudstone** (blue line - observed intensity at each step; red line - calculated pattern; solid grey line below - difference between observed and calculated intensities; vertical bars - positions of all Bragg reflections). Coloured lines are individual diffraction patterns of all phases.